UiA Universitetet i Agder

Master

Vibration-based structural health monitoring of a model truss bridge

Eivind Andreas M. Kvalvaag

Bjørn-Erik Elvebakk

Einar Garcia de Presno

INTERNAL SUPERVISOR

Zhiyu Jiang (UiA, Civil Engineering), Ajit Jha (UiA, Mechatronics),
Rein Terje Thorstensen (UiA, Civil Engineering)

EXTERNAL SUPERVISOR

Zhen Sun (University of Porto)

Universitetet i Agder, 2022

Faculty of Science and Technology

Department of Engineering

Obligatorisk egenerklæring/gruppeerklæring

Den enkelte student er selv ansvarlig for å sette seg inn i hva som er lovlige hjelpemidler, retningslinjer for bruk av disse og regler om kildebruk. Erklæringen skal bevisstgjøre studentene på deres ansvar og hvilke konsekvenser fusk kan medføre. Manglende erklæring fritar ikke studentene fra sitt ansvar.

1.	Jeg/vi erklærer herved at min/vår besvarelse er mitt/vårt eget arbeid, og at jeg/vi ikke har brukt andre kilder eller har mottatt annen hjelp enn det som er nevnt i besvarelsen.	☒
2.	Jeg/vi erklærer videre at denne besvarelsen: - ikke har vært brukt til annen eksamen ved annen avdeling/universitet/høgskole innenlands eller utenlands. - ikke refererer til andres arbeid uten at det er oppgitt. - ikke refererer til eget tidligere arbeid uten at det er oppgitt. - har alle referansene oppgitt i litteraturlisten. - ikke er en kopi, duplikat eller avskrift av andres arbeid eller besvarelse.	☒
3.	Jeg/vi er kjent med at brudd på ovennevnte er å betrakte som fusk og kan medføre annullering av eksamen og utestengelse fra universiteter og høgskoler i Norge, jf. Universitets- og høgskoleloven §§4-7 og 4-8 og Forskrift om eksamen §§ 31.	☒
4.	Jeg/vi er kjent med at alle innleverte oppgaver kan bli plagiatkontrollert.	☒
5.	Jeg/vi er kjent med at Universitetet i Agder vil behandle alle saker hvor det forligger mistanke om fusk etter høgskolens retningslinjer for behandling av saker om fusk.	☒
6.	Jeg/vi har satt oss inn i regler og retningslinjer i bruk av kilder og referanser på biblioteket sine nettsider.	☒

Publiseringsavtale

Fullmakt til elektronisk publisering av oppgaven

Forfatter(ne) har opphavsrett til oppgaven. Det betyr blant annet enerett til å gjøre verket tilgjengelig for allmennheten (Åndsverkloven. §2).

Alle oppgaver som fyller kriteriene vil bli registrert og publisert i Brage Aura og på UiA sine nettsider med forfatter(ne)s godkjennelse.

Oppgaver som er unntatt offentlighet eller tausehetsbelagt/konfidensiell vil ikke bli publisert.

Jeg/vi gir herved Universitetet i Agder en vederlagsfri rett til å

gjøre oppgaven tilgjengelig for elektronisk publisering: ☒JA ☐NEI

Er oppgaven båndlagt (konfidensiell)? ☐JA ☒NEI

(Båndleggingsavtale må fylles ut)

- Hvis ja:

Kan oppgaven publiseres når båndleggingsperioden er over? ☐JA ☐NEI

Er oppgaven unntatt offentlighet? ☐JA ☒NEI

(inneholder taushetsbelagt informasjon. Jfr. Offl. §13/Fvl. §13)

Preface

This master thesis is conducted at the Department of Engineering as a part of the Civil and Structural Engineering program at University of Agder in Grimstad. This is the concluding project in subject BYG508 and was finished in the fourth and final semester.

It is assumed that the reader has a fundamental knowledge of engineering and mathematics. The majority of this project is based on structural dynamics.

We would like to offer our gratitude to our main supervisor Zhiyu Jiang at University of Agder for his professional insight on dynamics and his help and guidance throughout this project: Thank you. We would also like to thank supervisor and sensor expert Ajit Jha at University of Agder, Rein Terje Thorstensen at University of Agder, and external supervisor and bridge expert Zhen Sun at University of Porto for their inputs and thoughts on the project. The group would also like to thank senior engineer Karl Berge Rød and Professor Kjell Gunnar Robbersmyr for loaning us the DEWESoft equipment and Endevco accelerometers.

The group also cooperated with a bachelor group that had the responsibility of building the model bridge, so the group would like to thank them for their work on the bridge.

The purpose of this thesis is to examine the change in the truss bridge's dynamic response when altering the physical properties. The study will be carried out experimentally by performing analytical and experimental modal analyses. The analyses will cover three cases involving the truss model bridge. These will cover one intact case and two different damage cases where the physical properties of the bridge are altered.

Abstract

Vibration-based methods with acceleration sensors are playing an increasingly important role in structural health monitoring of modern bridges. This master thesis investigates how the change in the truss bridge's dynamic response when altering the physical properties. The study will be carried out experimentally by performing analytical and experimental modal analyses. The analyses will cover three cases involving the truss model bridge. These will cover one intact case and two different damage cases where the physical properties of the bridge are altered. First, we created numerical model of a truss bridge along with a model bridge of the same bridge design. Second, we run an analytical modal analyse of the numerical model. The analytical modal analysis consisted of two cases, the first case was the bridge undamaged, the second was the bridge with one diagonal member removed. Third, we conducted two different types of modal analyses on the physical model, where one was classical, and one was operational. The classical was only with the bridge undamaged and done with low sensitivity sensors. The operational was done with high sensitivity sensors and consisted of three different cases. The first case was the bridge undamaged, the second was the bridge with one diagonal member removed, and the third was the bridge with one diagonal member loosened. Finally, we compared the different modal analyses to each other. The main finding is that both damage case 1 where the truss element is removed and damage case 2 where the element was loosened showed on average -6.49% and -8.37% decrease in the eigenfrequencies in the z-direction. The damage cases were applied on the element contributing to vertical stiffness, this was reflected in the result as the damage affected the vertical modes about 5x and 7.5x more than the lateral modes in damage case 1 and 2. The analytical modal analysis (AMA) result had discrepancies of 0-10% to the experimental modal analyses (CMA and OMA) in the undamaged case. The damage simulation in the AMA gave a significantly larger decrease of -9.83% in the lateral modes compared to the OMA which had only -0.87%. The thesis show that structural health monitoring based on vibration measurements can be achieved by instrumenting the bridge with accelerometers in key locations. By doing this we are able to measure the free vibrations of the bridge's superstructure. The raw vibration data from the measurements can then be decomposed to identify the bridge's mode frequencies. The mode frequencies are dependent on the bridge's structural stiffness and weight. Knowing this, any change in the eigenfrequencies can be treated as a change in stiffness of the superstructure. This may be caused by structural damage and should be investigated.

1 Table of content

List of figures

List of tables

Abbreviations

AMA	Analytical Modal Analysis
APDL	Ansys Parametric Design Language
CMA	Classic Modal Analysis
DOF	Degrees of freedom
FDD	Frequency Domain Decomposition
FEM	Finite Element Method
FFT	Fast Fourier Transformation
GUI	Graphic User Interface
MAC	Modal Assurance Criterion
MCF	Modal Complexity Factor
MEEL	Mesh Element Edge Length
MF	Modal Frequency
NA	Neutral axis
NRK	Norsk Rikskingkasting/Norwegian national broadcasting
OMA	Operational Modal Analysis
TC	Test Case

1 Introduction

1.1 Background

Using vibration properties to investigate damages on bridges has been done since the mid 70's, which lead to vibration-based structural health monitoring becoming highly focused as research discipline in the late 90's. There are already many advanced applications of SHM system on bridges all over the world [1]. With structural health monitoring system installed on 20 bridges in China, e.g. Tsing Ma bridge in Hong Kong. Were they summarized several vibration-based methodologies developed for SHM and damage detection [2]. The Øresund bridge in Denmark, were they used a continuous monitoring system on an 8km long bridge and focused on how operational modal analysis can used to provide useful information on the health of the bridge [3]. Figure 1 below is showing structural health monitoring on a bridge.

With more and more concern about the ageing structural degradation of bridges, together with more complex structures that need validation of their behaviour.

Figure 1 Structural health monitoring of a bridge [62]

Looking at the standards on bridges in Norway today, there are a lot of bridges that are in poor condition. There are reports out about this problem, example a rapport from 2022 that says about 5600 bridges out of 17000 in Norway have damages. Where another rapport states that over 1000 of 5600 birdges have damage which are so great that it has significant impact on the load bearing capacity of the bridges [4] [5].

In addition to that, about 5300 of 5600 bridges has damages that affect the traffic safety. This has mainly to do with corrosion of the railing. The reports said that some of the reasons for this was that the government would rather improve the main roads by e.g., making 4-lane highways, then priorities the bridge maintenance [4] [5].

Another report also points out that many bridges are closing in on the end of their designed lifetime, some are even over 100 years old, and that many of the bridges hasn't even been inspected. This is a very critical for the condition of the bridges and all these problems will lead to functional or structural failure if nothing is done [6].

The environmental and mechanical stresses on the bridge are also increasing with more traffic and extreme weather, which means the probability for damages and fractures will increase.

It is resource demanding to manually go out and inspect all these bridges to verify that they are safe to use. Nowadays many bridges lack a regular maintenance plan, but a strategy to maintain the structural sustainability through its whole lifetime is getting more and more used. This strategy, called preventive maintenance is often combined with structural health monitoring.

With the right technology this could be done automatically with sensors to detect different damages on the bridge and decide what condition the bridge is in without the need of a manually inspection [7]. The monitoring systems are getting more practical and economical, but two of the main problems are still the return of investment and how to properly design and implement the system. Its therefore relevant to investigate the possibility to use sensors that measure the differences in the frequency over time to detect possible damages and then give an early warning before a critical failure or collapse will occur.

1.2 Scope

The scope of the study is to examine the change in the truss bridge's dynamic response when altering the physical properties. The study will be carried out experimentally by performing analytical and experimental modal analyses. The analyses will cover three cases involving the truss model bridge. These will cover one intact case and two different damage cases where the physical properties of the bridge is altered. Below in Figure 2 is an illustration of the structural health monitoring process. The illustration shows what steps we focus on and how far in the process we go.

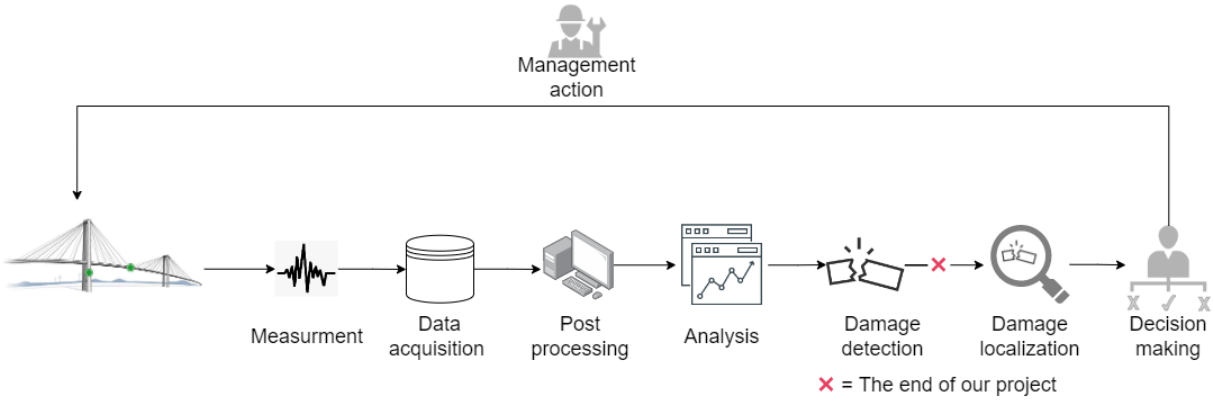

Figure 2 The process of structural health monitoring

2 Social perspective

In the introduction the group mention that there is a lot of bridges being in poor condition, this is negatively impacting the road infrastructure. Having a functional and safe road infrastructure are important to both the economic growth and quality of life [8]. These topics is highly relevant to the UN's Sustainability goals, and especially the goals 9.1 and goal 12.2. Goal 9.1 is about developing reliable, sustainable solid high-quality infrastructure. Goal 12.2 is about sustainable management and effective usage if natural resources [4] [9].

Vibration-based SHM is a possible method to improve the chances to reach these goals. The method will help locating possible damages on the bridge and then tell what condition the bridge is in. Which then can be used to form a basis for preventive maintenance. This can help to optimize the usage of the material and can prolong the lifetime of the bridge.

With this technology the bridge inspectors only need to mount the equipment one time and then monitor the bridge through its lifetime, and don't need to only rely on manually inspections of the bridge. This will make it easier for the inspectors to have control over what condition the bridges are in.

The maintenance backlog is a problem because of too many bridges and the inspections are too time consuming to keep up the maintenance. Structural health monitoring is a new tool with numerical models or digital twins to keep up the maintenance of bridges. By improving the maintenance system, it will also improve the general safety of bridges [4].

3 Theoretical background

3.1 Truss bridges

A truss structure consists of an array of straight beams connected in nodes. These beams are oriented in a series of triangles. Triangles are used because they are the only shape that can't be angularly distorted in the nodes without deforming the truss members longitudinally [10]. Truss connections are generally considered as pinned, meaning that they are free to rotate. Given the trusses are free to rotate, the truss members will only carry axial loads. In practice the truss members are often rigidly connected in the nodes by gusset plates. By eliminating rotation in the nodes, the critical buckling load is reduced for compression truss members. Although the trusses are rigidly connected, they are still considered jointed given that all the connected members intersect at a common point. In reality the truss elements will carry small, but usually negligible bending moments as a result of the rigid connections [11].

Truss bridges typically is a loadbearing superstructure, which consist of trusses and a substructure. The superstructure consists of one or more rows of triangles which as shown in Figure 3. Truss bridges uses the Steiner's theorem by efficiently arranging the loadbearing elements far away from the neutral axis of the bridge. The triangular shape of the trusses and the jointed nodes will distribute the loads applied into axial forces, thus eliminating bending moment. With no bending moment, the only deformations in the trusses are axial. As a result, truss bridges achieve a high bending stiffness while maintaining a relatively low self-weight and material usage. All these factors contribute to creating a stiff and rigid bridge span [12].

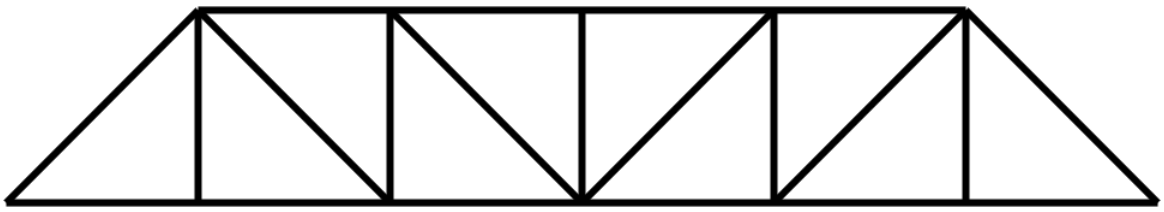

Figure 3 A truss bridge (Pratt bridge design, patented in 1844) made from triangular elements.

Truss bridges are popular because of their high utilization of materials, stiffness and low weight compared to other bridge types like concrete bridges. These bridges are commonly used for railroad bridges and road bridges requiring longer spans.

3.2 Normal truss bridge damage cases

The superstructure of truss bridges usually consists of steel elements. Due to large forces and tough environmental stresses, these elements are prone to a number of damage scenarios that are typical for steel.

3.2.1 Fatigue cracks

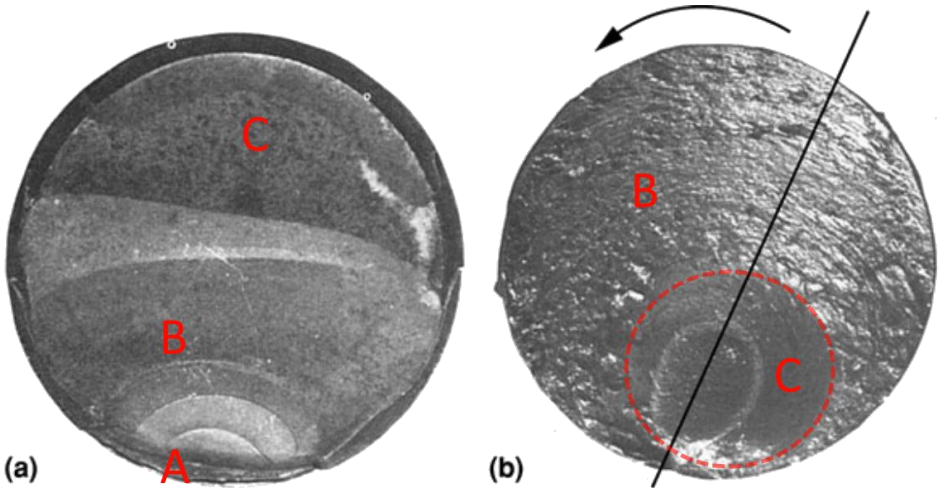

Figure 4 Example of fatigue cracked cross sections. (a) Result of unidirectional bending cycles. (b) Result from rotating bending cycles [49]

One of the most common damage cases of steel is fatigue due to repeated loading. When elements experience repeated cyclic loading with high enough magnitude, fatigue cracks will form on the surface. These initial cracks will continue to grow progressively as the loading cycles continue. As the cracks grow, they will reduce the effective area in cross section of the element. If these cracks are left unnoticed, the fatigue cracks will weaken the cross section to the point where a brittle failure will occur. These progressive steps can be seen in the failure cross section of element (a) in Figure 4. The figure shows crack initiation A, continuous growth of crack B, and the final fracture area C.

3.2.2 Corrosion

Another common damage instance is corrosion. The most common corrosion process occurs when the three necessary elements are in place: Iron (Fe), water (H_2O), and oxygen (O_2).

$$4Fe + 3O_2 + 6H_2O \rightarrow 4Fe(OH)_3 \; or \; 4FeO(OH) + 4H_2O \qquad (3.2.2.1)$$

This chemical reaction creates red rust. The corrosion process can be accelerated by several factors including the presence of chlorides. Chlorides are commonly used as road salts in the winter to stop ice from forming on the road surface. On bridges the road salts will often flow or splash on nearby steel elements causing the corrosion process to accelerate. Corrosion slowly eats away steel from the element's cross section, often small flakes at a time, weakening it and in some cases resulting in critical failure [13]. A common method to stop corrosion is coating the steel in a protective layer and thus removing key elements in the chemical reaction.

Figure 5 Rusted steel beam under a bridge [48]

If this layer is compromised through cracks or holes, either by mechanical damage or imperfections, the corrosion process has a place to start and can easily spread. Figure 5 shows a steel beam that has started corroding and the protective layer (green) is peeling off where rust is forming.

3.2.3 Stress corrosion cracking (SCC)

Cracking due to mechanical stresses and rust corrosion combined synergize in what is called stress corrosion cracking (SCC). This combination can lead to unexpected brittle failures in otherwise ductile metals [13]. When a crack occurs in a steel element, a new active (non-passive) surface appears. These fresh surfaces are highly reactive and corrode easily. The corrosion reaction causes the crack to expand and again exposing highly reactive metal. This cycle can lead to rapid crack growth and can result in mechanical failure in the respective component [13].

3.2.4 Mechanical damage

Figure 6 Damage to trusses caused by collision [50]

Mechanical damage as a result of collision is a less common, but often a significant damage case. Collision from vehicles such as cars, trucks and boats, carry enough energy to critically injure the superstructure of a truss bridge. In some cases, such as the I-5 Skagit River bridge, road vehicles colliding with key elements of the bridge can result in total bridge collapse [14] [15]. Non-critical collisions create permanent plastic deformations in the affected area. These deformations change the affected element's stiffness and loadbearing capacity by altering the cross sections geometry. Altering the cross section's geometry causes a displacement of the neutral axis which leads to eccentric loads. The eccentricity of the load generates greater deflections and a reduction of the critical buckling load. The increased sensitivity to deflections lowers the stiffness both in axial and rotational load cases. Mechanical damage in key elements of the superstructure can result in significant reduction in overall stiffness and capacity [16].

3.2.5 Buckling

Buckling is a failure mode that can occur under compressive loads. These types of failures are most common in slender beams or columns (flexural buckling), and locally in beams with a tall web under heavy bending loads (tortional buckling). [17] Some common buckling forms in columns can be seen in Figure 7.

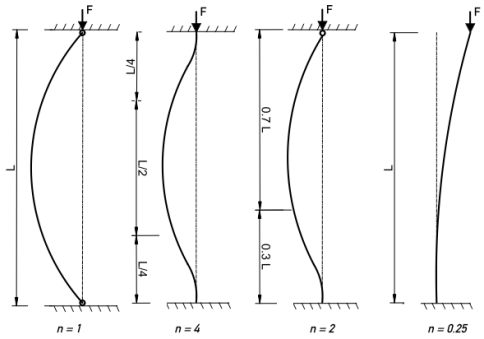

Figure 7 Buckling faliure modes of beam elements with different boundry conditons

Buckling failures often result in sudden collapse because of the abrupt loss of axial capacity relative to regular compressive deformations. This is because once the critical buckling load is met, the column will abruptly bend, causing an additional bending load due to the now eccentric cross section. The additional deformation will again create increased bending due to the PΔ-effect ($M = P \times \Delta$), where Δ is the deformation/eccentricity. [17] [18]

The critical buckling load (P_{cr}) for non-eccentric loads is defined by Euler's formula for buckling:

$$P_{cr} = \frac{\pi^2 EI}{(l_0)^2} \tag{3.2.5.1}$$

l_0 is the effective length factor accounting for the column's mounting method as shown in Figure 7. The critical buckling load is greatly reduced by eccentric loads. Eccentric loads are loads acting on an element offset from the neutral axis, thus creating a bending moment ($M_e = P \times e$) in the beam. The bending moment will deform the column as the load increases, this gives a gradual and more predictable buckling form. The Secant Buckling Formula builds on Euler's work by accounting for eccentricity (e) in the system and is given by [18] [17]:

$$\sigma_{max} = P\left[\frac{1}{A} + \frac{e \times c}{I} sec\left(\frac{\pi}{2}\sqrt{\frac{P}{P_{cr}}}\right)\right] \tag{3.2.5.2}$$

Where c is the distance from the neutral axis to the furthest point in the cross section. Due to the eccentricity the beam will bend when loaded. This results in a lower axial stiffness and will reduce the capacity due to combined forces of bending and compression. The eccentricity can be a result of the joint's structural design or by mechanical damage in the structure. Eccentric loaded columns with corbels are a common example (as shown in Figure 8). [18]

Figure 8 shows a common column with a corbel and its deformations due to axial and eccentric loads.

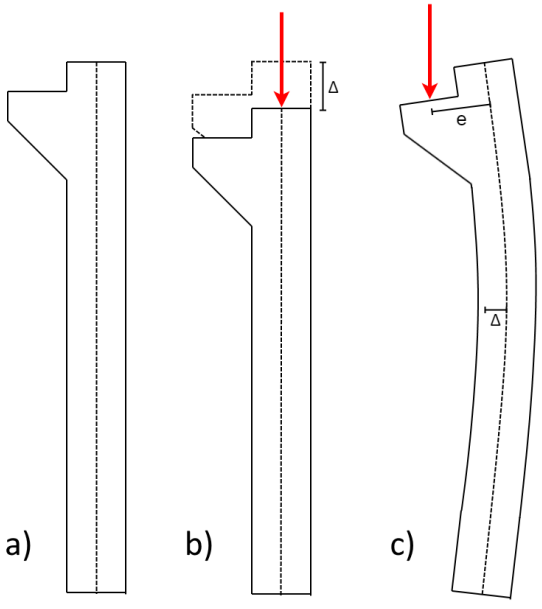

Figure 8 Column with corbel (a) under axial (b) and eccentric (c) load

The eccentric loaded column bends due to the moment created by the offset eccentric load ($M_e = P \times e$).

3.3 Structural health monitoring

Structural health monitoring is about observation and analysis of an engineering structure such as a bridge. This is done by mounting sensors to get response measurements that can be monitored over time and analyse the changes in the material and geometric properties. The main purpose is to use this in a long-term to get an update regarding the condition of the bridge and if it's capable of working as intended. This monitoring is done while the bridge is aging and getting worn down by the operational environments. This can also be used after extreme events or accidents on the bridge to locate if the bridge has any damages and if it's safe to use [19].

It's important to identify features in the acquired data to determine if its damaged or undamaged, where it often uses a feature extraction method. This is based on correlating measured system response quantities, like vibration amplitude or frequency [19].

3.4 Structural dynamics

Dynamics are often broken down into two analyses. The first one is free vibration, where the initial disturbance caused by static equilibrium is setting the system in motion. The system is moving freely without any further external forces, the properties of the structure is the only factor causing the motion. The system consists of mass and stiffness, together this causes the system to oscillate, which is called natural frequency. The second analyse is when the system is affected by an external force and the forced vibration will occur [20]. Degree of freedom is a known term when modelling structures, which is explained by how many motion variables you have in the analysis.

3.4.1 Mode shapes and eigenfrequency

Eigenfrequency or natural frequency is the frequency of the system when it's not being exposed from any external forces. Multi degree of freedom system has multiple modes of vibration, which each have their own natural frequency. They also each have a distinct deformation shape that is called mode shape. This means a system can have many different mode shapes, each with its own frequency. In Figure 9 below it shows the first and second mode shape of a simple beam with fixed ends.

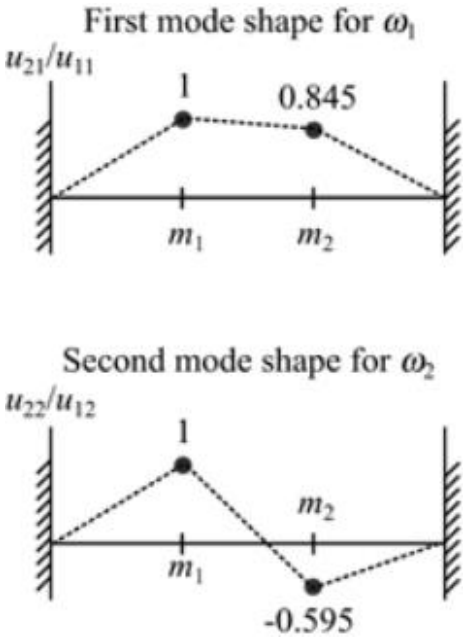

Figure 9 Illustration of first and second bending mode shape [21]

To solve this problem and find the different modes, it will be easier to look at a system where the load is zero and damping is neglected.

$$m\ddot{x} + kx = 0 \tag{3.4.1.1}$$

In equation 3.4.1.1 the displacement "*x*" can varies in both time and position. This can be simplified by using "*t*" as a function of time and "*u*" is a function for position only. From SDOF system the sinusoidal was the form by variation of displacement with time. It's an assumption that the from will be similar with MDOF as well, so the equation can be written as [20].

$$x = u \sin \omega t \tag{3.4.1.2}$$

Now that "*u*" is not a function of time, the equation 3.4.1.2 only relies on the sine term. Combining this with the equation 3.4.1.1 from the start will give equation 3.4.1.3.

$$(k - \omega^2 m)u \sin \omega t = 0 \tag{3.4.1.3}$$

Equation 3.4.1.3 is usually named the characteristic equation. Two of the reason this equation can be true, is that either "*u*" or "$sin(\omega t)$" is zero, this imply that the system doesn't vibrate.

This leads to look at the last option, which is that the matrix "$(k - \omega^2 m)$" doesn't have an inverse, which leads to equation 3.4.1.4 [20].

$$det(k - \omega^2 m) = 0 \tag{3.4.1.4}$$

Solving this will find the values of natural frequency, the number of natural frequencies will be the same as how many degrees of freedom the system. All these frequencies can be substituted into equation 3.4.1.5.

$$(k - \omega^2 m)u = 0 \tag{3.4.1.5}$$

With an undamped system with two degrees of freedom, that is harmonically loaded. Then derive the equation of motion, to get equation 3.4.1.6.

$$\begin{bmatrix} m_1 & 0 \\ 0 & m_2 \end{bmatrix}\begin{bmatrix} \ddot{x}_1 \\ \ddot{x}_2 \end{bmatrix} + \begin{bmatrix} k_1 + k_2 & -k_2 \\ -k_2 & k_2 \end{bmatrix}\begin{bmatrix} x_1 \\ x_2 \end{bmatrix} = \begin{bmatrix} P \sin \omega_P t \\ 0 \end{bmatrix} \tag{3.4.1.6}$$

By applying the equation 3.4.1.4 from earlier, can the frequencies of the system be found, in equation 3.4.1.7.

$$(k_1 + k_2 - \omega^2 m_1)(k_2 - \omega^2 m_2) - k_2^2 = 0 \tag{3.4.1.7}$$

The two natural frequencies "ω_1" and "ω_2" can now be solved and by substituting each frequency the mode shapes can also be found. The form of the steady state response is expected to be like equation 3.4.1.8 [20].

$$\begin{bmatrix} x_1 \\ x_2 \end{bmatrix} = \begin{bmatrix} X_1 \\ X_2 \end{bmatrix} \sin \omega_P \, t \tag{3.4.1.8}$$

Then substituting and differentiating into the equation of motion to get equation 3.4.1.9.

$$\begin{bmatrix} k_1 + k_2 - m_1\omega_P^2 & -k_2 \\ -k_2 & k_2 - m_2\omega_P^2 \end{bmatrix}\begin{bmatrix} X_1 \\ X_2 \end{bmatrix} = \begin{bmatrix} P \\ 0 \end{bmatrix} \tag{3.4.1.9}$$

By standard methods can the matrix equation be inverted, and the two masses gets the resulting amplitude as in equation 3.4.1.10 [20].

$$\begin{bmatrix} X_1 \\ X_2 \end{bmatrix} = \begin{bmatrix} k_2 - m_2\omega_P^2 \\ k_2 \end{bmatrix} \frac{P}{m_1 m_2(\omega_1^2 - \omega_P^2)(\omega_2^2 - \omega_P^2)} \tag{3.4.1.10}$$

3.4.2 Single degree of freedom

Systems that are known as single-degree-of-freedom, can describe the dynamic behaviour with the use of only one coordinate. The system is affected by a single displacement variable. Using this to get a better understanding of how the vibration works on the system and to simplify the main principles of a bigger system with multiple degrees of freedom [20].

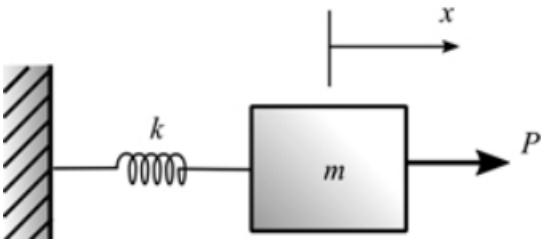

Figure 10 Illustration of a SDOF system [21]

In Figure 10 above, you can see a system that consists of a cube that contains the mass "m". Between the wall and the cube is a spring with the stiffness "*k*" that moves in a linear movement.

An external force "*P*" is working on the mass and causes the mass to have a displacement, and the displacement of the mass is described as "*x*". In this system the damping force is neglected, but the damping is described as "*c*".

From Newton's second law combined with Hook's law we can get equations from the different forces:

$$P_s = kx(t) \quad The\ stiffness\ force \tag{3.4.2.1}$$

$$P_d = \dot{c}x(t) \quad The\ damping\ force \tag{3.4.2.2}$$

$$P_m = ma = m\ddot{x} \ The\ inertia\ force \tag{3.4.2.3}$$

From Newtons's second law, the resultant force is equal to mass times acceleration can we get the equation of motion for the system [20]:

$$m\ddot{x} + c\dot{x} + kx = P(t) \tag{3.4.2.4}$$

This can be simplified by putting both "*c*" and "*P(t)*" equal to zero, this is called an undamped free vibration system [20]:

$$m\ddot{x} + kx = 0 \tag{3.4.2.5}$$

This equation will be more complex in a multi-degree-of-freedom system.

Using standard mathematical techniques to solve this second-order ordinary differential equation. Complex exponential or sine and cosine functions can be used to express the general solution in many different forms, as the form [20]:

$$x = A\sin(\omega t + \varphi) \tag{3.4.2.6}$$

In this form we have some new variables, the *"A"* is for amplitude, *"t"* is the time, "φ" is for phase angel and the "ω" is the circular natural frequency, which is a parameter that describes an equivalent circular motion from the angular velocity and is usually measured in radians per second [20]:

$$\omega = \sqrt{\frac{k}{m}} \tag{3.4.2.7}$$

The vibration can be measured in a more intuitive way, which is called naturals frequency "f_n". The natural frequency is how many cycles of vibration the system has in one second. In the system, there is also a natural period "T_n" , which is how long it takes to complete a cycle [20].

$$f_n = \frac{1}{T_n} = \frac{\omega_n}{2\pi} = \frac{1}{2\pi}\sqrt{\frac{k}{m}} \tag{3.4.2.8}$$

$$T_n = \frac{2\pi}{\omega_n} = 2\pi\sqrt{\frac{k}{m}} \tag{3.4.2.9}$$

3.4.3 Multiple degree of freedom system

This is a system with two or more degrees of freedom, that is affected by free vibration. MDOF- and SDOFs dynamic behaviour have most of the same basic principles.

One of the differences is that's there many motions to consider, this involves vectors of displacements, velocities, accelerations and nodal forces that are working together. The structural mass, damping and stiffness can be described by these vectors through the use of a matrix.

The other one is that MDOF system can move in multiple directions and therefore vibrate in multiple deformed shapes [20].

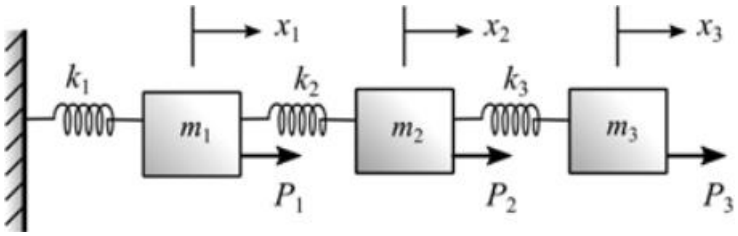

Figure 11 Illustration of a MDOF system [21]

From Figure 11 above is a model a system, here with three degrees of freedom. The setup of the model is similar, and the method is still the same. The system now has three masses and three springs.

The forces can be described with the same method as earlier but it's necessary to divide the three masses. Relations of the displacement-force can be written in the form:

$$x_1 x_2 = P_{11} P_{12} P_{13} P_{21} P_{22} P_{23} \tag{3.4.3.1}$$

With the drawing of a free body diagram of each mass with the relevant forces on it and the use of Newton's second law, the equations will be.

$$P_1 + c_2(\dot{x}_2 - \dot{x}_1) + k_2(x_2 - x_1) - c_1\dot{x}_1 - k_1 x_1 = m_1\ddot{x}_1 \tag{3.4.3.2}$$

$$P_2 - c_2(\dot{x}_2 - \dot{x}_1) - k_2(x_2 - x_1) = m_2\ddot{x}_2 \tag{3.4.3.3}$$

This can also be arranged into a matrix equation 3.4.3.4.

$$\begin{bmatrix} m_1 & 0 \\ 0 & m_2 \end{bmatrix}\begin{bmatrix} \ddot{x}_1 \\ \ddot{x}_2 \end{bmatrix} + \begin{bmatrix} c_1 + c_2 & -c_2 \\ -c_2 & c_2 \end{bmatrix}\begin{bmatrix} \dot{x}_1 \\ \dot{x}_2 \end{bmatrix} + \begin{bmatrix} k_1 + k_2 & -k_2 \\ -k_2 & k_2 \end{bmatrix}\begin{bmatrix} x_1 \\ x_2 \end{bmatrix} = \begin{bmatrix} P_1 \\ P_2 \end{bmatrix} \tag{3.4.3.4}$$

The expression can also be written more compactly by denoting the matrices and vectors, where we simplify it to "*m*" as mass matrix, "*k*" as stiffness matrix and "*c*" as damper matrix. The "*f*" is for the load vector and "*x*" is for the displacement vector. This is known as the equation of motion for MDOF systems [20].

$$m\ddot{x} + c\dot{x} + kx = f \tag{3.4.3.5}$$

3.5 Modal analysis

The modal analysis is deciding the inherent dynamic characteristics of a system by placing it into forms of natural frequency, damping factors and mode shapes. This is used to create a mathematical model to understand the dynamic behaviour.

By converting the problem from MDOF into a system with new coordinates, the mass matrix and the stiffness matrix will decouple. This procedure will make it simpler to look at and solve MDOF system. By dividing the MDOF system into many SDOF systems, which can now be solved separately. The procedure can be used in both undamped and proportionally damped systems [21].

There are several types of modal analysis such as Analytical Modal Analysis (AMA), which is modal analysis based on simulation and then there are Experimental Modal analysis which is either Classical Modal analysis (CMA) or Operational Modal Analysis (OMA) [22].

Looking at the spatial model and the modal model, it's the orthogonality properties of the system that holds them together. Considering an undamped MDOF system and creating an equation of the "r_{th}" and "s_{th}" modes [23].

$$([K] - \omega_r^2[M])\{\varphi\}_r = \{0\} \tag{3.5.1}$$

$$([K] - \omega_s^2[M])\{\varphi\}_s = \{0\} \tag{3.5.2}$$

Further the "r_{th}" equation gets multiplied with $\{\varphi\}_s^T$, the "s_{th}" equation multiplied with $\{\varphi\}_r^T$, and solve out the parentheses.

$$\{\varphi\}_r^T[K]\{\varphi\}_s = \{\varphi\}_r^T\omega_s^2[M]\{\varphi\}_s \tag{3.5.3}$$

$$\{\varphi\}_s^T[K]\{\varphi\}_r = \{\varphi\}_r^T\omega_r^2[M]\{\varphi\}_r \tag{3.5.4}$$

Subtracting the (4.4.6.4) gives.

$$(\omega_s^2 - \omega_r^2)\{\varphi\}_r^T[M]\{\varphi\}_s = 0 \tag{3.5.5}$$

The two possible solutions are that the two angular natural frequency is the same or not, in this case it was already assumed that $\omega_s^2 \neq \omega_r^2$ [23].

$$\{\varphi\}_r^T[M]\{\varphi\}_s = 0 \tag{3.5.6}$$

Taking the (4.4.6.6) and substituting it into (4.4.6.4) with *r≠s*.

$$\{\varphi\}_r^T[K]\{\varphi\}_s = 0 \tag{3.5.7}$$

Because of the two equations above the mode shapes must be orthogonal to each other with consideration on the K and M matrices.

$$\{\varphi\}_r^T[M]\{\varphi\}_r = m_r \tag{3.5.8}$$

$$\{\varphi\}_r^T[K]\{\varphi\}_r = k_r \tag{3.5.9}$$

And then the natural frequency will be.

$$\omega_r = \sqrt{\frac{k_r}{m_r}} \tag{3.5.10}$$

Orthogonality of the system is about how orthogonal the distinct natural frequency is to each other's with respect to the mass of the system and stiffness of the matrix. Shown in matrix form under.

$$[\varphi]^T[M][\varphi] = [\cdot m_i.] = \begin{bmatrix} m_1 & \cdots & 0 \\ \cdots & \cdots & \cdots \\ 0 & \cdots & m_n \end{bmatrix} \tag{3.5.11}$$

$$[\varphi]_T[K][\varphi] = [\cdot m_i.] = \begin{bmatrix} k_1 & \cdots & 0 \\ \cdots & \cdots & \cdots \\ 0 & \cdots & k_n \end{bmatrix} \tag{3.5.12}$$

$$[\cdot \omega_r^2.] = [\cdot k_i.][\cdot m_i.]^{-1} \tag{3.5.13}$$

Where the "*k*" and "*m*" stand for the modal matrix for the stiffness and the mass. Further the orthogonal modal properties can be used by going from a general coordinate system to a modal coordinate system [23].

$$x = \{\varphi\}q \tag{3.5.14}$$

$$\ddot{x} = \{\varphi\}\ddot{q} \tag{3.5.15}$$

Then we use the equation of motion for a multi degree of freedom system together with these two equations and multiply inn $\{\varphi\}^T$.

$$\{\varphi\}^T[M]\{\varphi\}\{\ddot{q}\} + \{\varphi\}^T[K]\{\varphi\}\{q\} = \{0\} \tag{3.5.16}$$

The orthogonal properties to the modal forms are then used to divide the system into multiple independent equations with only one degree of freedom. Here with mode "*r*".

$$m_r\{\ddot{q}\} + k_r q = 0 \tag{3.5.17}$$

The system with multi degree of freedom is now divided into multiple one degree of freedom systems. To find the complete solution of the equation of motion, all the independent linear systems are added together [23].

$$\{X(t)\} = \varphi_1 q_1(t) + \varphi_2 q_2(t) + \varphi_3 q_3(t) + \varphi_n q_n(t) = [\varphi]q(t) \tag{3.5.18}$$

3.5.1 Analytical Modal Analysis

Analytical Modal Analysis is a simulation based modal analysis, where the modal parameters are obtained through finite element models [24] [22].

The finite element method is often used to perform an analytical modal analysis, but it always occurs some errors when making the FEM model of the real structure. This is not only due to the simplifying of the real structure, but it may also be because if the uncertainties from the geometrical and material properties. This is why an experimental modal analysis is often used to calibrate the finite element model, which then can be used as a real representative of the structure [25].

3.5.2 Classical Modal Analysis

In Classical Modal Analysis (CMA), the measurements are usually performed by impact hammer or by modal shakers. Where the impact is known and the results are measured usually by either triaxial or uniaxial accelerometers, so CMA is a known input and output Analysis [22].

The Hammer test is a modal analysis test where you use a hammer as the excitation device. This is one of the more popular excitation devices in recent years. This device is more efficient to use than a shaker device and doesn't add any masses to the bridge. The test structure is hit by the hammer to excite a broad range of frequencies. The impulse response from the hammer to the structure contains excitations at each of the system's natural frequencies [26].

3.5.3 Operational Modal Analysis

Operational Modal Analysis or OMA is an analysis that gives an understanding of a structure's dynamic behaviour and/or its inherent dynamic properties. This will improve the safety, performance, and reliability, etc. the analysis is performed by solving a numerical model which is based on the structure, it is solved either by physical measurements or by computer simulations [22].

The results will be several modes which are described by their modal parameters such as natural frequency, modal damping, and mode shapes, etc. [22].

Measurements are usually done by implementing an impact hammer or modal shaker as input force. But since OMA is an output-only analysis, it does not matter what input force is used, since it is the resulting measurements that are the focus. The vibrations are usually measured by triaxial or uniaxial accelerometers.

OMA has several advantages, such as testing with true boundary conditions, actual environmental conditions, vibrations levels and frequency range, etc. In addition to making, it possible to test structures that may be difficult to excite input force upon, since OMA can be used with only accelerometers, it will make the setup simpler and faster [22].

OMA originated from Civil Engineering applications such as natural input modal analysis or ambient modal analysis for buildings, wind turbines, dams, bridges, etc. but today OMA is also used in Mechanical engineering [22].

3.5.4 Modal Assurance Criterion

The modal assurance criterion is used for statistical indicate differences in mode shapes. It is sensitive to large differences and insensitive to small differences. When having mode shapes from analytical model and mode shapes obtained experimentally, MAC can be used to pair them. The MAC value is bounded between 0 and 1, where 1 is the fully consistent mode shape [27].

3.5.5 Modal complexity factor

Modal Complexity Factor (MCF) is a factor that indicates if the mode shapes have high or low complexity. With the scale bounded between 0 and 1. 0 indicates a real-value mode shape, and the higher the factor number is, the higher the complexity is [28]. The MCF can be divided in MCF 1 and MCF 2, where MCF 1 is defined from the phase. Which mean to consider any two consecutive elements from the eigenvector and then make these two 90 degrees apart in phase. MCF 2 is amplitude-weighted, this factor relies on both the phase angle and the moduli of the model shape elements [29]. An example of a MCF plot is shown in Figure 12. Here all the nodes and their magnitude (radial length) and phase (degree) are plotted. A low MCF value will appear as a straight line as the movements will be 180 degrees apart in phase.

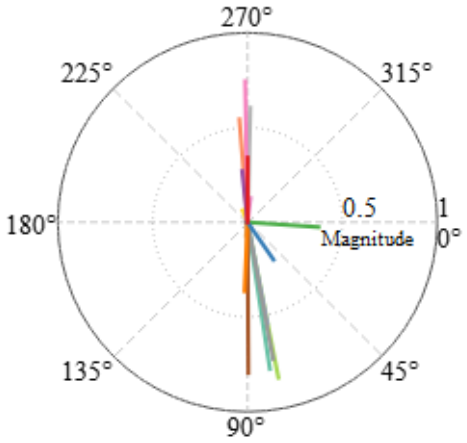

Figure 12 Example of MCF plot, radial value = magnitude, degrees = phase

$$MCF_r = 1 - \frac{(S_{xx}-S_{yy})^2+4S_{xy}^2}{(S_{xx}+S_{yy})^2} \quad (3.5.5.1)$$

$$S_{xx} = Re\{\Psi_r\}^T Re\{\Psi_r\} \quad (3.5.5.2)$$

$$S_{yy} = Im\{\Psi_r\}^T Re\{\Psi_r\} \quad (3.5.5.3)$$

$$S_{xy} = Re\{\Psi_r\}^T Im\{\Psi_r\} \quad (3.5.5.4)$$

3.5.6 Fast Fourier Transformation

Fast Fourier transformation refers to a group of algorithms when calculating the Fourier transformation of a signal. The Fourier transformation is about converting a signal that is a function of time into a function of angular frequency. FFT is often used synonymous with Fourier transformation [30].

The signal can be expressed as sum of multiple sine functions with different frequencies, amplitudes and phases. The amplitude and the phase are described as a function of frequency with the use of Fourier transformation [30].

If the time function is periodic, the signal can be put together of a series of sine functions with frequencies that are multiples of the frequency with which the period repeats. The Fourier transformation then only have value for discrete frequencies, so it becomes discrete. If the time function is finite in time, it will have the same effect as the time functions is periodic [30].

An instrument called spectral analyser is used when performing a Fourier transformation. The instrument will always use FFT-algorithm because they are more efficient than other algorithms [30].

The FFT is the decomposed discrete Fourier transformation equation, put into number of short transforms, and then recombined. Here $e^{-\frac{i2\pi}{N}}$ is a primitive Nth root of 1.

$$X_k = \sum_{N=0}^{N-1} x_n \, e^{-\frac{i2\pi kn}{N}} \quad k = 0, \dots, N-1, \quad (3.5.6.1)$$

3.5.7 Frequency domain decomposition

Frequency domain decomposition (FDD) is one of the more popular output-only system identification techniques, especially in structural health monitoring. It is a technique for modal analysis using the frequency response given output data to generate a system realization [31].

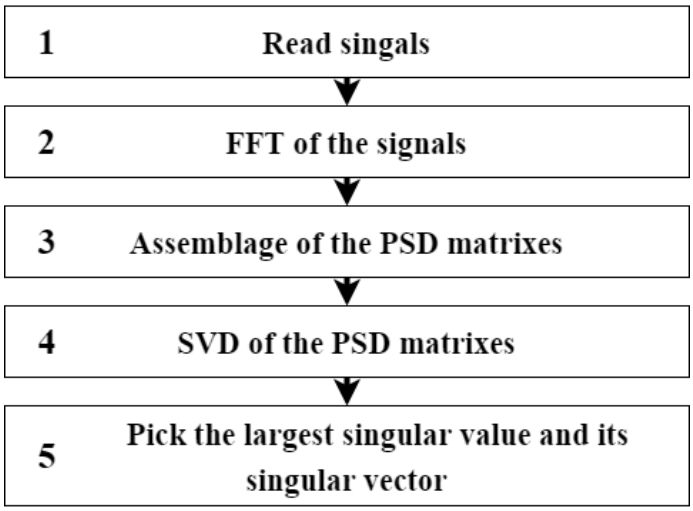

Figure 13 Frequency domain decomposition (FDD) flowchart

The FDD takes the Singular Value Decomposition (SVD) of the Power Spectral Density (PSD) matrix, this is also known as a periodogram or "Welsh's" spectrum. The SVD is created from the measurements made in the operational modal analysis test. By plotting the SVD components for each frequency line, one can identify the natural frequency. This can be done even when the modes are closely spaced. By selecting the peaks from the plotted lines given by the singular values [32].

3.6 Finite element method (FEM)

Setting up and solving partial differentials and integrals are often done by using a method called finite element method. This method is used in engineering to break down whole systems into smaller pieces or elements, where the solution is known or easier to find. This is done because the behaviour of the system can't be predicted with closed-form equations [33].

To use this method, it's necessary to define the geometry into several points that are called nodes, which each consists of a set of degrees of freedom. This DOF can be displacement, temperature, etc. and the inputs to the system will decide what these sets are based on [33].

Some of the elements have a closed-form solution that is known, like beams. Other elements, like continuum elements, need a numerical integration over the element to estimate the interaction among the degrees of freedom [33].

The model is a combination of all the individual elements, which creates a set of equations that expresses the system that can be analysed. Useful information about how the system moves can then be given by solving these equations [33]

The more elements there are, the better the expression of the system gets. When the number of elements reaches infinite, the expression will become perfect. But since it isn't possible to divide the system into an infinite number, the method will produce the exact solution to an estimate, to get as close to the answer to the problem as possible.

This can be hard to do by hand when the number of elements gets excessive, and the number of equations to solve gets higher. Therefore, the finite element method is often associated with computer programs. The program will set up and solve large sets of equations and can also help with visualization [33].

3.6.1 Element type

When selecting the element type, it is the nodal/element DOF which are chosen and that is the reason for element type has to be selected when applying the finite element method. There are many different types of elements which can be used, e.g line elements such as truss, beam, and frame etc., which has 2 nodes, one in each end of the line. Another element type is surface elements which are 4-noded quadri-lateral, 8-noded quadri-lateral and 3-noded irregular etc., which as mentioned in the names have 4, 8 and 3 nodes. Then there is solid, where there are 8-noded hexagonal form (brick), 6-noded pentagonal form (wedge) and 4-noded tetrahedron form (tet). And then there are special purpose, and are Gap, Rigid and Hook [34].

3.6.2 Mesh size

When analysing an object, it has to be meshed and what that does is dividing the object into smaller arbitrary number of regions, in such a way the whole object is covered. The small regions are called finite elements and must be connected in their corner points. The finite elements corner points are called nodes. so meshing divides an object into elements and nodes, which is necessary to achieve an accurate result, when applying the finite element method [35] [36]. A mesh is fine if the mesh size is small and is coarse if the mesh size big. This is why mesh size is important, because the finer the mesh is the more accurate the results become. But it will take more time to calculate the equations and it may not be necessary to have the whole object fine meshed. If the object has known weak spots, the object can have a coarser mesh size and the specific areas around the weak spots can be meshed with a finer mesh size [37].

3.6.3 Convergence

Mesh Convergence is about how many finite elements the Finite element model or object must have to ensure that the result from the analysis is not affected by eventual changes in mesh size. By performing the mesh convergence any additional refinement of the mesh will not affect the results from the analysis, and this makes the finite element model and the results it produces mesh independent. This means that the system response (deformation, stress, etc.) to the finite element model will converge to a repeatable solution, which poofs that the results are accurate, and any additional refinement of the mesh is unnecessary [38].

3.7 Measuring hardware

Measuring relevant data under static and dynamic loading conditions can be done by equipping an object with a number of different sensors. The best suited sensors are dependent on the load case and desired measurements.

The equipment for data acquisition and postprocessing hardware has changed and improved rapidly over the past decades. To do a vibration test requires multiple hardware components. The basic equipment's you need to perform a test is and excitation device, accelerometers, data acquisition, recording device and some sort of postprocessing software. Below in Figure 14 is an illustration of the basic equipment's [26].

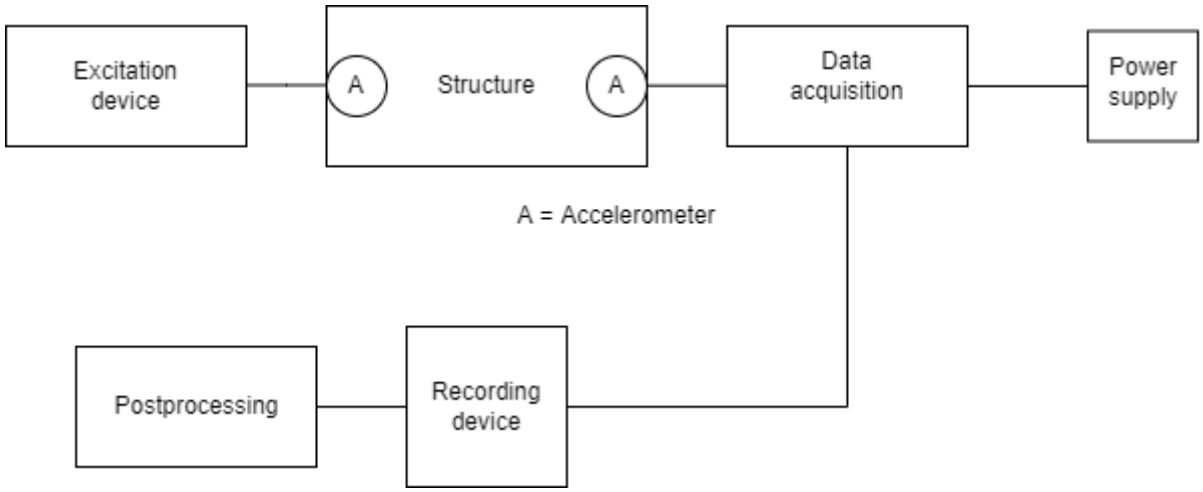

Figure 14 Hardware devices used to perform a vibration test

3.7.1 Accelerometers

Accelerometer sensors are used to measure the acceleration of an object. These sensors are used for both vibration measurements and tracking of larger movements. Vibrations are often monitored in machinery in industrial plants, turbines, etc. These machines and structures are vulnerable to some frequencies generated by the operation. In some cases, it can be critical to avoid resonant frequency ranges and other damaging ranges. These ranges can create fatigue cracks or lead to other mechanical failure modes. [39]

By measuring the forces (F) applied to a small mass (m), can the sensor determine the acceleration (a) by solving Newton's second law of motion. The force applied is calculated by reading the displacement (x(t)) of a small spring connected to the mass (m). [39]

$$F = m \times a \tag{3.7.1.1}$$

$$F = k \times x(t) \tag{3.7.1.2}$$

$$a = \frac{k \times x(t)}{m} \tag{3.7.1.3}$$

By finding the acceleration of the sensor, the velocity (v) and change in position (x) can be calculated by the following formulas.

$$\int a\, dt = \Delta v + C_1 \tag{3.7.1.4}$$

$$\int v\, dt = \Delta x + C_2 \tag{3.7.1.5}$$

By using this method in three axes can in theory the exact change in position be found, assuming the starting velocity (C_1) and position (C_2) is zero. The three-dimensional equation will be:

$$\iint a_x\, d^2t + \iint a_y\, d^2t + \iint a_z\, d^2t = \Delta x + \Delta y + \Delta z \qquad (3.7.1.6)$$

However, the process is quadratically sensitive to inaccuracies in the acceleration measurements. Thus, the rate of growth in error will lead to inaccuracies beyond acceptable within 10 to 20 seconds. This makes position tracking by double integration only viable in combination with other methods. This method is used in some subsea navigation methods for drones and submarines in combination with long- and ultrashort baseline systems [40].

Rotational acceleration of the system can be detected using two spaced out accelerometers. By comparing data from the two sensors, the variation in acceleration can be interpreted as rotation. The angle of the sensor can also be found by measuring the direction of the gravitational pull on the mass at rest.

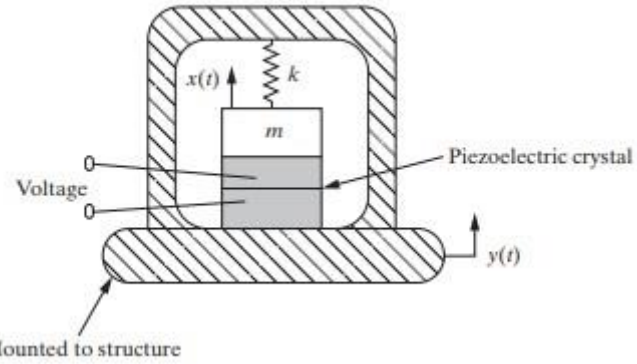

Figure 15 Illustration of a piezoelectric accelerometer, Taken from chapter 2.6 of Engineerig Vabration book [26]

Above in Figure 15 is an illustration of a piezoelectric accelerometer. Piezoelectric accelerometers use the piezoelectric effect of a material to measure the dynamic changes in the mechanical variables. It gets an electric signal in response to a quantity, property, or condition by converting one form of energy to another, which then can be measured. They have a wide frequency response and high sensitivity, which makes them good for vibration testing [41].

While piezoresistive accelerometers use the piezoresistive effect, that is the ability of a material's resistivity to change when a mechanical force occurs. The accelerometers measure high frequency in short durations but have low sensitivity [41].

4 Research question

How to monitor the structural health condition of a steel bridge based on vibration measurements?

Subquestions

- How to instrument sensors on a truss bridge to obtain the structural dynamics properties?
- How will applying damage to the truss bridge affect the dynamic properties?
- How can damage be discovered using sensor data?
- *What are the discrepancies between different methods, i.e., AMA, CMA, and OMA, in the modal analysis results?*

4.1 Limitations

- In this study it will only be focused on modal analysis as method, i.e., AMA, CMA, and OMA.
- Only accelerometers are used as the experiments focus on measuring dynamic cases.
- A true 1:1 digital model (digital twin) is time consuming and difficult to make, that is why the group has chosen to make a simplified numerical model.
- In this study the group will only focus on the first six steps described in the structural health monitoring process (see Figure 2). The group will not include any damage localization methods.
- In this thesis the group will be focusing on the global modes in the modal analyses.

5 Case and Materials

This study will use a simple truss bridge with a two-meter span as its subject. The truss bridge was designed by Dr. Zhen Sun of the University of Porto for this study. The design of the bridge is commonly found in short road and railway bridges. The truss bridge will be represented as a physical model with a corresponding numerical model. The numerical model is made using ANSYS Mechanical APDL.

5.1 Model bridge

The model bridge used in the dynamic tests is a single span truss bridge as shown in Figure 16.

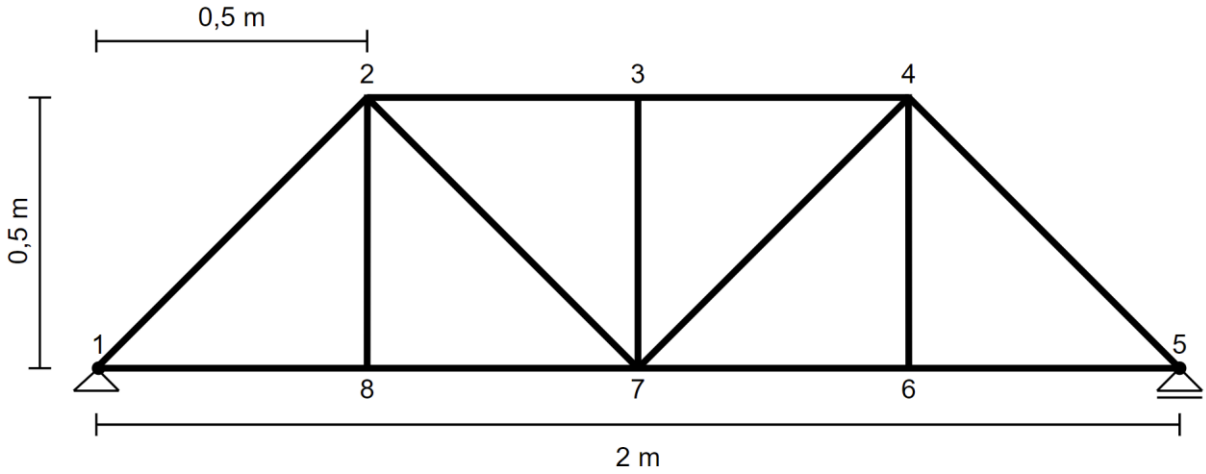

Figure 16 Sketch of the model bridge.

The truss members used in the model bridge were steel L-profiles. The L-profile elements are 20 mm x 20 mm with a 2 mm thickness (see Figure 17). The Young's Modulus for the steel used is 210 GPa. The Poisson's ratio for the steel is 0.3.

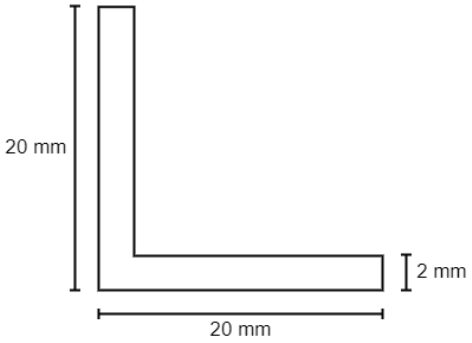

Figure 17 L-profile cross section dimensions

The bridge has a span of 2 meters, is 0.5 meters tall and 0.5 meters wide. The two vertical truss planes are connected in each node. There are no diagonal trusses in the horizontal plane. In each node, the truss members are held together with steel brackets, acting as gusset plates. The brackets secure each beam with 2 bolts to achieve virtually 0 DOF for the truss elements in the nodes, as is common in real truss bridges. The bolts used were each tightened to the recommended 11 Nm according to the mechanical handbook. [42]

The bridge mounts are pinned connections made by connecting 2 plates on the test bench to a plate on the underside of the model bridge as shown in Figure 18. To create a static indetermined system, the holes in the connection plates are widened to allow for horizontal movement on one side. This is often the case for full size bridges too as they are equipped with expansion joints to allow for expansion and contraction in the materials due to creep etc.

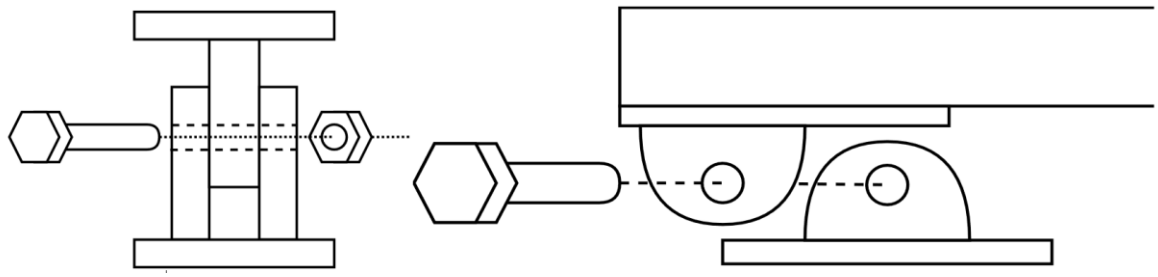

Figure 18 Sketch of mounts used to secure the model bridge to the test bench

5.1.1 Damage case 1

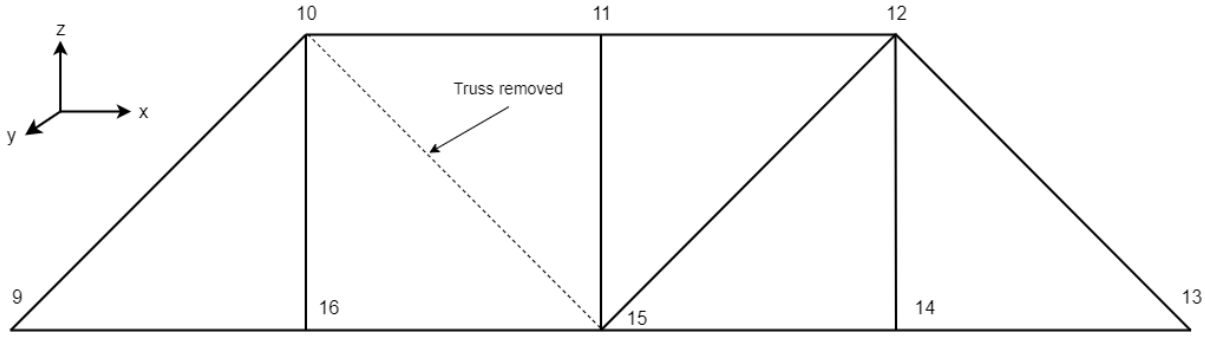

Figure 19 Damage case 1

In the first damage case, the diagonal truss element connecting node 10 and 15 in the second plane is removed (see Figure 19).

5.1.2 Damage case 2

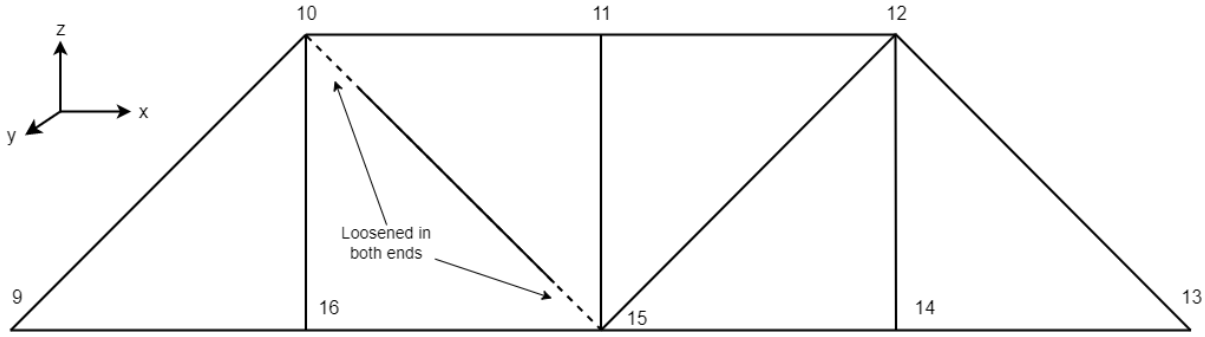

Figure 20 Damage case 2

In the second damage case, the diagonal truss element connecting node 10 and 15 in the second plane are loosened in both nodes. The screws were kept tight enough so the truss element would not move under vibration but could not effectively transfer any forces.

5.2 Numerical modelling of bridge

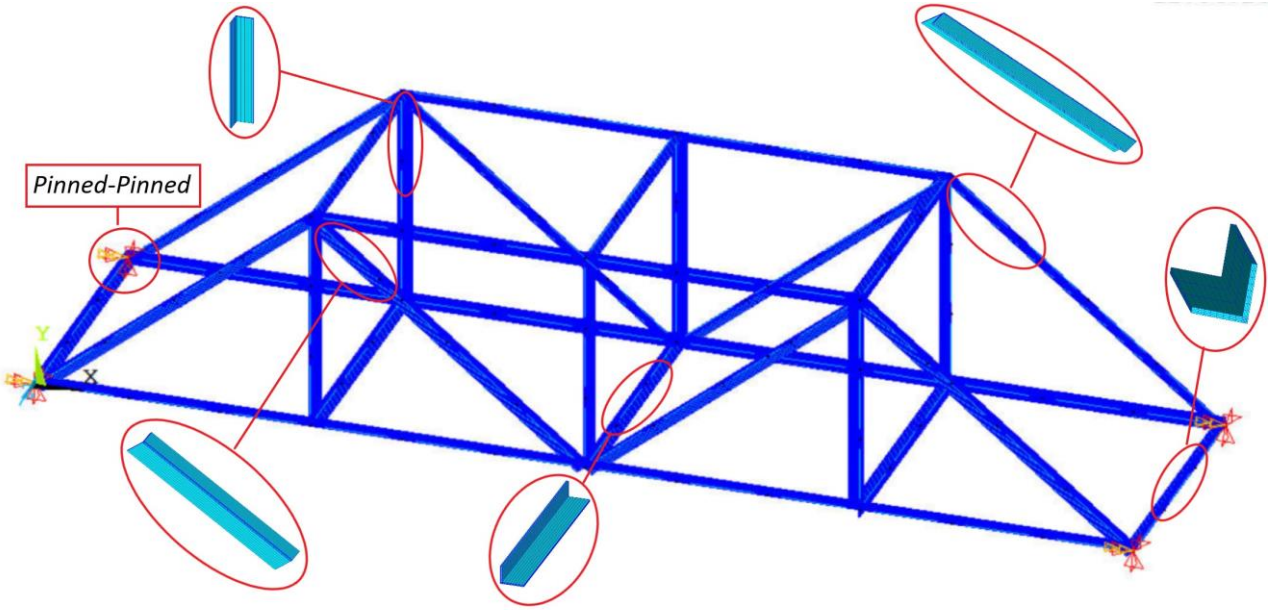

Figure 21 Picture of the Numerical bridge model. The model is 1:1 to physical model, with boundary condition Pinned-Pinned, mesh element edge length 0.01 and cross-section 20x20x2

The numerical FEM model is a digital representation of the physical truss bridge, meaning the cross-section, material properties and dimensions are identical to the physical model. The digital model only deviates in node connections where the physical model uses brackets. The numerical model uses instead the command “glued lines” to connect the lines between the different key points where the brackets would be. The eccentricity caused by connecting the brackets to the edge of the truss cross-section is deemed negligible by a sensitivity study (see study under the method chapter 7.7.5).

5.3 Tests conducted

Table 1 Overview and detailed information about the tests conducted

Test	Description	Results
TC 1.1 AMA (Undamaged)	Analytical Modal Analysis (AMA) of the numerical bridge model. Method detailed in chapter 6.2 on page 31.	Results are presented in Table 3 under chapter 7.2 on page 41.
TC 1.2 AMA (Damaged)	Analytical Modal Analysis (AMA) of the damaged numerical bridge model. (Damage case 1 detailed in chapter 5.1.1 on page 24). Method detailed in chapter 6.2 on page 31.	Results are presented in Table 4 under chapter 7.2 on page 41.
TC 2.1 Hammer test (Y-direction)	6 strikes with a hammer on each column in the first plane. (Column 2-8, 3-7 and 4-6). Method detailed in chapter 6.3 on page 33.	Results are presented in Figure 31 and Table 5 under chapter 7.2.1 on page 43.
TC 2.2 Hammer test (Z-direction)	6 strikes with a hammer on each beam. (Beam 10-4, 11-3 and 12-2). Method detailed in chapter 6.3 on page 33.	Results are presented in Figure 32 and Table 5 under chapter 7.2.1 on page 43.
TC 3.1 OMA (Undamaged, Y direction)	Random strikes with a small wood element. Method detailed in chapter 6.4 on page 35.	Results are presented in Figure 33, Figure 34 and Table 6 under chapter 7.2.2 on page 44.
TC 3.2 OMA (Undamaged, Z direction)	Random strikes with a small wood element. Method detailed in chapter 6.4 on page 35.	Results are presented in Figure 39, Figure 40 and Table 9 under chapter 7.2.2 on page 44.
TC 3.3 OMA (Damage case 1, Y-direction)	Random strikes with a small wood element. (Damage case 1 detailed in chapter 5.1.1 on page 24). Method detailed in chapter 6.4 on page 35.	Results are presented in Figure 35, Figure 36 and Table 7 under chapter 7.2.2 on page 44.
TC 3.4 OMA (Damage case 1, Z-direction)	Random strikes with a small wood element. (Damage case 1 detailed in chapter 5.1.1 on page 24). Method detailed in chapter 6.4 on page 35.	Results are presented in Figure 41, Figure and Table 10 under chapter 7.2.2 on page 44.

TC 3.5 OMA (Damage case 2, Y-direction)	Random strikes with a small wood element. (Damage case 2 detailed in chapter 5.1.2 on page 24). Method detailed in chapter 6.4 on page 35.	Results are presented in Figure, Figure and Table 8 under chapter 7.2.2 on page 44.
TC 3.6 OMA (Damage case 2, Z-direction)	Random strikes with a small wood element. (Damage case 2 detailed in chapter 5.1.2 on page 24). Method detailed in chapter 6.4 on page 35.	Results are presented in Figure 43, Figure 44 and Table 11 under chapter 7.2.2 on page 44.
TC 4.1 Damping ratio test	Soft strike on the center column (3-7) with bottom of hand. Isolates first lateral bending mode for damping calculations. Method for calculation is shown in chapter 6.6 on page 38.	Results are presented in Figure 58 in chapter 7.6 on page 60.

5.4 Test setup

5.4.1 Test instruments

A range of sensors and datalogging equipment was used to record and log data from the tests conducted on the physical model. This equipment was borrowed from the mechatronics lab or purchased in connection with this experiment.

5.4.1.1 Sensors

The truss bridge was equipped with accelerometers in key locations to measure the dynamic frequency response.

In the CMA we used three Endevco 713-2k-240 triaxial piezoresistive accelerometer along with three Endevco uniaxial accelerometers. They weigh 7.5 grams, have a scale of 2000 g and max frequency of 1500 Hz. These are shock sensors and have a sensitivity of 0.030 mV/ms^2 which is very low [43].

In the OMA we used four piezoelectric deltashear accelerometer type 8344 from Brüel and Kjær. These are high sensitivity sensors with a sensitivity of 250 mV/ms^2. With a weight of 157 grams and a frequency range of 0.2-3000 Hz. For these sensors, we used a multi-purpose 4-channel input module type 3050 from Brüel and Kjær as data acquisition device [44].

5.4.1.2 Datalogging

The computer used for datalogging in the CMA is a custom built DEWESoft® Sirius Modular computer. The configuration had two SIRIUS Waterproof Rugged IP67 Data Acquisition System modules for sensor inputs and one SBOX Waterproof Rugged IP67 Data Processing Computer for datalogging. The processing computer was running Windows 10 with DEWESoft's own datalogging software (DEWESoftX). The hardware configuration had two rows of DB9 connectors allowing for 16 total sensors [45].

5.5 Software

5.5.1 Ansys Mechanical APDL

Ansys is a program for modelling and analysis, that uses the finite element method.

There are two different ways of using the program. The first is the GUI which stands for "Graphic User Interface" and is the manual interface that comes up when starting the program. The second is the script/Syntax language which is APDL (Ansys parametric design language), which can be used for making a script that consists of several commands and when the script has been run then the program will automatically model and perform analyses. [46]

5.5.2 MATLAB

Matlab is a script/programmer software, which can be used as simple as a calculator or as advanced as running large, advanced scripts which solve complex analysis.

In this project, Matlab will mainly be used to process the raw data from the accelerometers to get the frequency domain signal and then plot the result in a graph and compare it to the result from AMA FEM.

5.5.3 BK Connect

BK Connect is a software to use for recording of measurements. In the software one can create a 3D model of the structure and set up a pre-plan for all the sensors and recordings. The program has innovative features and functions which help reduce the risk of errors happening. [47]

5.5.4 PULSE OMA

PULSE OMA is an abbreviation, which stands for PULSE Operational Modal Analysis and is a post-processing tool. That performs modal analysis of a structure or object with the measured time data output of said object or structure. Some of the fields of usage are testing Civil Engineering structures such as offshore structures, wind loads on buildings etc. it can also be used on large Mechanical structures such as ships and submarines which are hard to excite antically.

In this project, PULSE OMA will be used to postprocess the recorded accelerometer data from BK Connect [28].

PULSE OMA uses 2 different identification techniques for identifying modes in an operational modal analysis, the first is Frequency Domain technique, which is a peak-picking technique based on using SVD curves (Singular Value Decomposition curves) to pick modes. This is done by using FDD (Frequency Domain Decomposition) in different forms such as enhanced and curved-fit FDD. Because the input force is unknown and the decomposition that PULSE OMA uses, there will entail a risk of overestimating the modal damping.

The second identification technique PULSE OMA uses are Time Domain Technique which is a Stochastic Subspace Identification technique (SSI), which is based on Discrete-time stochastic space Models, which is given by [22].

1. The State Equation, which is the Model of the dynamic of the system

$$X_{t+1} = Ax_t + w_t \tag{5.5.4.1}$$

2. And Observation (output) equation, which is the Model of the output of the system

$$y_t = Cx_t + v_t \tag{5.5.4.2}$$

Where "w_t" is process noise, "v_t" is Measurement noise and Model order is the Dimension of "A" [22].

6 Method

In this chapter, we describe our methods for data gathering, software, building of models, physical testing, and the analysis and processing of our results. The thesis is a quantitative methodology where we gathered test results from lab testing and computer programs.

6.1 Literature review

To start the thesis, a literature study was carried out to find relevant sources and widen our knowledge of the main topics of the research question. The main topics, which was looked into were truss bridges, digital twins, dynamics and measuring instruments. We also had useful sources from a report about Digital Twin and Structural health monitoring from a pre-project, two of the authors wrote the third semester.

All three of the authors had a class in dynamics and therefore used information from the lecture books "Mechanical Vibration" and "Structural Dynamics" in addition to relevant knowledge gathered through searches.

To get more knowledge about the software, we used MathWorks for MATLAB and the book "Mechanical APDL for Finite Element Analysis" for ANSYS.

Search method

- Define the topics relevant to our research question.
- Choose good databases to use for the research
- Choose keywords and different synonyms
- Start the research

In this thesis we mainly used Google Scholar and Google as database for our research, but also through Science Direct, Research gate and Elsevier. In Google Scholar the group used the advanced search function as a specifying method, where we chose out the age, language, and author. For dynamics and truss bridges we looked at articles from the last ten years, while SHM we wanted newer information, so we looked at articles from the last five years. The search was done in English to get a wider span of articles. There were also used boolean-operations like "OR", "AND" and "NOT".

6.2 Analytical modal analysis (AMA)

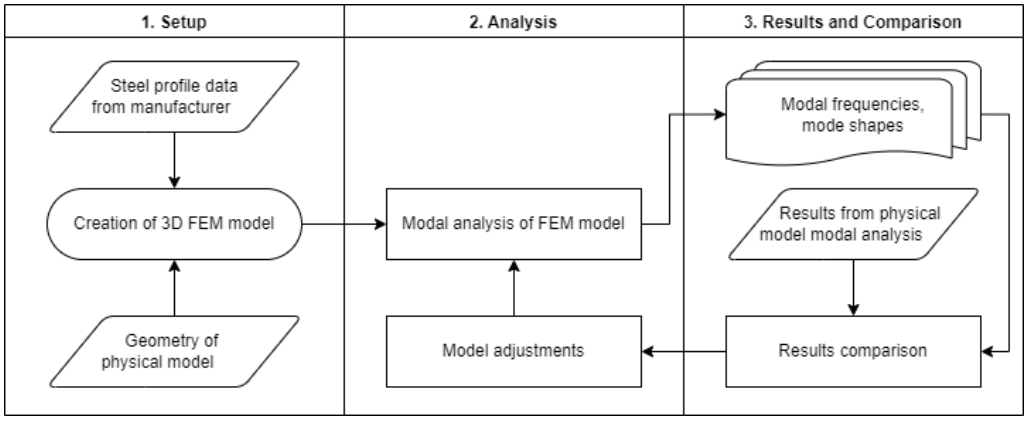

Figure 22 Analytical modal analysis flow chart

The analytical modal analysis (AMA) will serve as the reference for the results from the modal analyses on the physical model. Comparing the frequencies from the AMA to the results from the modal analyses on the physical counterpart can help identify the modal frequencies and their corresponding mode shapes.

1. Setup

The AMA is done in ANSYS Mechanical APDL. The modelling and analysis are done using the APDL (Ansys parametric design language) script approach in ANSYS using Notepad++. This way changes to the model can easily be made by changing parameters in the script.

The mechanical properties for the material, shown in Table 2, are given by the steel manufacturer and are entered into ANSYS.

Table 2 Material properties from manufacturer

Mechanical property	Value
Young's modulus (E)	210 GPa
Possion's ratio	0.3
Material density	7850 kg/m³

A custom L-profile matching the physical counterpart is created in ANSYS. The dimensions used are 20 mm x 20 mm with a 2 mm thickness as seen in Figure 17. After the profile and mechanical properties are defined, the geometry of the bridge can be made. The ANSYS analytical model is a simplified version of the physical bridge, meaning elements such as the brackets, bolts and nuts in each node are not included in the analytical counterpart. The measurements of the geometry are identical to the physical model detailed in the case chapter 5 under chapter 5.1 Model bridge).

The analytical 3D model was created by defining all the key points by their coordinates, and then connecting them using lines. When all the key points are connected, the lines can be defined by element type and cross-section. The element type used for this analysis is beam 188. This was chosen through a third-party Ansys Mechanical APDL manual [33], by using section 4.6.2 Top-Down Element selection: Process of elimination. All the key point are "glued" as a result of using the "glue lines" command, meaning that the lines connected in the same key point move dependent on each other (not jointed). This is to mimic the effect of the brackets on the physical model.

When the lines are defined the model can be meshed. Meshing the model applies the element type and cross section to the lines. The necessary mesh resolution or mesh element edge length (MEEL) was

determined by a sensitivity study (chapter 6.7.2 Mesh Element Edge Length). This sensitivity study showed that 0.01 was sufficient and little to no further benefit could be gained by using finer mesh. Before running the analysis, the boundary conditions must be applied. A sensitivity study was conducted to find the most comparable boundary conditions to the results from the physical modal analyses (see chapter 6.7.3 and 6.7.4). The pinned-pinned boundary conditions proved to be the closest to the physical model and are thus used in all the analyses done using ANSYS.

2. Analysis

When the 3D model is complete, the modal analysis can be run. By inputting the start and end frequencies as 0 in the analysis and modes to 42, the analysis will find the first 42 modes regardless of frequency. The 42 first mode covers the 0-260 Hz range used in the physical modal analyses.

3. Results and comparison

The ANSYS modal analysis returns the modal frequencies and mode shapes for the specified modes under the “General postproc” tab.

The results from the FEM AMA conducted in ANSYS are then compared to the results of the physical modal analyses. From here adjustments are made to the model to find the most comparable configuration (i.e., boundary conditions, young’s modulus, glued lines etc.).

6.3 Classic Modal Analysis, Hammer test (Control test)

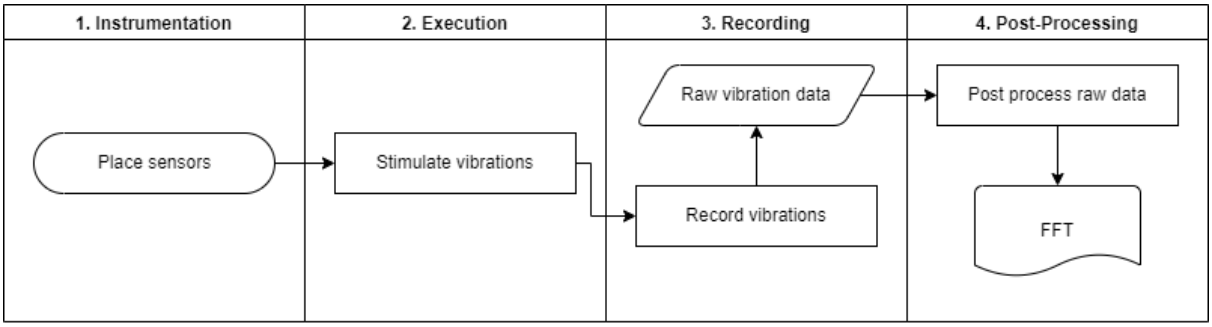

Figure 23 Flowchart of the control test method

The initial classical modal analysis (CMA) tests conducted with the low sensitivity accelerometers and the DEWESoft datalogging and processing system serves as a control for later tests. The main objective of these tests was to extract the modal frequencies for comparison.

1. Instrumentation

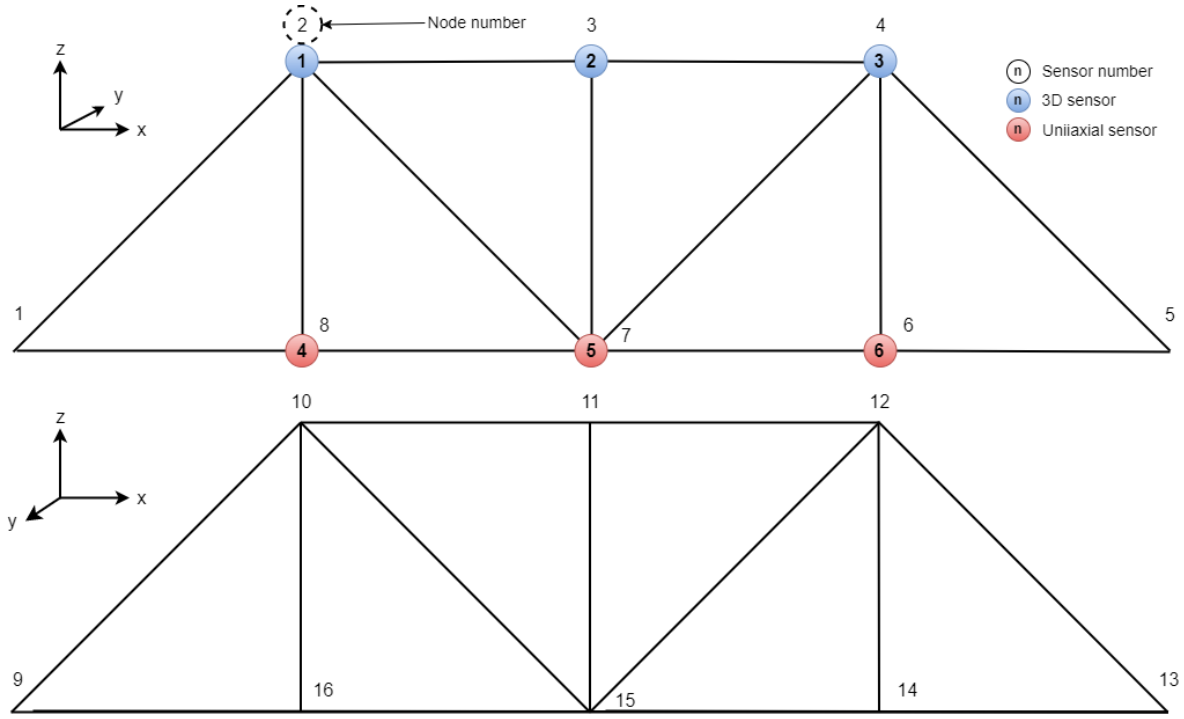

Figure 24 Sensor placements during control tests

The sensor placements for the tests were chosen based on the mode shapes from AMA and experimenting with various locations. It is favourable for the 3D sensors to be located where the model bridge experiences the most complex and varied movements, thus the 3D sensors were placed in the top nodes (node 2, 3 and 4). The uniaxial sensors were placed in the Y direction in the lower nodes. The bridge was only instrumented on one side as it is assumed to be symmetrical. The current placement also covers a more beneficial variance of relevant nodes. A thin and strong double-sided tape was used to mount the sensors to the bridge.

2. Execution

To stimulate vibration in the bridge model, initial displacement was created with a hammer. The impact location and strength were determined early by experimenting. Impact location and strength only affected the clarity of the modes and the unwanted noise, not the frequencies.

All tests were carried out by hitting the middle of the vertical columns and the horizontal beams connecting each side with low to moderate force. This was done to stimulate as many modes as possible. The impact velocity of a typical strike was calculated to be 1.14 m/s (see Figure 25) with some variance as it was done manually. Each beam and column were hit 6 times with 10 seconds in-between to get clear results.

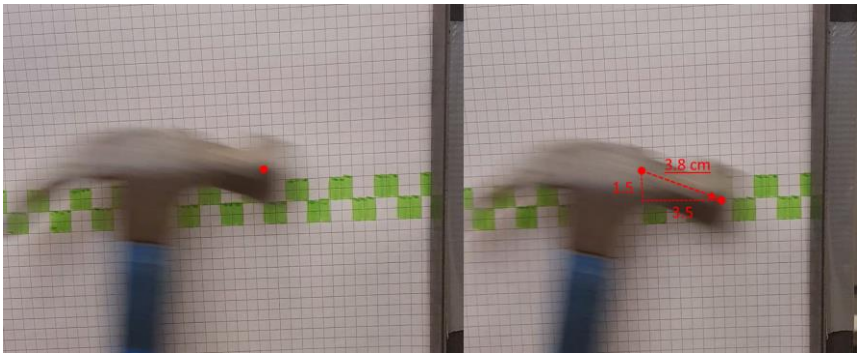

Figure 25 Measurement of impact velocity (distance traveled in 1 frame)

3. Recording

The setup for the recording is done in the DEWESoft X software running on the datalogger computer. Here the sample rate was set to 3125 s/sec and the relevant sensor axes were highlighted.

During the recording, the model bridge's free vibrations are picked up by the accelerometers. The raw sensor data is recorded and stored by the DEWESoft datalogger for post-processing or to be exported. The sensor data is stored individually so that each sensor can be analysed and compared.

4. Post-Processing

The recorded raw senor data was exported from DEWESoft X and analysed using MATLAB. The modal frequencies are acquired by using a FFT (Fast Fourier Transformation). The FFT decomposes the raw vibration data into the separate frequencies that the raw signal consists of. The modal frequencies are identified by the consistency and clarity of the peak values in the FFT. The modal frequencies are compared to the ANSYS results to help identify the corresponding mode and modal shape.

6.4 Operational Modal Analysis (OMA), Main test

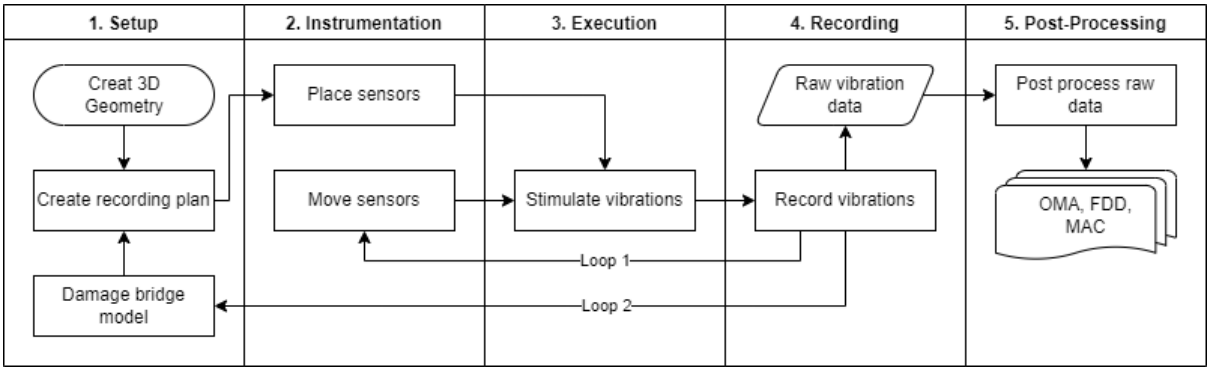

Figure 26 Flowchart of the main test method

The main testing of the bridge was done using a set of 4 high sensitivity piezoelectric deltashear accelerometers. The scope of the test is to extract the modal frequencies and then compare these with the frequencies we extract from the bridge with damage.

1. **Setup**

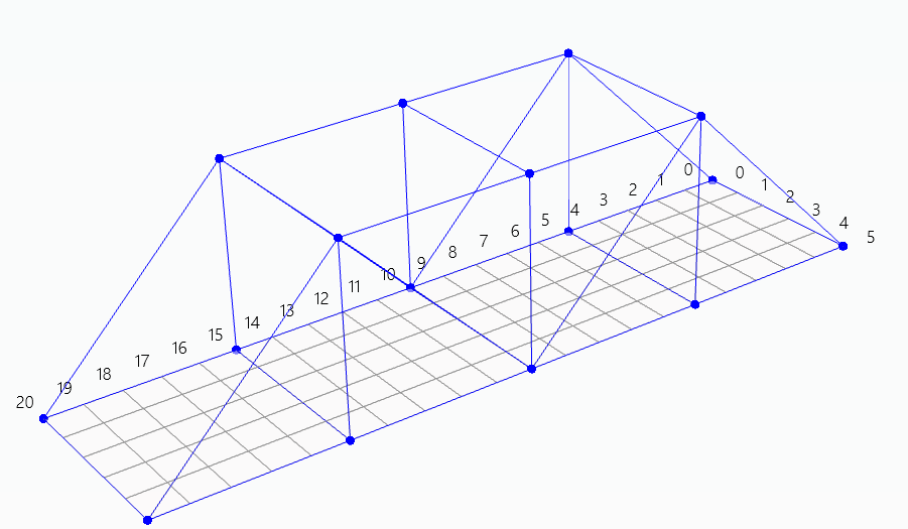

Figure 27 3D model in BK Connect

To be able to use the operational modal analysis (OMA) tool in the post-processing software, a 3D model of the test subject must be created in BK Connect before the testing begins. The 3D model consists of the simple geometry containing the physical model's corresponding nodes (as seen in Figure 27. When the 3D model is complete the recording plan can be created. If the model contains more nodes than available sensors, the vibration test will have to be done in multiple recordings to cover all nodes. These recordings must be pre-planned in the recording software. The recording plan gives the order of the nodes that will be recorded and what sensor will be placed in the specific nodes (see example in Figure 28). This metadata will later be used in the post-processing data to combine the separate recordings.

One sensor will be the designated reference point for all the recordings and will not be moved. The reference sensor should be placed in a node with large amount of movement [44].

2. Instrumentation

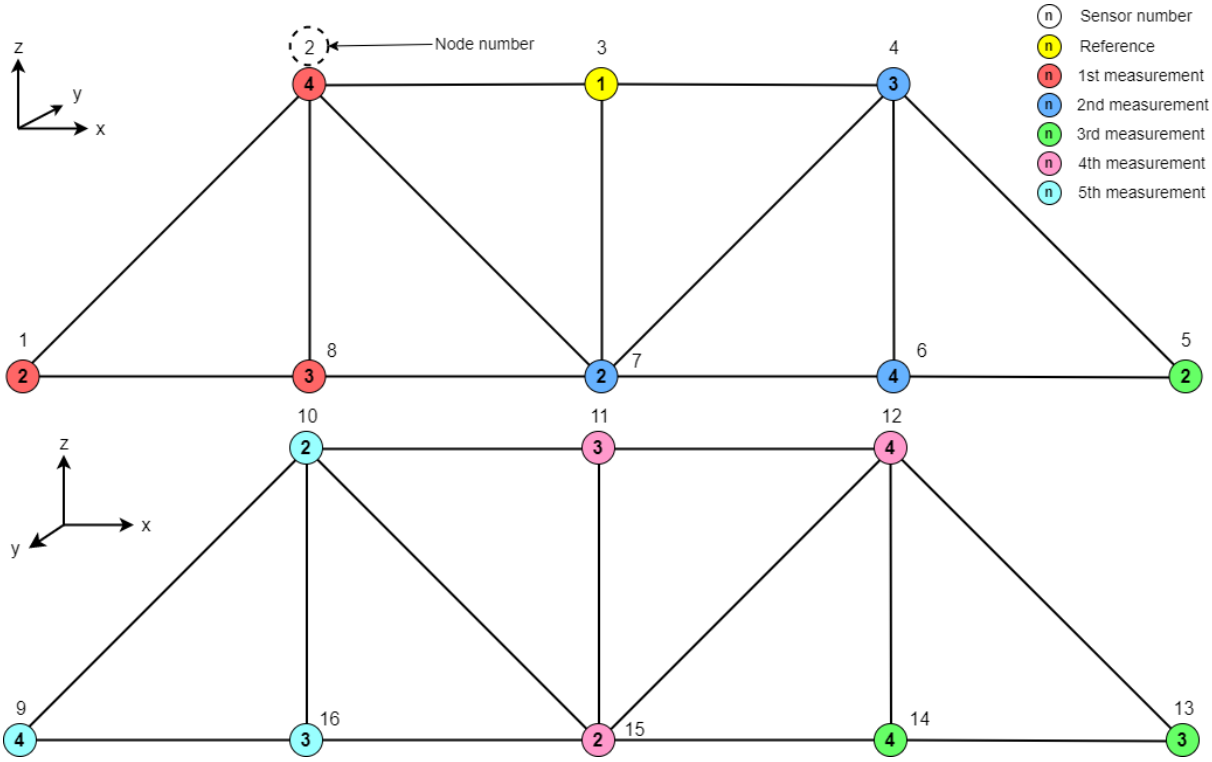

Figure 28 Sensor placement, main test

The sensors are then mounted to the bridge according to the recording plan with the numbered sensors placed in their designated nodes as seen in Figure 28. The reference sensor is fixed in node 3. The sensors are mounted using double-sided tape. It is crucial that the tape used will not affect the results by adding dampening or excess movement to the mounted sensors. It is therefore important to use a thin and strong tape to prevent this.

3. Execution

Stimulating vibrations in the bridge model is done by lightly tapping the bridge with an object. Using softer materials to stimulate vibration will decrease the frequencies range stimulated in the system. As we are looking for modal frequencies in the 0-200 Hz range, we used a small wooden element in this experiment.

It is important to stimulate vibrations at different locations and with different intensities [44]. During the recording period, the bridge model was tapped on every element in random order, multiple times, with varying intensity and direction. This is done to stimulate as many of the potential modes of the model as possible.

4. Recording

While the bridge is being stimulated, a computer is recording the sensor data. The recordings should be proportional in length to the lowest frequency being tested. Given the lowest frequency (f) the minimum recording time is found by [44]:

$$Time = \frac{1}{f} \times 1000 \qquad (6.4.1)$$

Using the lowest frequency from ANSYS of 15 Hz, the recordings should be minimum of 67 seconds long. Given the minimum time and the number of elements that need to be stimulated our recordings were set to 180 seconds. The frequency cut-off of the recording was set to 800 Hz as we are only

looking at the 0-200 Hz range. The recording software automatically adjust the sampling rate of the sensors based on the cut-off.

After the recording was complete the sensors were moved to the next position in the recording plan and the recording process is repeated (Loop 1 in Figure 26). After all the nodes are recorded in the desired directions, simulated damage can be applied to the physical model and the process can be repeated (Loop 2 in Figure 26).

5. **Post-processing**

The raw vibration data and the 3D model are then imported into the post-processing software. The software combines all the recordings using the reference sensor and 3D geometry. After combining the raw data, the FDD (Frequency Domain Decomposition) can be created. This is used together with the MATLAB FFTs to identify all the modal frequencies of the model bridge. By matching the recorded vibrations and their respective frequencies to the 3D model, the mode shapes can be extracted. The movement of the mode shapes are compared to the AMA and mode theory to identify the modes (i.e., one arch is the first bending mode).

Pinpointing the modes in the damage cases was done by comparing the movements of the mode shapes to the undamaged case.

6.5 Damage cases

Applying simulated damage to the model bridge is done by altering the bridge's elements or geometry. By modifying the characteristics, such as the stiffness or weight, the bridge's modal frequencies will be altered.

6.5.1 Damage case 1

The first damage case serves as a control damage test to determine the significance of altering the geometry of the model bridge. By examining the effect on the modal frequencies from this test, further decisions can be made based on the results. Given the negligible change, more significant damage will be applied in the following test cases.

Altering the geometry of the bridge is done by removing the diagonal truss element connecting nodes 10 and 15 (see Figure 19 on page 24). This is a key element in the superstructure and will reduce the stiffness of the bridge.

6.5.2 Damage case 2

The second damage case is a simulated damage scenario. The diagonal truss element connecting nodes 10 and 15 are loosened by untightening the screws in both ends (see Figure 20 on page 24). By doing this the weight is still present but the truss element will not contribute to any significant stiffness in the superstructure. This effect is similar to cases of heavy corrosion, critical cracking, or damage to the gusset plates (see page 5).

6.6 Damping properties

The damping ratio of a mode can be found by looking at the reduction in amplitude from one peak (n) to the next (n+1) as seen in Figure 30. By using the average of multiple peaks, an accurate estimate can be made. MATLAB was used to process the raw vibration data from PULSE OMA and export it to Excel for calculation of the damping ratio. The result from the calculations is presented in chapter 7.6 on page 60.

The damping ratio is given by:

$$\xi = \frac{\delta}{\sqrt{\delta^2+(2\pi)^2}} \tag{6.6.1}$$

Where:

$$\delta = \ln\left(\frac{x_n}{x_{n+1}}\right) \tag{6.6.2}$$

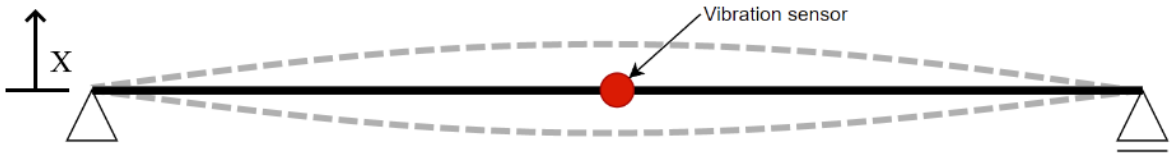

Figure 29 Simply supported beam vibrating, first bending mode

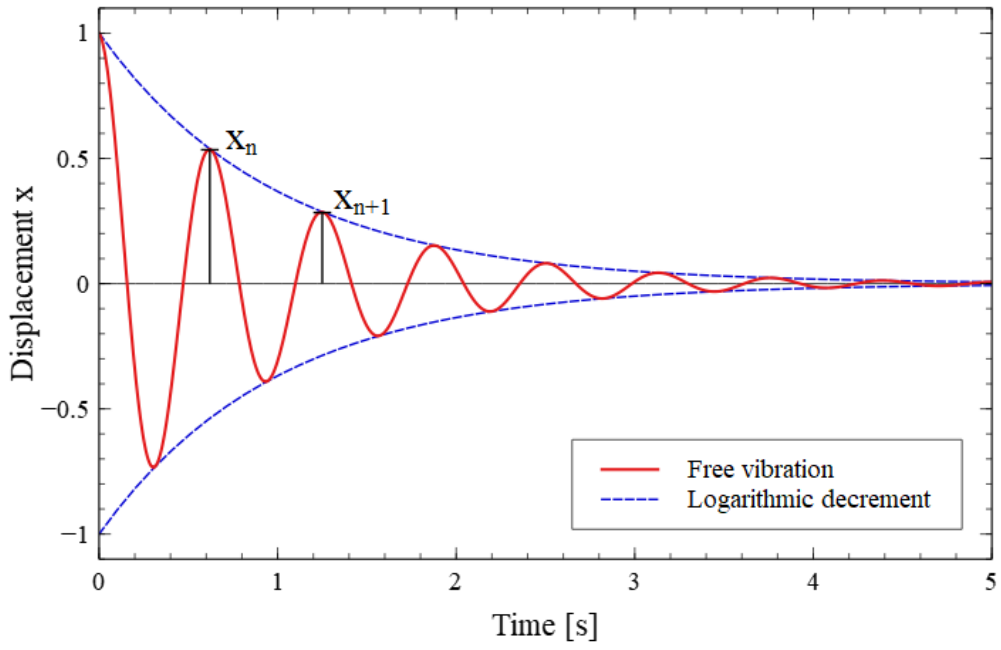

Figure 30 Damping ratio illustration, free vibration of beam in Figure 29

6.7 Sensitivity studies

Several sensitivity studies were conducted to assess the impact of certain variables and inaccuracies. By analysing and comparing results from these studies we can determine the precision required to get accurate results from our simulations among other things. These studies were also used to choose the amount of damage necessary to get significant alteration in the frequency response to get more evident results.

6.7.1 Benchmark of Numerical model (FEM VS model superposition principle)

A simple beam was made to see if the result from the example in MATLAB and the result in Ansys is the same. This was done to see if what we have done in Ansys is correct. This will compare the FEM that Ansys uses to the superpositions method that MATLAB uses, but with the same inputs, the result will be the same in theory. (see chapter 7.7.1 on page 61)

The result show that the simple beam made in Ansys has only 0-6‰ deviation in frequency from the superposition method it was controlled against. This means that we have chosen the right element type and material properties when creating the FEM model.

6.7.2 Mesh Element Edge Length

Each beam in the truss bridge model is divided into smaller elements by ANSYS when running an analysis. The accuracy of the results from the Finite Element Method (FEM) is reliant on the resolution of the beams. Mesh Element Edge Length (MEEL) is the length of the elements ANSYS uses in its FEM analysis. That means that a smaller MEEL gives greater resolution and thus more accurate results. To find a sufficient MEEL for our truss bridge analyses we conducted a convergence study using our ANSYS model (see chapter 7.7.2 on page 61).

The results show virtually no further accuracy achieved with MEEL lower than 0,01 meters. Thus, all further analyses done in ANSYS will use a MEEL of 0,01 meters.

6.7.3 Boundary conditions of the FEM model

The ANSYS model's boundary condition impacts the modal frequencies significantly. Therefore, a comparison of the results from the physical OMA testing was done to find the most comparable boundary condition without changing the young's modulus. The three boundary conditions tested were pinned-pinned, clamped-clamped and statically determined. Clamped-clamped allows for no displacement or rotation in the boundary nodes. Pinned-pinned allows for rotation in the vertical plane and no displacement. Statically determined allows for rotation in the vertical plane and displacement in the x-axis at one end of the model.(see chapter 7.7.3 on page 63) The result shows that Pinned-Pinned with an average of 8.5% frequency deviation, is the most accurate boundary condition.

6.7.4 Young Modulus reduction test

After the evaluating the different boundary conditions in the AMA the numerical model is calibrated further by adjusting the young's modulus. Each boundary condition was tested to not only get the closest average, but also the closest behaviour.

The test was to let the Young Modulus go from 0% reduction to 30% reduction with a 5% interval and then do a comparison to Pulse OMA's result. Then if the result was not adequate, a finer tune reduction was done to get the AMA result as close to Pulse OMA as possible. (See chapter 7.7.4 on page 6461).

After the reduction test, pinned-pinned with 13% reduction in the young's modulus was chosen as the best fit, with an average of 1.31% frequency deviation.

6.7.5 Eccentric in connections

The physical bridge model uses bracket plates to connect the truss elements in each node. The brackets attach to the edge of the truss element causing an eccentric load, meaning that the force vector is offset from the truss element's neutral axis. To analyse the potential effect from this eccentricity a sensitivity study has been conducted. To examine the influence of the eccentrically loaded trusses all elements in the digital model were offset 10 and 20 millimetres from the neutral axis and a modal analysis was done (see chapter 7.7.5 on page 65). The results show that the impact of the eccentricity is negligible.

Following this sensitivity study, we conclude that the eccentricity due to the mounting method on the physical model will not significantly impact the result of this study and can therefore be ignored.

6.7.6 Buckling with eccentricity

Eccentricity can be a result of the structural design of a connection or from mechanical damage from vehicle collisions. These eccentricities can significantly impact the structural integrity of the superstructure. To determine the impact on buckling, an assortment of eccentricities that realistically occur in the model bridge was used. (See chapter 7.7.6 on page 66)

The results show that initial eccentricity has a significant impact on the elements' critical buckling load. Further, the impact reduces as the eccentricity grows. Buckling will be considered as a potential damage case for the testing.

7 Result

7.1 Analytical Modal Analysis (AMA) (Finite Element Method)

In this chapter the result from the AMA is shown. For more information about the method see chapter 6.2 on page 31, and to read more about the case see chapter 5.2 on page 25.

Table 3 Undamaged from TC 1.1 AMA (Undamaged) in *Table 1*

Mode Number	Frequency [Hz]	Mode Number	Frequency [Hz]
1	15.61 Hz	22	164.33 Hz
2	37.10 Hz	23	171.51 Hz
3	50.54 Hz	24	177.63 Hz
4	68.58 Hz	25	181.38 Hz
5	75.05 Hz	26	185.03 Hz
6	91.37 Hz	27	186.25 Hz
7	106.71 Hz	28	191.21 Hz
8	112.61 Hz	29	193.20 Hz
9	113.54 Hz	30	200.51 Hz
10	115.07 Hz	31	202.39 Hz
11	117.97 Hz	32	205.91 Hz
12	121.15 Hz	33	208.55 Hz
13	129.35 Hz	34	214.72 Hz
14	133.64 Hz	35	216.70 Hz
15	136.06 Hz	36	222.82 Hz
16	148.60 Hz	37	226.60 Hz
17	152.43 Hz	38	229.72 Hz
18	154.49 Hz	39	232.01 Hz
19	157.58 Hz	40	236.45 Hz
20	160.43 Hz	41	238.18 Hz
21	162.94 Hz	42	239.38 Hz

Table 3 above shows the frequencies from the AMA done through ANSYS. The result is from the undamaged case, which has boundary conditions Pinned-Pinned and this showcases all the modes and frequencies from 0 to 256.63 Hz, this was done to get the frequency range.

Table 4 Damage Case 1 from TC 1.2 AMA (Damaged) in *Table 1*

Mode number	Frequency [Hz]	Mode number	Frequency [Hz]
1	16.02 Hz	22	165.15 Hz
2	34.79 Hz	23	171.95 Hz
3	44.43 Hz	24	177.06 Hz
4	55.70 Hz	25	182.97 Hz
5	68.79 Hz	26	186.13 Hz
6	76.59 Hz	27	191.75 Hz
7	92.97 Hz	28	193.73 Hz
8	106.79 Hz	29	199.58 Hz
9	112.65 Hz	30	203.05 Hz
10	113.73 Hz	31	205.31 Hz
11	115.52 Hz	32	207.98 Hz
12	117.75 Hz	33	214.76 Hz
13	124.01 Hz	34	217.60 Hz
14	133.59 Hz	35	223.42 Hz
15	136.49 Hz	36	228.09 Hz
16	148.49 Hz	37	228.75 Hz
17	152.65 Hz	38	229.84 Hz
18	155.12 Hz	39	235.34 Hz
19	156.92 Hz	40	236.68 Hz
20	160.94 Hz	41	239.44 Hz
21	164.33 Hz	42	241.31 Hz

Table 4 above is the frequencies and modes from damage case 1 taken from AMA through ANSYS. This is to show the frequencies in the same frequency range as above, which means mode 1 to 42.

7.2 Modal extraction from vibration data

To extract the modal frequencies from the raw vibration recordings from TC 2.1, TC 2.2, and TC 3.1-3.6 from Table 1, the data needs to be post-processed. The raw data contains multiple frequencies overlapped. Identifying the overlapping frequencies was done by decomposing the signal using a FFT (Fast Fourier Transformation) or a FDD (Frequency Domain Decomposition). These methods are described in the theory background chapter on page 17 and 18.

7.2.1 Classical Modal Analysis (CMA) (Hammer test)

See method chapter 6.3 on page 33, and case chapter 5.1 on page 23 to get an overview of the CMA.

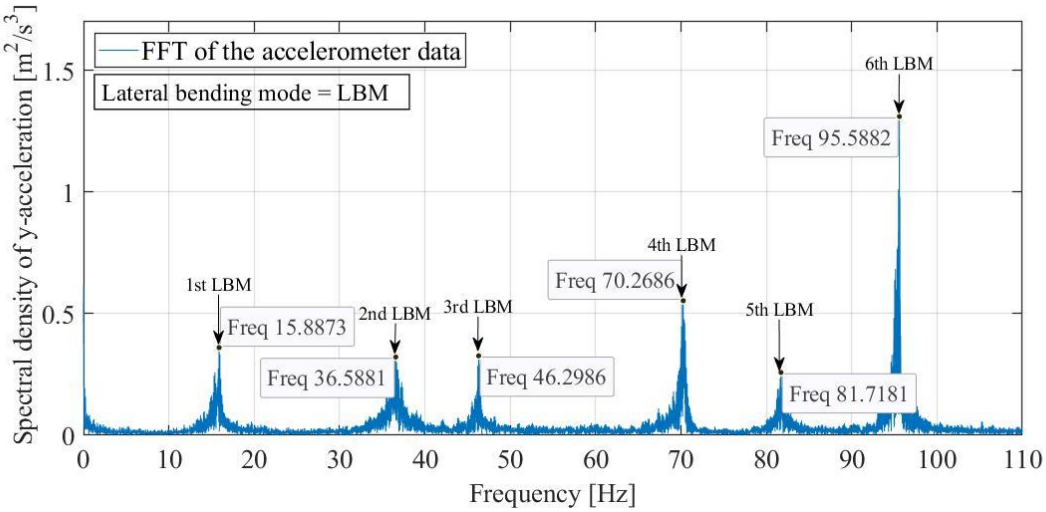

Figure 31 Shows the FFT of the accelerometer data in from TC 2.1 Hammer test (Y-direction) in *Table 1*

The Figure 31 above and Figure 32 below show the FFT from Matlab of the accelerometer data from the TC 2.1 Hammertest in Table 1. The peaks are where the modes are expected to be and have been highlighted. Where the blue line is the FFT and the arrows show where the expected modes are, both in Y- and Z-direction.

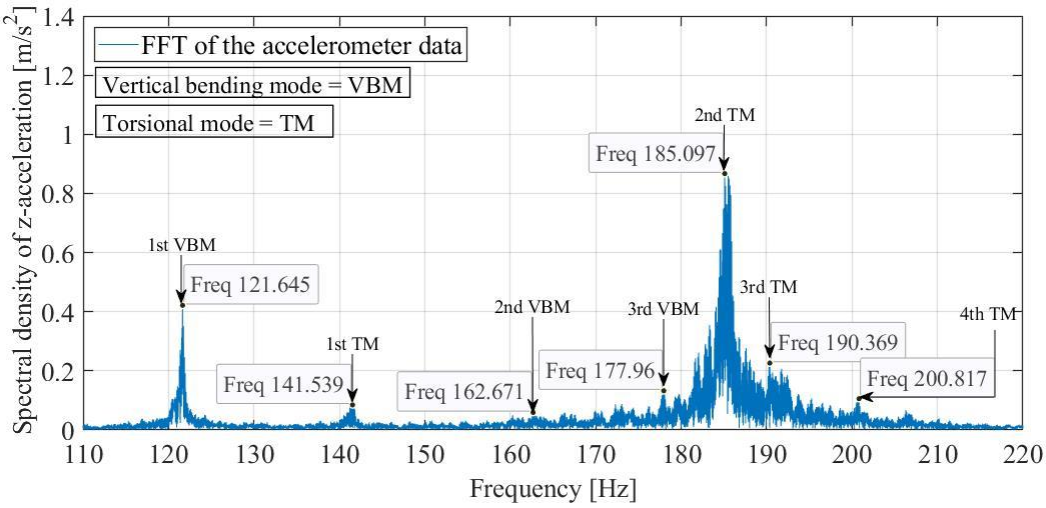

Figure 32 Shows the FFT of the accelerometer data from TC 2.2 Hammer test (Z-direction) in *Table 1*

Table 5 below shows the frequencies from the TC 2.1 Hammer test in both Y- and Z-directions, which are expected to be modes.

Table 5 Shows the Frequencies from the TC 2.1 Hammertest

Mode	Y-direction	Z-direction
1	15.89 Hz	121.65 Hz
2	36.59 Hz	141.54 Hz
3	46.40 Hz	177.96 Hz
4	70.27 Hz	185.10 Hz
5	81.72 Hz	190.37 Hz
6	95.59 Hz	200.82 Hz

7.2.2 Operational Modal Analysis (OMA)

See method chapter 6.4 on page 35, and case chapter 5.1 on page 23 to get an overview of OMA.

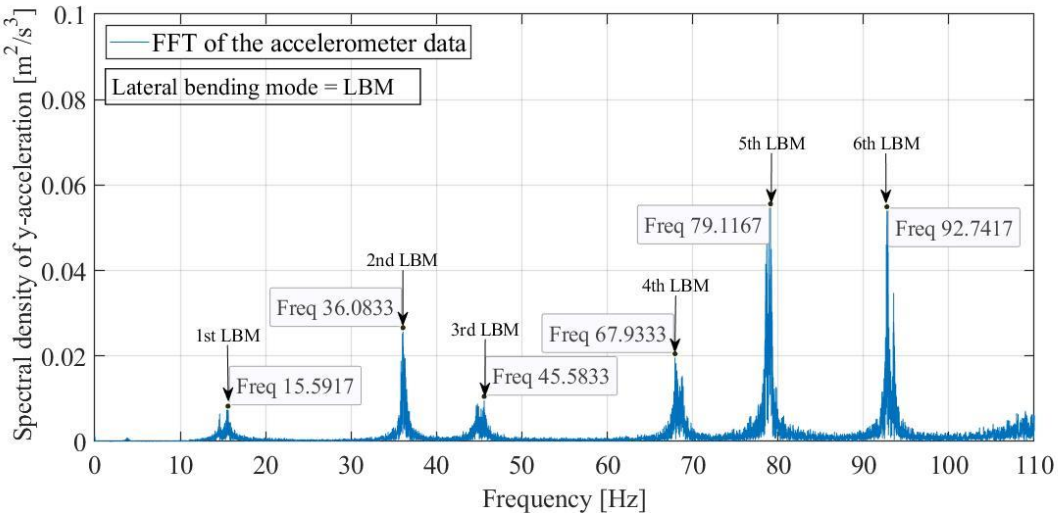

Figure 33 FFT of the accelerometer data from BK Connect, TC 3.1 OMA (Undamaged, Y-direction) in *Table 1*

Figure 33 above show the FFT done in Matlab of the raw accelerometer data from BK Connect in the Y-direction, the blue line is the FFT of the raw data and the arrows are the expected modes.

Figure 34 below shows the FDD from Pulse OMA, done on the raw accelerometer data from BK Connect, in Y-direction. The blue SVD line is the main line, which is used to select the peaks, that gives the frequencies and their estimated mode shapes

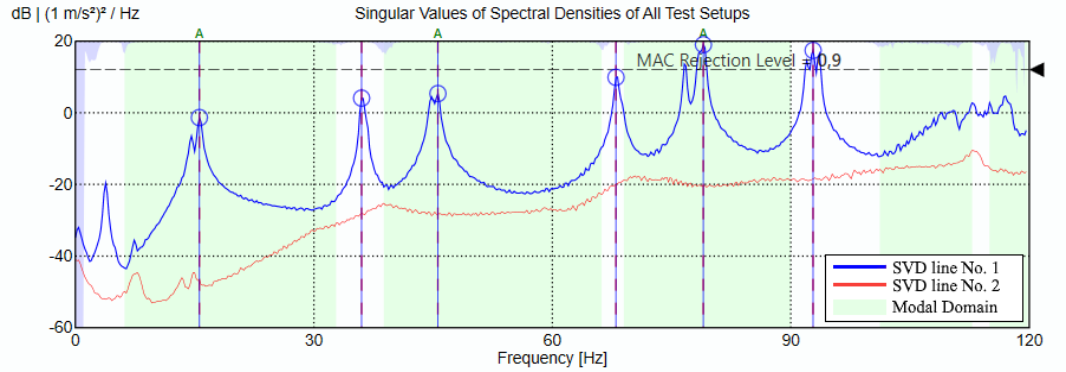

Figure 34 FDD done in Pulse OMA of the accelerometer data from BK Connect, TC 3.1 OMA (Undamaged case, Y-direction) *in Table 1*

Table 6 below shows the frequencies from FFT and FDD from the Undamaged case and the percentage difference between them in Y-direction.

Table 6 Overview of the frequencies from FFT, FDD and percentage difference, undamaged case in Y-direction

Modes	FFT	FDD	Percentage difference
1	15.59 Hz	15.60 Hz	+ 0.06 %
2	36.01 Hz	36.10 Hz	+ 0.25 %
3	45.58 Hz	45.60 Hz	+ 0.04 %
4	67.93 Hz	68.00 Hz	+ 0.10 %
5	79.12 Hz	79.10 Hz	- 0.03 %
6	92.74 Hz	92.80 Hz	+ 0.06 %

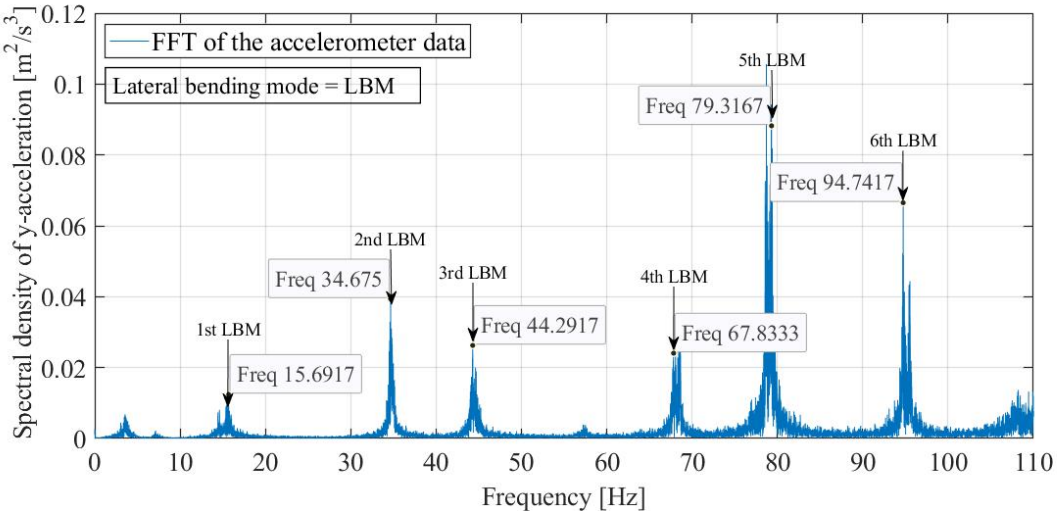

Figure 35 FFT of the accelerometer data from BK Connect, from TC 3.3 OMA (Damage case 1, Y-direction) in *Table 1*

Figure 35 above Shows the FFT done in Matlab of the accelerometer data from BK Connect of the Damage case 1. The blue line is the FFT, and the arrows are the expected modes.

Figure 36 below is the FDD from Pulse OMA of the same accelerometer data from Damage case 1, taken from BK Connect. The blue line is the main SVD line, which is used to choose the peaks and mode shapes.

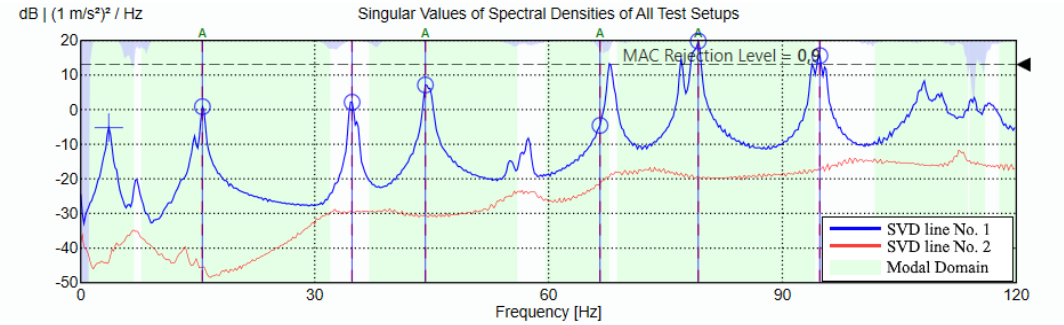

Figure 36 FDD done in Pulse OMA of the accelerometer data from BK Connect, TC 3.3 OMA (Damage case 1, Y-direction) in *Table 1*

Table 7 below shows the comparison of the frequencies from FFT and FDD of Damage case 1 in Y-direction and percentage difference between them.

Table 7 Overview of the frequencies from FFT and FDD Damage Case 1, Y-direction

Modes	FFT	FDD	Percentage difference
1	15.69 Hz	15.60 Hz	- 0.58 %
2	34.68 Hz	34.60 Hz	- 0.23 %
3	44.29 Hz	44.20 Hz	- 0.20 %
4	67.83 Hz	67.80 Hz	- 0.04 %
5	79.32 Hz	79.20 Hz	- 0.15 %
6	94.74 Hz	94.80 Hz	+ 0.06 %

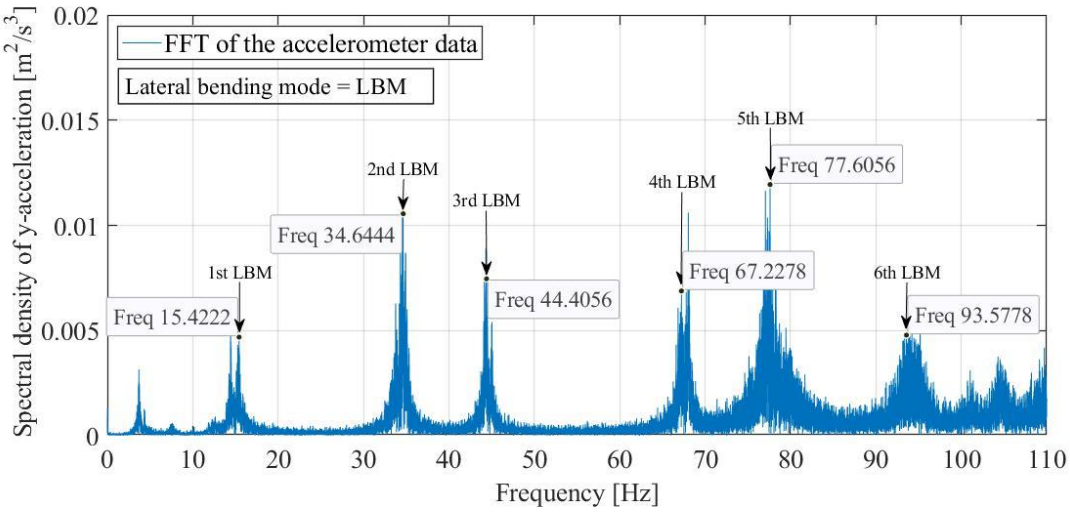

Figure 37 FFT of the accelerometer data from BK Connect, TC 3.5 OMA (Damage Case 2, Y-direction) *in Table 1*

Figure 37 above shows the FFT done in Matlab from the raw accelerometer data from BK Connect of Damage case 2. The blue line is the FFT, and the arrows are where the expected modes are.

Figure 38 below shows the FDD of the same accelerometer data from BK Connect of Damage case 2. Where the blue line is the main SVD line, which is used to select the peaks, were the modes are.

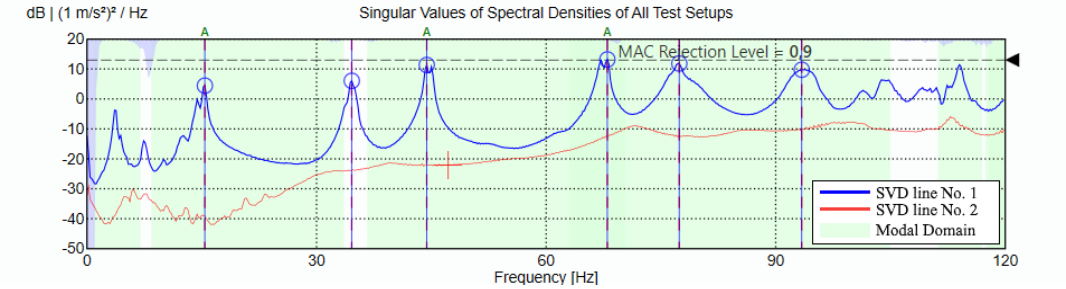

Figure 38 FDD done in Pulse OMA of the accelerometer data from BK Connect, TC 3.5 OMA (Damage Case 2, Y-direction) in *Table 1*

Table 8 OMA modal frequencies from the undamaged and damaged cases in the Y-direction

Modes	FFT	FDD	Percentage difference
1	15.42 Hz	15.40 Hz	- 0.13 %
2	34.64 Hz	34.60 Hz	- 0.12 %
3	44.41 Hz	44.40 Hz	- 0.02 %
4	67.23 Hz	67.20 Hz	- 0.04 %
5	77.61 Hz	77.40 Hz	- 0.27 %
6	93.58 Hz	93.40 Hz	- 0.19 %

Table 8 above is the frequencies from the FFT and FDD form Damage case 2 in Y-direction. As well as the percentage difference between them.

The FFT done in Matlab of the accelerometer data from the Undamaged case in Z-direction from BK Connect is showcased in Figure 39 below.

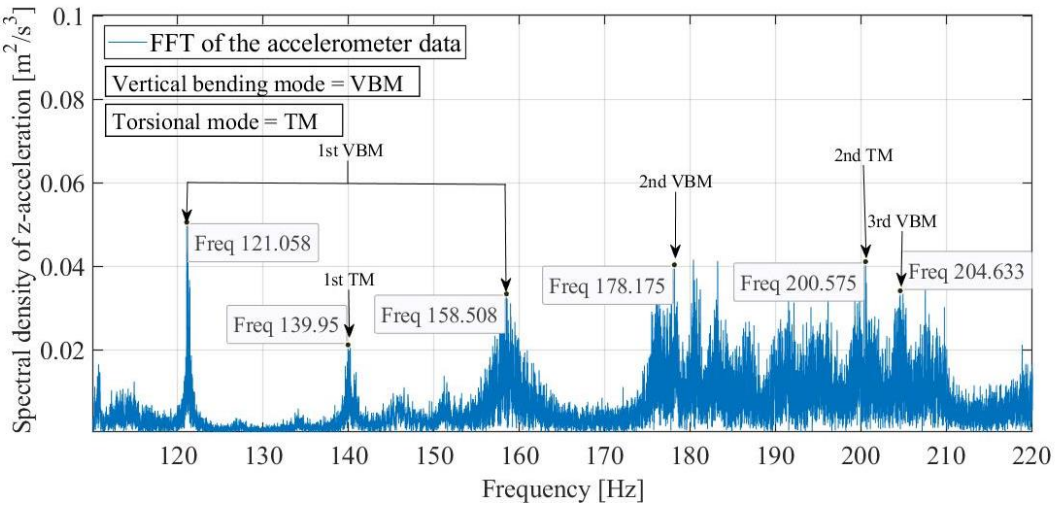

Figure 39 FFT of the accelerometer data from BK Connect, TC 3.2 OMA (Undamaged case, Z-direction) in *Table 1*

Figure 40 below shows the FDD done in Pulse OMA, of the accelerometer data obtain in BK Connect of the Undamaged case in Z-direction.

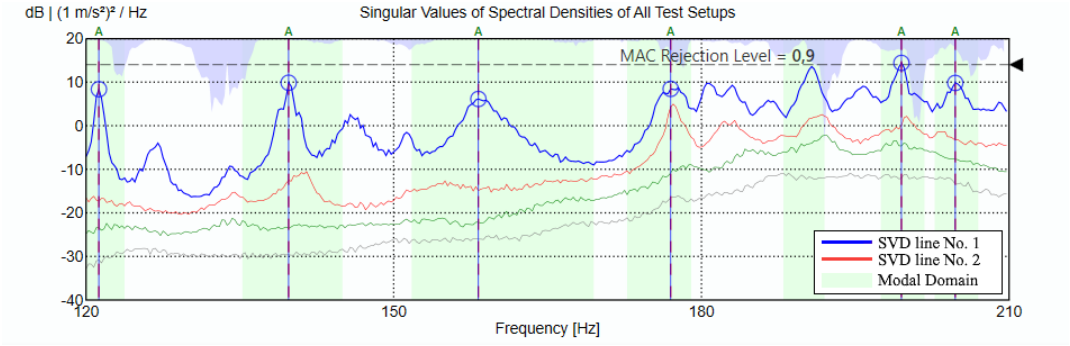

Figure 40 FDD of the accelerometer data from BK Connect, TC 3.2 OMA (Undamaged case, Z-direction) in *Table 1*

Table 9 below shows the frequencies from the FFT and FDD in the Undamaged case, in addition to the percentage difference between them.

Table 9 Overview of the FFT and FDD frequencies and the percentage difference in undamaged case in Z-direction

Modes	FFT	FDD	Percentage difference
1	121.06 Hz	121.20 Hz	- 0.12 %
2	139.95 Hz	139.80 Hz	- 0.11 %
3	158.51 Hz	158.20 Hz	- 0.20 %
4	178.18 Hz	177.00 Hz	- 0.67 %
5	200.57 Hz	199.40 Hz	- 0.59 %
6	204.63 Hz	203.00 Hz	- 0.80 %

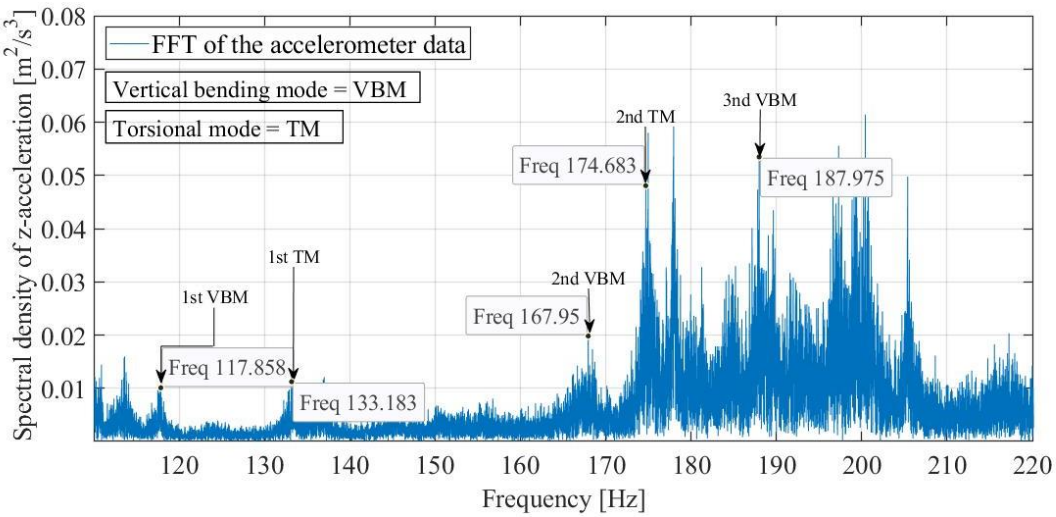

Figure 41 FFT of the accelerometer data from BK Connect, TC 3.4 OMA (Damage case 1, Z-direction) *in Table 1*

Figure 41 shows the FFT done in Matlab of the accelerometer data from BK Connect in Damage case 1 in Z-direction.

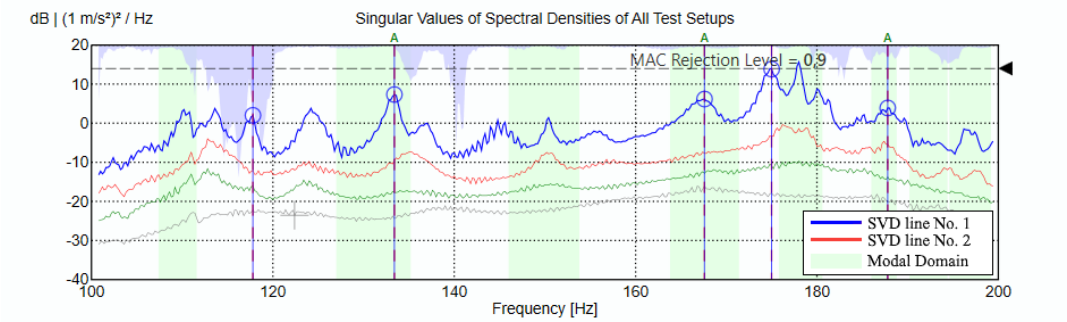

Figure 42 FDD of the accelerometer data from BK Connect in TC 3.4 OMA (Damage case 1, Z-direction) in *Table 1*

Figure 42 above shows the FDD performed in Pulse OMA, with the accelerometer data from BK Connect of Damage case 1 in Z-direction.

Table 10 below shows the frequencies from FFT and FDD as well as the percentage difference between the two.

Table 10 Overview of the FFT and FDD frequencies and percentage difference in damage case 1 Z-direction

Modes	FFT	FDD	Percentage difference
1	117.86 Hz	117.75 Hz	- 0.09 %
2	133.18 Hz	133.50 Hz	+ 0.24 %
3	167.95 Hz	167.5 Hz	- 0.27 %
4	174.68 Hz	174.75 Hz	+ 0.04 %
5	187.98 Hz	188.00 Hz	+ 0.01 %

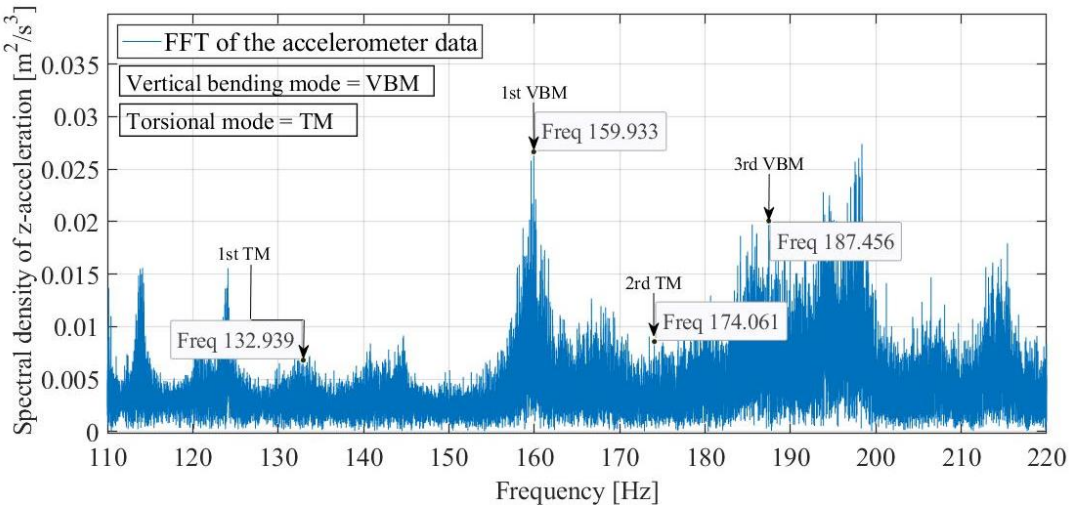

Figure 43 FFT of the accelerometer data from BK Connect, TC 3.6 OMA (Damage case 2, Z-direction) *in Table 1*

Figure 43 above shows the FFT done in Matlab of the raw accelerometer data from BK Connect in Damage case 2 in Z-direction. Where the arrows are the expected modes

Figure 44 below shows the FDD done in Pulse OMA of the same accelerometer data from BK Connect. Where the lines with the circles are the selected peaks, where the modes are.

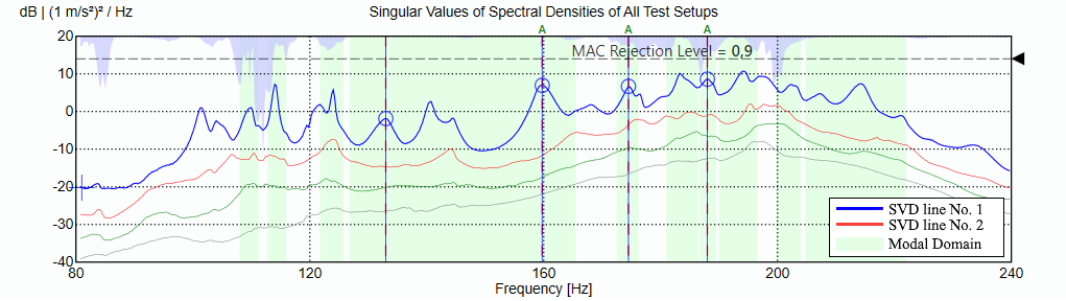

Figure 44 FDD of the accelerometer data from BK Connect in TC 3.6 OMA (Damage case 2, Z-direction) *in Table 1*

Table 11 below is a comparison of the frequencies from the FFT done in Matlab and the FDD done in Pulse OMA, as well as the percentage difference between the two.

Table 11 Overview of the FFT and FDD frequencies and percentage differnece in damage case 2 Z-direction

Modes	FFT	FDD	Percentage difference
1	132.94 Hz	132.50 Hz	- 0.33 %
2	159.93 Hz	159.75 Hz	- 0.11 %
3	174.06 Hz	174.50 Hz	+ 0.25 %
4	187.46 Hz	188.00 Hz	+ 0.29 %

7.3 Analytical vs experimental modal analyses

Comparing the analytical modal analysis to the experimental modal analyses (OMA and CMA) gives an indication of the similarities of the numerical model and the physical counterpart.

Table 12 Analytical vs experimental modal analyses, lateral modes, with OMA as baseline, %Δ = percentage difference from OMA

Mode	OMA	CMA	%Δ	AMA	%Δ
1	15.60 Hz	15.89 Hz	1.86%	15.61 Hz	0.06 %
2	36.10 Hz	36.59 Hz	1.36%	37.10 Hz	2.77 %
3	45.60 Hz	46.40 Hz	1.75%	50.54 Hz	10.83 %
4	68,00 Hz	70.27 Hz	3.34%	68.58 Hz	0.85 %
5	79.10 Hz	81.72 Hz	3.31%	75.05 Hz	-5.12 %
6	92.80 Hz	95.59 Hz	3.01%	91.37 Hz	-1.54 %

Table 12 shows the comparison of the modal analyses done of the numerical and physical model. The table shows the percent difference from the OMA to use as a comparison. The AMA gives increase in frequencies in all the modes except for mode 5 and 6. The values from the table is plotted in. The CMA gives consistent higher frequencies (2.44% on average) than the OMA (see explanation in the discussion chapter 8.2).

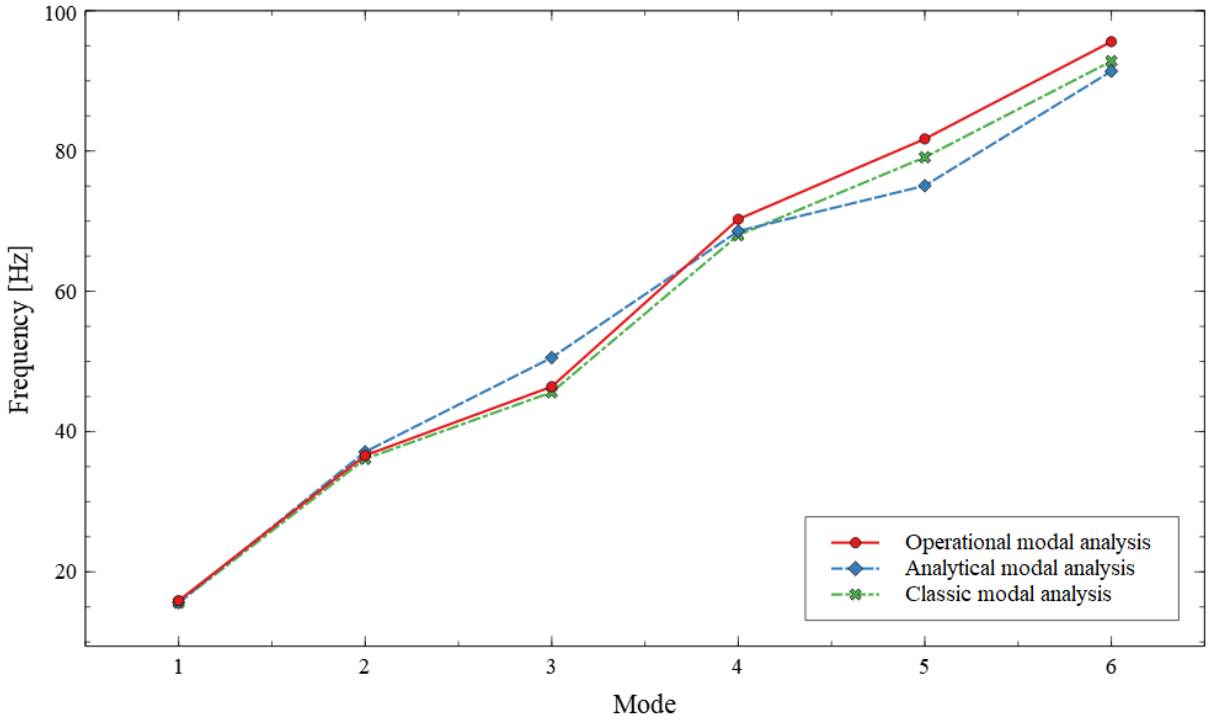

Figure 45 Analytical vs experimental modal analyses, lateral modes (first 6 bending modes)

7.4 Mode shapes

The mode shapes acquired from the operational modal analysis gives an understanding of the actual movements of the model bridge in free vibration. These mode shapes can be compared to the analytical FEM modal analysis.

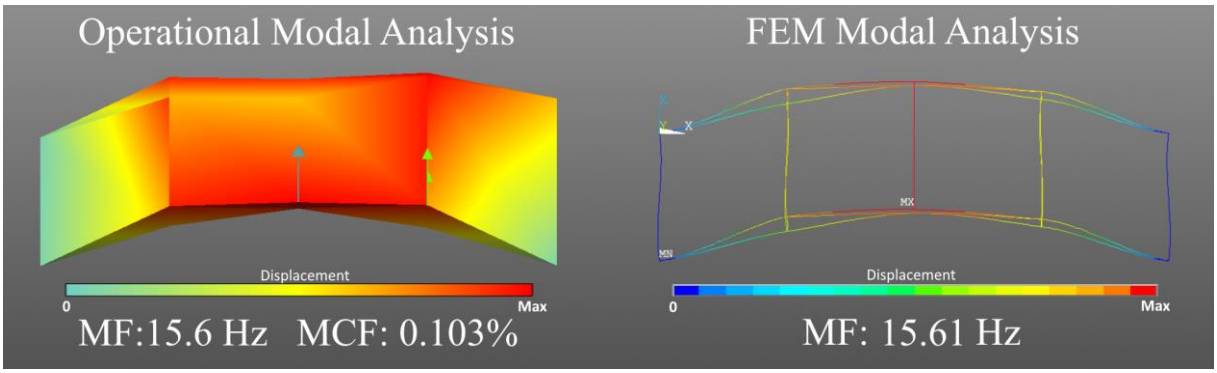

Figure 46 First lateral bending mode shape comparison OMA vs FEM MA (top-down view)

Figure 46 show the comparison of the analytical FEM Modal Analysis and the recorded Operational Modal Analysis first lateral bending mode. The recorded OMA mode shape has a Modal Complexity Factor (MCF) of 0.103% and was found at 15.6 Hz.

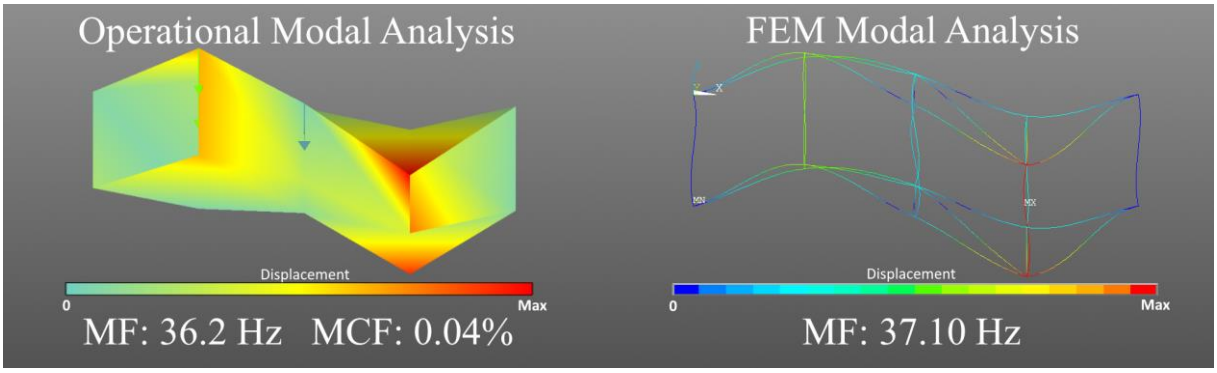

Figure 48 Second lateral bending mode shape comparison OMA vs FEM MA (top-down view)

Figure 48 shows the comparison of the second lateral bending mode. The recorded OMA shape was found at 36.2 Hz with a MCF of 0.04%. The MCF of the OMA mode shape is plotted in Figure 47. The plot resembles a straight line as the phase of each side of the model is 180 degrees from the other.

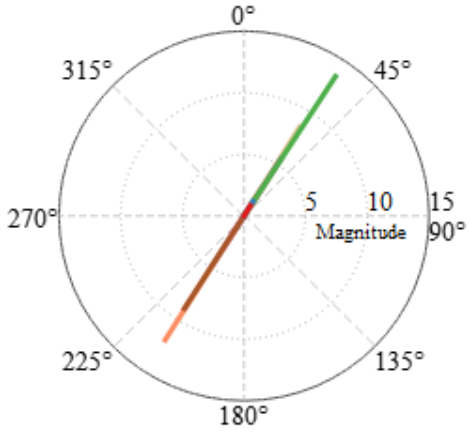

Figure 47 MCF plot 2nd lateral bending mode, MCF=0.04%, radial = magnitude, degree = phase

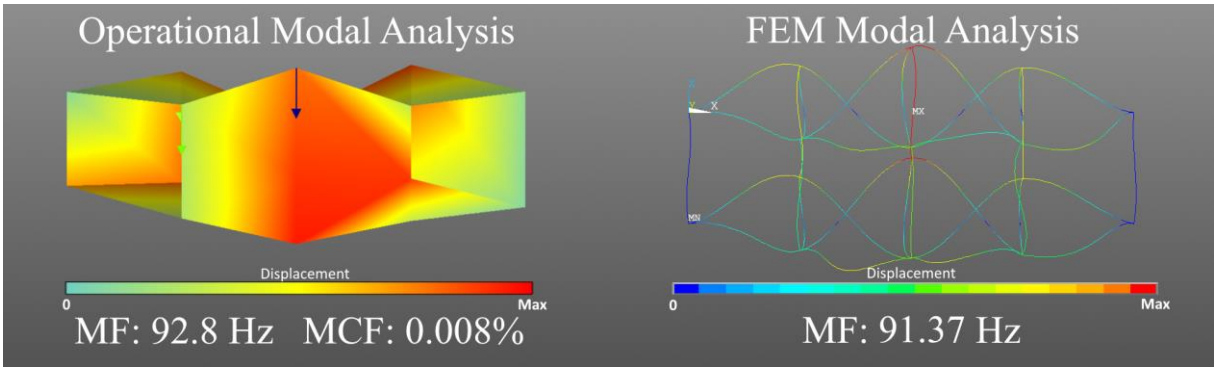

Figure 49 6th lateral bending mode shape comparison OMA vs FEM MA (top-down view)

Figure 49 shows the comparison of 6th lateral bending mode. The recorded OMA shape was found at 92.8 Hz and has a MCF of 0.008%.

The first torsional mode is found at 139.8 Hz. The mode shape has clear opposite movements with a 180-degree phase delay, as shown in Figure 50, creating a twisting movement of the bridge. The MCF of the OMA mode shape is plotted in Figure 51.

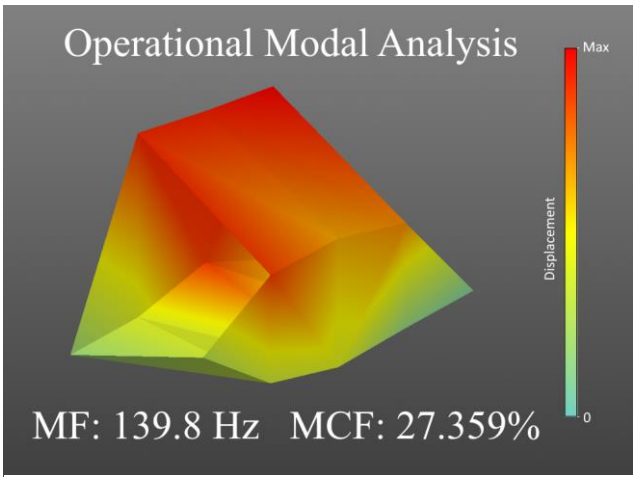

Figure 50 First torsional mode shape (isometric view)

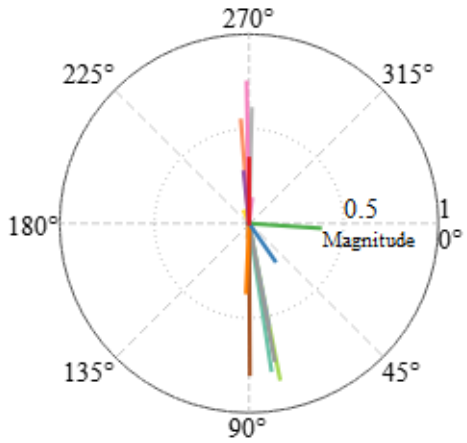

Figure 51 MCF plot of 1st torsional mode, MCF = 27.4%, radial = magnitude, degree = phase

Figure 52 shows a comparison of two vertical bending modes. Both have the single arch characteristic of the first bending mode yet have a 37 Hz difference in frequency. The first mode shape (1.a and 1.b in Figure 52) has the majority of its movement in the top nodes of the bridge, while the second mode shape (2.a and 2.b) has the most movement in the bottom-middle node.

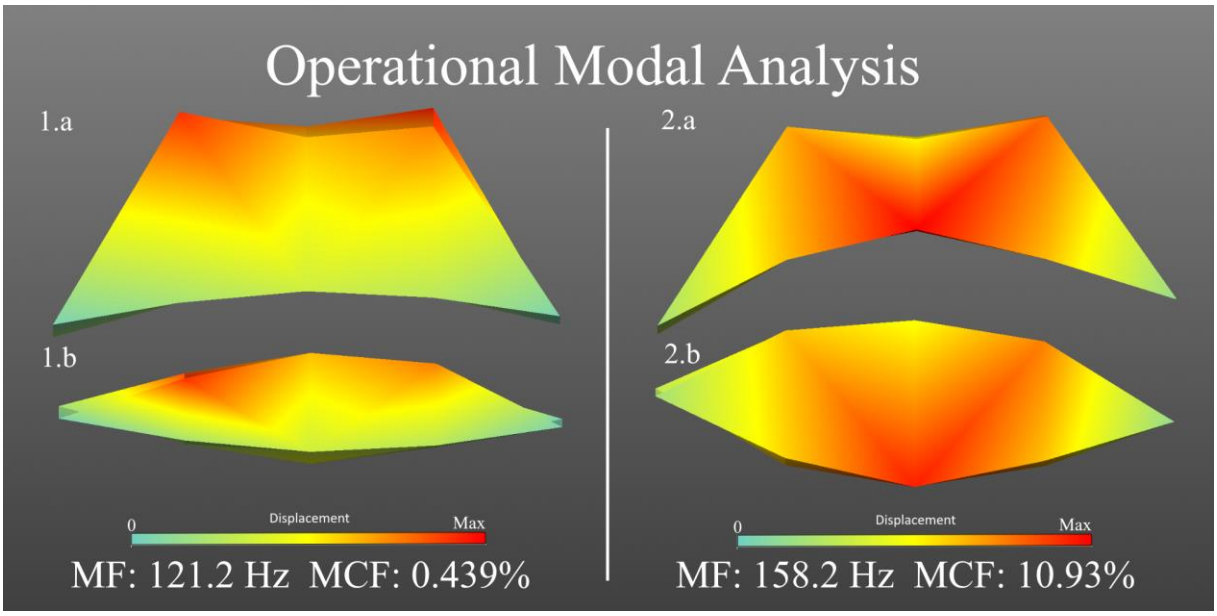

Figure 52 Comparison of two vertical bending modes

The vertical bending modes displayed in Figure 52 has a modal assurance criterion (MAC) of 0.7401 as shown in Table 13. This indicates that the modes have similar movements yet have a significant gap in frequencies. The MAC index is described in theory background chapter 3.5.4 on page 16.

Table 13 Extract of MAC table for vertical modes

	121.2 Hz	139.8 Hz	158.2 Hz
121.2 Hz	1	0.03982	0.7401
139.8 Hz	0.03982	1	0.03344
158.2 Hz	0.7401	0.03344	1

7.5 Damage cases

The damage cases of the model bridge described in chapter 6.5 on page 37 was tested using an OMA (Operational Modal Analysis) and compared with the FEM AMA (Analytical Modal Analysis) where applicable. The results from these tests give the basis to describe the impact of the damage applied.

7.5.1 Lateral modes

Table 14 Damage case 1 and 2 results from the OMA, lateral modes, where %Δ = percentage difference from undamaged

Mode	Undamaged	Damage Case 1	%Δ	Damaged Case 2	%Δ
1	15.6 Hz	15.6 Hz	0.00%	15.4 Hz	-1.28%
2	36.1 Hz	34.6 Hz	-4.16%	34.6 Hz	-4.16%
3	45.6 Hz	44.2 Hz	-3.07%	44.4 Hz	-2.63%
4	68.0 Hz	67.8 Hz	-0.29%	67.2 Hz	-1.18%
5	79.1 Hz	79.2 Hz	0.13%	77.4 Hz	-2.15%
6	92.8 Hz	94.8 Hz	2.16%	93.4 Hz	0.65%

The results from tests TC 3.3 and TC 3.5 from Table 1 on page 26 are shown in Table 14 above and showcases the damage case's lateral modal frequencies. These values are plotted in Figure 53 below and the percent difference from undamaged are shown in Figure 54.

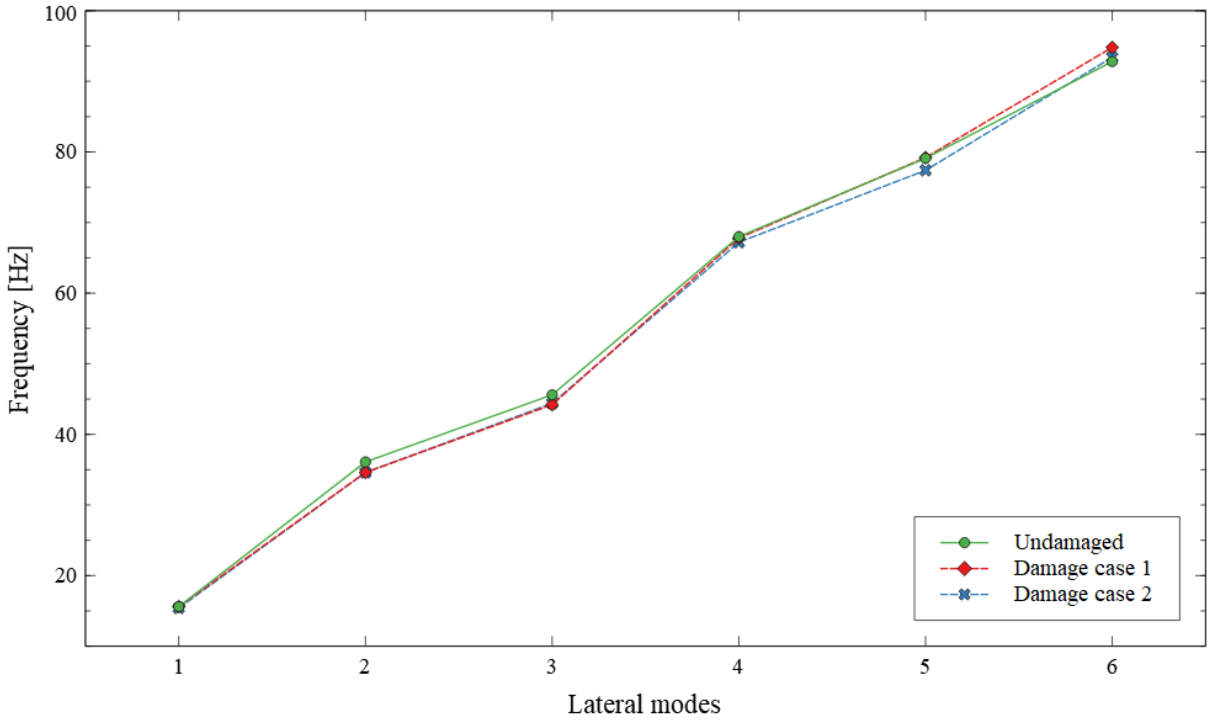

Figure 53 Damage case results (OMA), lateral modes (Y)

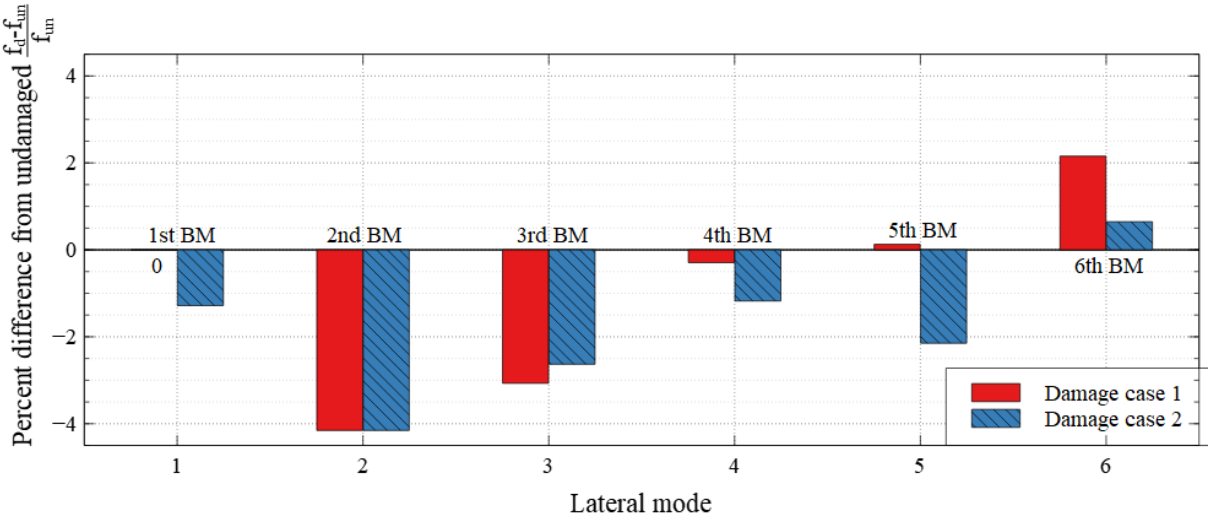

Figure 54 Damage case results (OMA), lateral modes (Y), percent difference from undamaged case

The results from the OMA damage cases from the PULSE OMA software show the effect of the modifications made to the bridge. All the lateral modes of the model bridge, except from the 5th and 6th mode, are reduced as a result of the damage applied. The change in frequency ranges from a 2.15% increase to a 4.16% decrease, the average being -0.87% for damage case 1 and -1.79% for case 2.

The first damage case can be compared to the FEM AMA damage simulation. These results are presented in Table 15 and Figure 55.

Table 15 Damage case 1 results, OMA compared with AMA (FEM), where %Δ = percentage difference from undamaged

Mode	OMA Undamaged	OMA Damage Case 1	%Δ	FEM Undamaged	FEM Damage case 1	%Δ
1	15.6 Hz	15.6 Hz	0.00%	15.61 Hz	16.02 Hz	2.65 %
2	36.1 Hz	34.6 Hz	-4.16%	37.10 Hz	34.79 Hz	-6.25 %
3	45.6 Hz	44.2 Hz	-3.07%	50.54 Hz	44.43 Hz	-12.09 %
4	68.0 Hz	67.8 Hz	-0.29%	68.58 Hz	55.70 Hz	-18.78 %
5	79.1 Hz	79.2 Hz	0.13%	75.05 Hz	68.79 Hz	-8.33 %
6	92.8 Hz	94.8 Hz	2.16%	91.37 Hz	76.59 Hz	-16.18 %

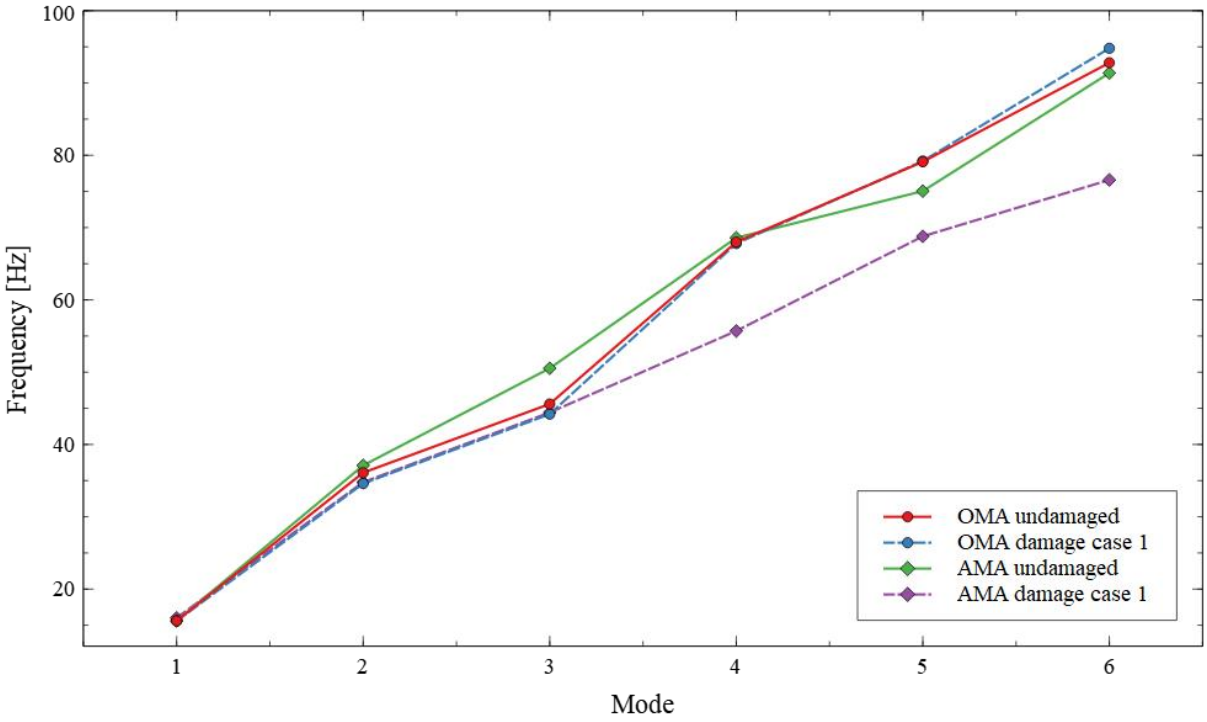

Figure 55 Damage case 1 results, OMA vs AMA

The FEM AMA gives a significantly larger decrease in frequency in all modes when removing the diagonal truss element in damage case 1. The average change in frequency is -0.87% for the OMA and -9.83% for the FEM AMA. The maximum decrease in the OMA case was 4.16% (bending mode 2) compared to the 18.73% (bending mode 4) in the FEM AMA.

7.5.2 Vertical modes

Table 16 Damage case 1 and 2 results from the OMA, vertical modes, where %Δ = percentage difference from undamaged

Mode	Undamaged	Damage Case 1	%Δ	Damaged Case 2	%Δ
1	121.2 Hz	117.8 Hz	-2.85%	Not observed	-
2	139.8 Hz	133.5 Hz	-4.51%	132.5 Hz	-5.22%
3	158.2 Hz	Not observed	-	159.8 Hz	0.98%
4	177.0 Hz	167.5 Hz	-5.37%	Not observed	-
5	199.4 Hz	174.8 Hz	-12.36%	174.5 Hz	-12.49%
6	203.0 Hz	188.0 Hz	-7.39%	188.0 Hz	-7.39%

The results from tests 3.4 and 3.6 from Table 1 on page 26 shows the damage case's vertical modes and are shown in Table 16 above. The 3rd mode in damage case 1 and the 1st and 4th mode in damage case 2 was not observed in the OMA (see discussion chapter for a hypothesis). The results are plotted in Figure 56 and the percent change in frequency is plotted in Figure 57 below.

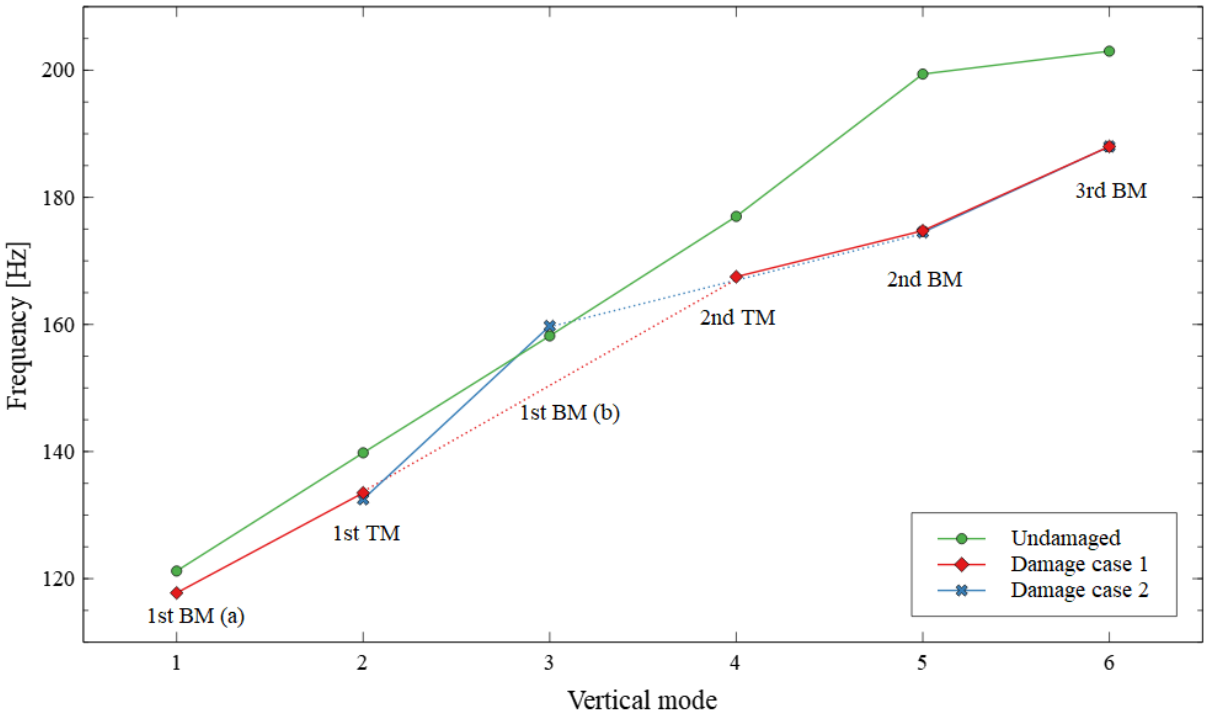

Figure 56 Damage case results compared with undamaged (OMA), vertical modes (Z). BM = Bending Mode, TM = Torsional Mode. (1st BM (a) and (b) see Figure 52)

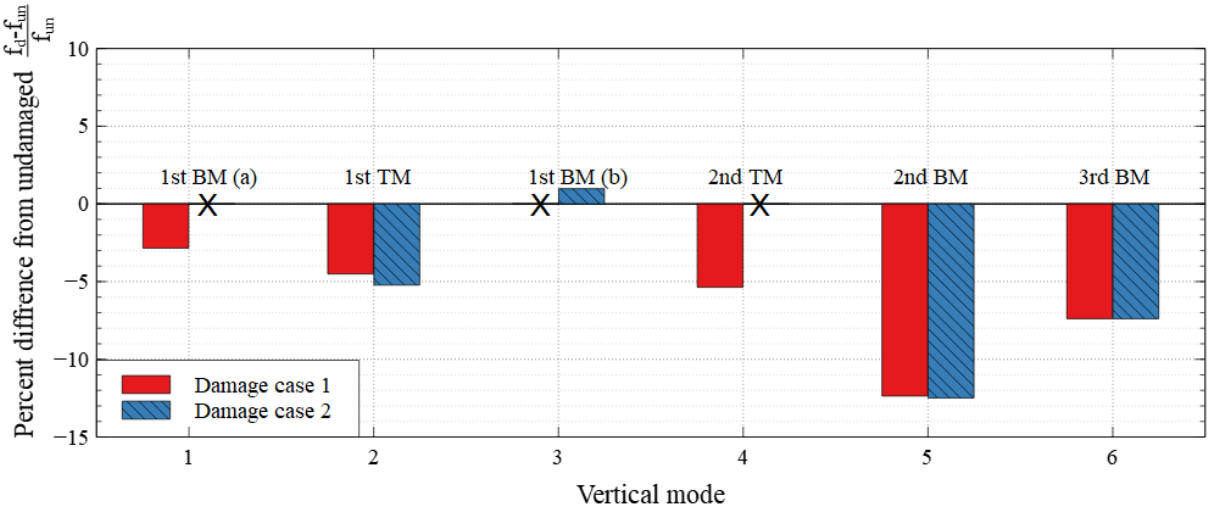

Figure 57 Damage case results (OMA), vertical modes (Z), percent difference from undamaged case. BM = Bending Mode, TM = Torsional Mode and X = not observed (1st BM (a) and (b) seeFigure 52)

The vertical modes are incomplete as some modes does not appear in all the damage cases. The ones that did were all significantly lower except the first bending mode (b). This mode is unclear in the damage cases and will not be considered but was worth mentioning. Figure 52 on page 54 displays the comparison of the two single arch bending modes that appeared in the undamaged OMA test.

The average change in frequency was -6.49% for damage case 1 and -8.37% for the second damage case excluding the first bending mode (b). Both cases had the largest decrease in mode 5 where case 1 was -12.36% and case 2 was -12.49%.

7.6 Damping properties

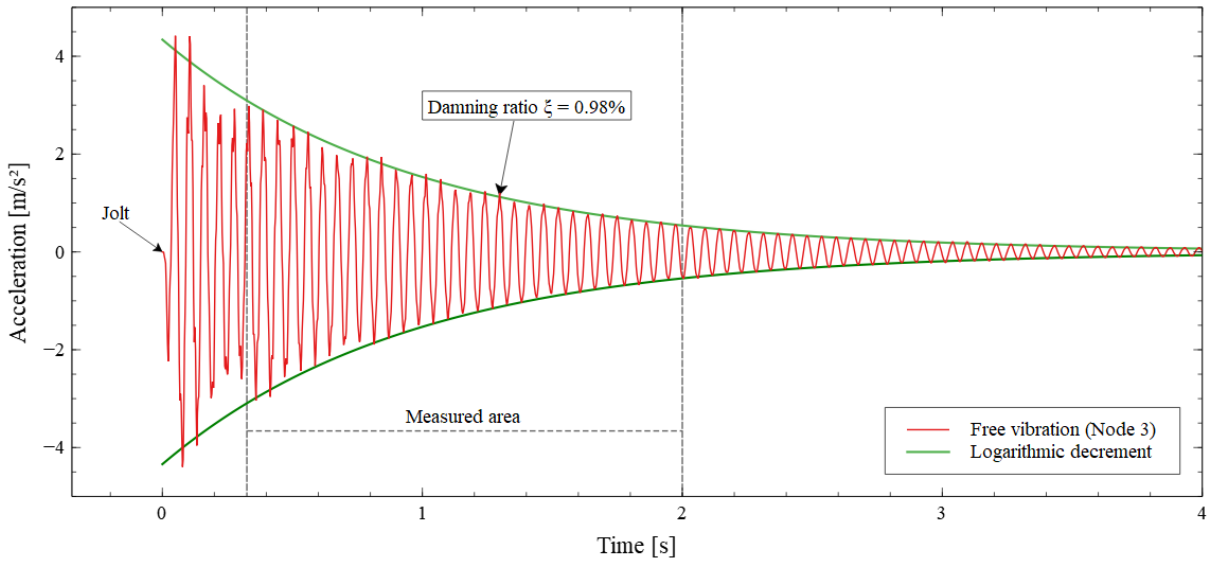

Figure 58 Results from damping ratio test, shows free vibrations of 1st BM recorded in node 3 (test 5.1 from Table 1)

The damping ratio was found by examining the raw data from the node 3 sensor recording during the soft impact tests (test 5.1 from Table 1) and applying the method described in chapter 6.6 on page 38. The average ratio from one peak to the next (δ) was calculated from using 30 peaks (from 0.325 to 2 seconds, see marked area on Figure 58 above). The damping ratio was found to be 0.980% in node 3 for the first lateral bending mode by using formula 6.6.1 and 6.6.2 on page 38.

7.7 Sensitivity studies

The results from the sensitivity studies in chapter 6.7 on page 38 are presented in this chapter. These studies analyze the effect of changing variables in the tests performed to find the impact or best fit for further use in the study.

7.7.1 Benchmark of the numerical model (FEM VS model superposition principle)

Table 17 Shows the Eigenfrequencies from the Single beam test from Matlab and AMA FEM, the ‰Δ is per mille difference between Matlab and AMA FEM in the different boundary conditions

Boundary condition	Pinned-Pinned			Clamped-Clamped		
Mode	Matlab	AMA FEM	‰Δ	Matlab	AMA FEM	‰Δ
1	0.2340 Hz	0.2345 Hz	2.03‰	0.5317 Hz	0.5313 Hz	- 0.81‰
2	0.9377 Hz	0.9375 Hz	- 0.20‰	1.4662 Hz	1.4632 Hz	- 2.07‰
3	2.1174 Hz	2.1076 Hz	- 4.61‰	2.8815 Hz	2.8650 Hz	- 5.73‰
4	3.7571 Hz	3.7425 Hz	- 3.89‰	4.7442 Hz	4.7287 Hz	- 3.26‰

Table 17 above shows the first 4 eigenfrequencies from the FEM control study, with the per mil difference. It was tested 2 different kinds of boundary conditions. This was done to have multiple tests and to be sure that what was done in Ansys when preforming the AMA, was right.

7.7.2 Mesh Element Edge Length

MEEL [m]	Mode 1 [Hz]	Mode 2 [Hz]	Mode 3 [Hz]
0.0005	20.0725	43.3285	55.3268
0.0010	20.0725	43.3286	55.3269
0.0030	20.0726	43.3290	55.3275
0.0050	20.0729	43.3299	55.3286
0.0070	20.0734	43.3311	55.3303
0.0100	20.0744	43.3340	55.3341
0.0500	20.1214	43.4625	55.5077
0.1000	20.2671	43.8581	56.0437

Table 18 Frequencies for mode 1-3 of the truss bridge with different MEEL

Table 18 shows each MEEL tested and the resulting modal frequencies in mode 1-3. Normalizing the results to the finest resolution gives the percent deviation from the most accurate result. Plotting the normalized results in a graph will visualize the convergence of accuracy (see Figure 59).

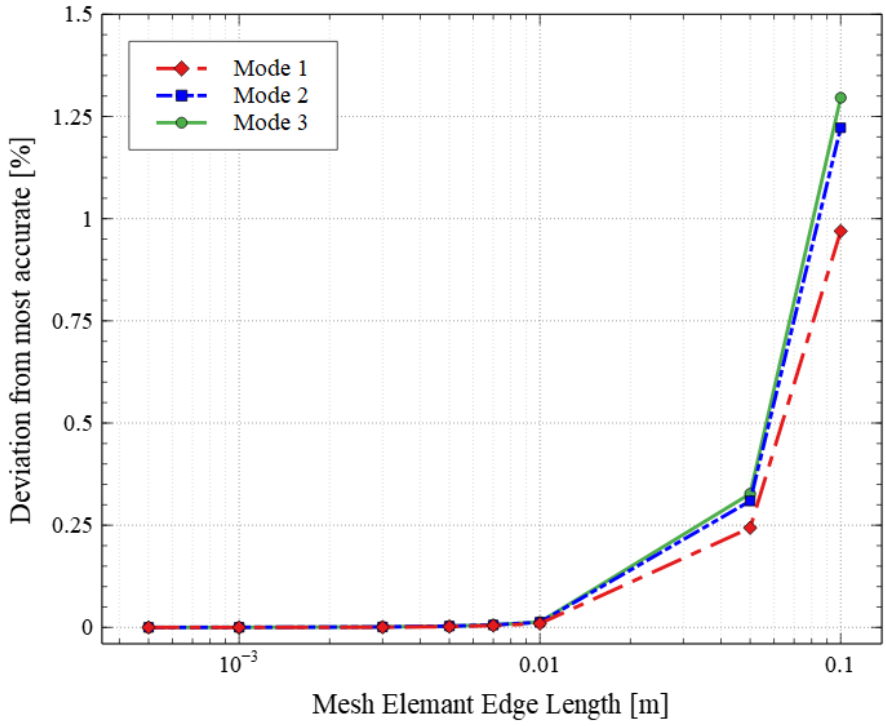

Figure 59 MEEL Convergence test, (logarithmic x-axis)

Figure 59 shows negligible deviation in frequency (<0,013%) from 0,005 to 0,01 meters MEEL and a clear increase in deviation with MEEL greater than 0,01 meters. A MEEL of 0,1 meters gives an increase in frequency of about 1% in the first 3 modes.

7.7.3 Boundary conditions of the FEM model

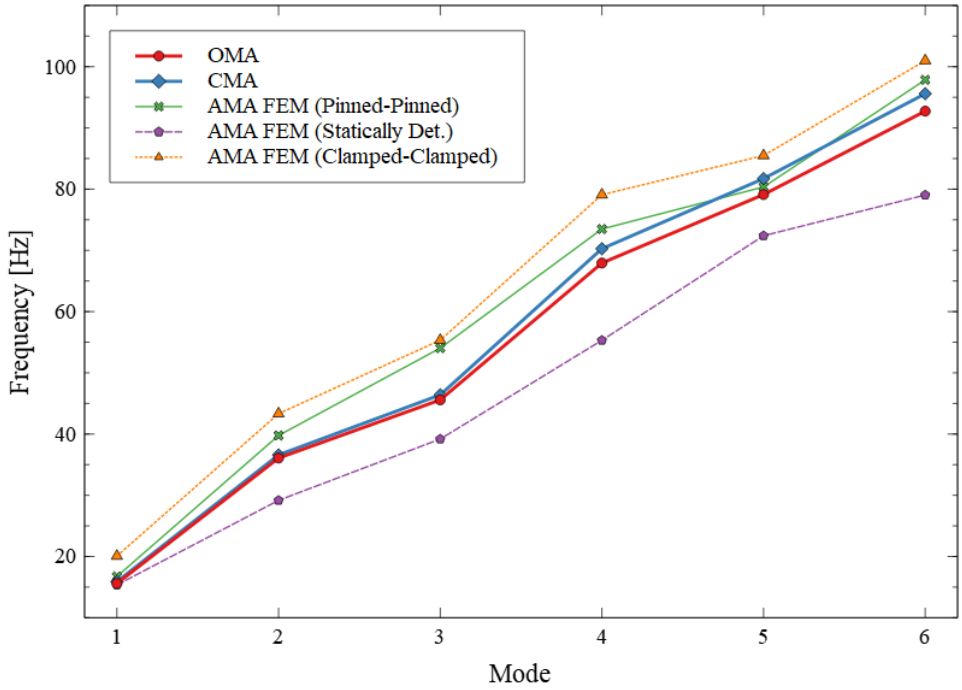

Figure 60 Comparison of different boundary conditions in the FEM AMA to the OMA and CMA results

Figure 60 shows the comparison of the two physical tests (OMA and CMA) with the FEM AMA of digital model. The FEM model was tested with three different boundary conditions to find the closest one to the physical model. The one with the closest behaviour and frequencies to the OMA will be considered the most comparable.

Table 19 Comparison of different boundary conditions in the FEM model and the OMA, where %Δ = percentage difference to OMA

Mode	OMA	AMA Static determined	%Δ	AMA Pinned-Pinned	%Δ	AMA Clamped-Clamped	%Δ
1	15.6 Hz	15.36 Hz	-1.55%	16.73 Hz	7.25%	20.07 Hz	28.68%
2	36.1 Hz	29.17 Hz	-19.20%	39.77 Hz	10.16%	43.33 Hz	20.04%
3	45.6 Hz	39.19 Hz	-14.07%	54.04 Hz	18.50%	55.33 Hz	21.35%
4	68 Hz	55.31 Hz	-18.66%	73.48 Hz	8.07%	79.09 Hz	16.31%
5	79.1 Hz	72.39 Hz	-8.48%	80.36 Hz	1.59%	85.49 Hz	8.07%
6	92.8 Hz	79.04 Hz	-14.83%	97.85 Hz	5.44%	100.99 Hz	8.82%

Pinned-pinned has the most comparable frequencies to the OMA results (without adjusting the young's modulus) with an average of 8.50% frequency deviation. Statically determined which is theoretically the most correct came second with an average of -12.80% deviation in frequency from OMA.

7.7.4 Young's Modulus reduction test

Table 20 AMA Young Modulus reduction test

	Pinned-Pinned	Clamped-Clamped	Static Determined
Mode	13% reduction	20 % reduction	11 % reduction
1	15.61 Hz	17.96 Hz	15.63 Hz
2	37.10 Hz	38.78 HZ	37.47 Hz
3	50.54 Hz	49.72 Hz	50.57 Hz
4	68.58 Hz	70.78 Hz	68.74 Hz
5	75.05 Hz	76.59 Hz	75.23 Hz
6	91.37 Hz	90.51 Hz	91.40 Hz

Table 20 above shows the selected results from the reduction test from the AMA. The young's modulus was adjusted to best fit the OMA results.

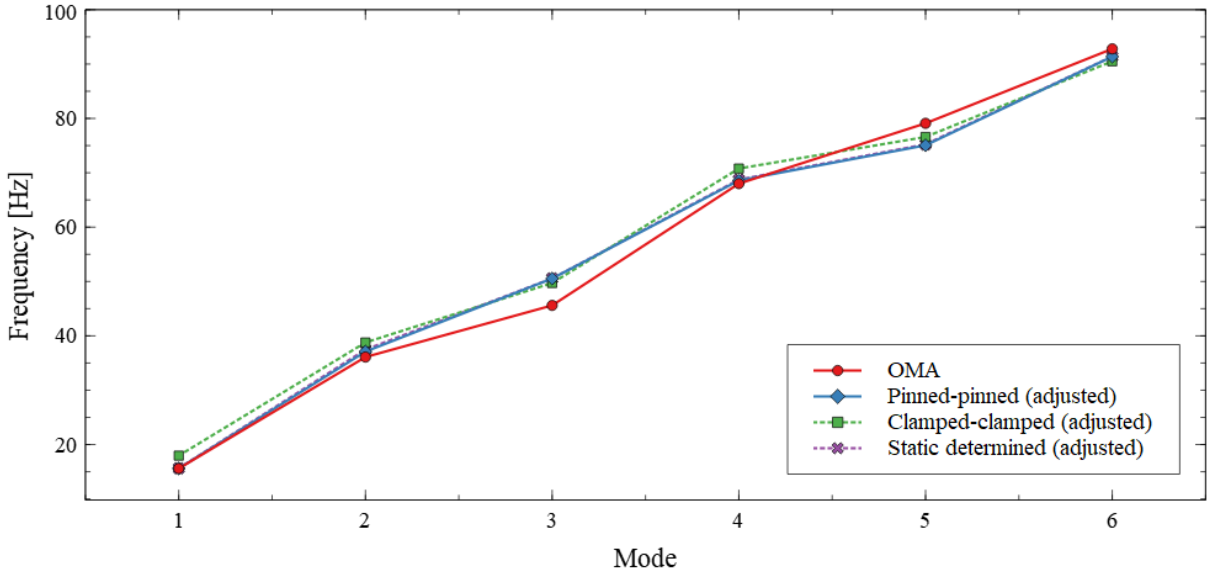

Figure 61 Different boundary conditions with adjusted young's modulus compared to OMA

Table 21 below shows the adjusted boundary conditions compared to the OMA with the percent difference (%Δ). The values from Table 21 are plotted above in Figure 61.

Table 21 OMA compared to the adjusted boundary condition cases

Mode	OMA	AMA Static determined	%Δ	AMA Pinned-Pinned	%Δ	AMA Clamped-Clamped	%Δ
1	15.60 Hz	15.63 Hz	0.19 %	15.61 Hz	0.06 %	17.96 Hz	15.13 %
2	36.10 Hz	37.47 Hz	3.80 %	37.10 Hz	2.77 %	38.78 HZ	7.42 %
3	45.6 0Hz	50.57 Hz	10.90 %	50.54 Hz	10.83 %	49.72 Hz	9.04 %
4	68,00 Hz	68.74 Hz	1.09 %	68.58 Hz	0.85 %	70.78 Hz	4.09 %
5	79.10 Hz	75.23 Hz	-4.89 %	75.05 Hz	-5.12 %	76.59 Hz	-3.17 %
6	92.80 Hz	91.40 Hz	-1.51 %	91.37 Hz	-1.54 %	90.51 Hz	-2.47 %

The pinned-pinned boundary condition is the closest with an average difference from the OMA of 1.31%.

7.7.5 Eccentricity in the connection

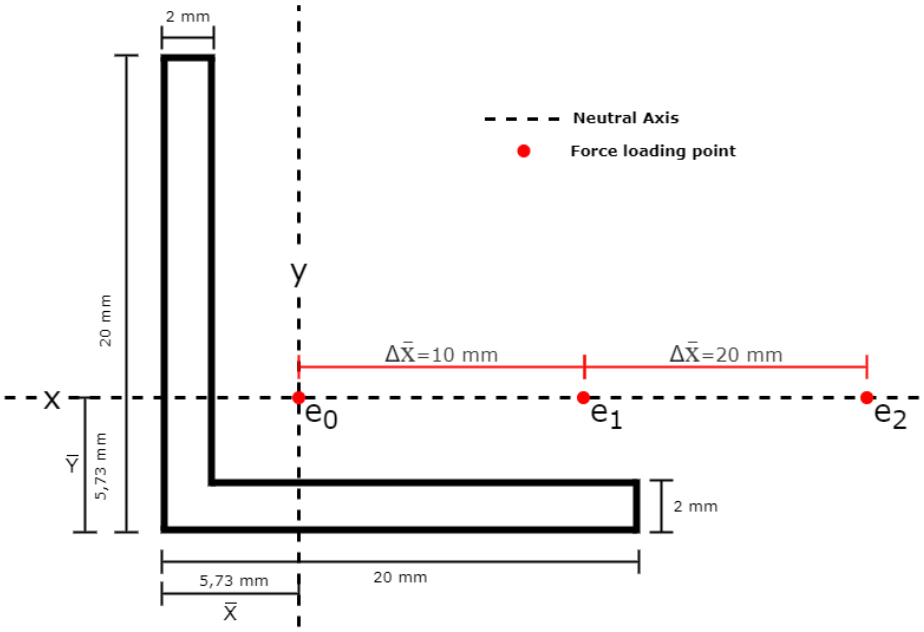

Figure 62 Eeccentricity in the connections cases

By moving the cross section 10 mm and 20 mm in the ANSYS model the impact of eccentricity in the connections will be identified. A modal analysis was done for all eccentricity in the connection's cases. The results, in hertz, from the analysis are shown in Table 22. The 0 mm eccentricity case is the control.

Table 22 Results from modal analysis with eccentric loaded trusses

Mode	0 mm	10 mm	20 mm
1	20.073	20.073	20.073
2	43.330	43.292	43.242
3	55.329	55.305	55.274
4	79.080	79.047	79.001
5	85.476	85.311	85.114
6	100.972	100.802	100.595
7	118.509	118.449	118.374
8	126.066	126.581	126.940
9	127.992	128.044	128.045
10	128.648	128.437	128.193

Normalizing the frequencies from the modal analysis in Table 22, to the control load case (0 mm) shows the percent deviation. The deviation from the control is interpreted as the eccentricity's impact on the model.

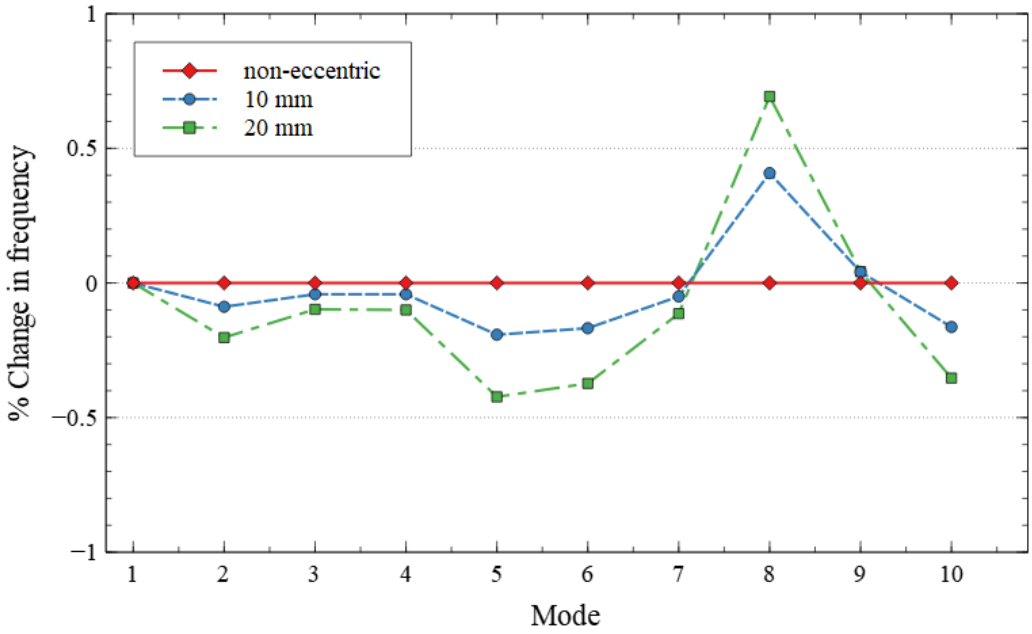

Figure 63 Normalized results from eccentric load case

Figure 63 shows that there is negligible impact from the eccentrically loaded trusses. The first 4 modes, which are the most relevant to our tests, are affected less than 0,2% by the eccentricity. Following this sensitivity study, we conclude that the eccentricity due to the mounting method on the physical model will not significantly impact the result of our study and can therefore be ignored.

7.7.6 Buckling with eccentricity

The critical buckling load is largely dependent on the eccentricity of the force in the load case. Figure 64 shows the buckling capacity with varying amount of eccentricity. The inputs used in the calculations are from the diagonal L-profile in the model bridge, as shown in Table 23, as this is the critical element when considering buckling. The connections are assumed to be pinned.

Table 23 Input variables to buckling formula

Variable	Value
Young's modulus (E-module)	200 000 MPa
Area	76 mm^2
2nd moment of area	2880 mm^4
Length	707 mm
c (distance from NA to edge)	14.26 mm
e (eccentricity)	0.01, 1, 2.5, 5, 10, 20 mm
P (load)	x
σ max	235 MPa

The formula used is a simplified version of the secant buckling formula and is written as:

$$\sigma = P\left[\frac{1}{A} + \frac{e \times c}{I} sec\left(\sqrt{\frac{P}{EI}} \times \frac{L}{2}\right)\right] \quad (7.7.6.1)$$

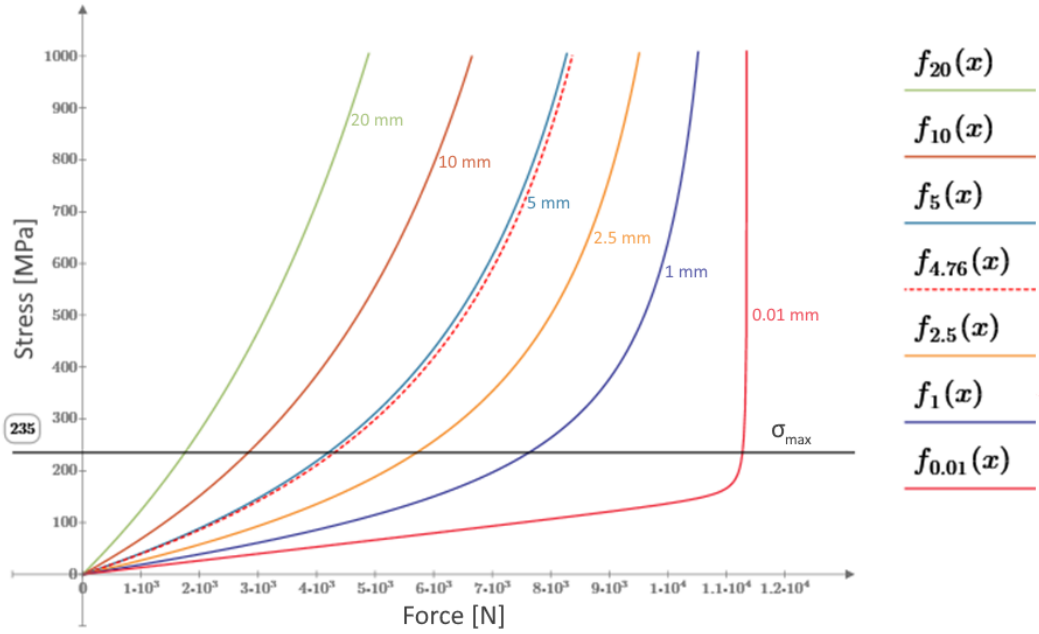

Figure 64 Critical buckling load with varying eccentricity

Figure 64 shows formula 7.7.6.1 plotted with an assortment of eccentricities. Buckling occurs as the stress in the element reaches the material capacity. When the eccentricities approach 0 mm the secant buckling formula returns the same value as Euler's formula. Increasing the eccentricity greatly reduces the critical buckling load. The model bridge has an eccentricity of 4.76 mm, this gives a reduction of the critical buckling load of 60.7%. In the case of mechanical damage causing the middle of the beam to bend 20 mm from its neutral axis, the resulting eccentricity would reduce the buckling capacity by 84.5%. See Table 24 for full critical load list.

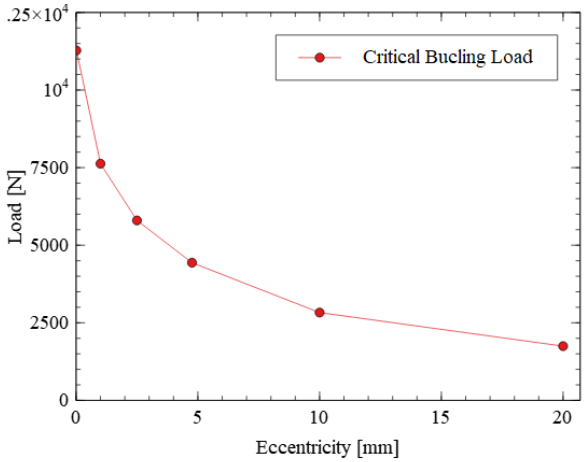

Eccentricity [mm]	Load [N]
0.01	11274.69
1	7626.09
2.5	5798.06
4.76	4436.53
10	2829.31
20	1747.53

Table 24 Result from secant buckling formula

Figure 65 Plotted critical buckling load in relation to eccentricity from Table 24

Figure 65 shows the critical buckling load in relation to the eccentricity. The loaded element's sensitivity (reduction in critical buckling per millimeter eccentricity) reduces as the eccentricity grows.

8 Discussion

8.1 Analytical and experimental modal analyses of the truss bridge model

In order to validate and control our results from the experimental modal analyses of the truss bridge model, a numerical counterpart was made in ANSYS Mechanical APDL. The analytical modal analysis (AMA) using the FEM gave an overview of what modes could be expected at different frequencies. This was used frequently throughout the study to identify modes. The numerical model was also used as a comparison to the physical model to analyse the discrepancies between an analytical solution and the results from the experimental modal analyses.

The numerical model used was a simplified version of the physical bridge model (see Figure 21). Meaning that the brackets, bolts, and nuts used to secure and connect the truss elements on the physical model were not included in the FEM numerical model. This makes the physical bridge slightly stiffer and heavier, which affects the dynamic properties.

Several sensitivity studies were performed in relation to the AMA (see chapter 7.7.1 to 7.7.4). This was done to calibrate the numerical model to the physical bridge model. The calibration was done by adjusting the young's modulus with different boundary conditions until the most comparable case was found. This was found to be pinned-pinned boundary conditions with a 13% reduction of the young's modulus (see Table 21). This combination gave a satisfactory behaviour compared to the results from the experimental modal analyses (see Figure 61). With this adjusted case, the average difference in frequency to the OMA was found to be 1.31% over the first 6 lateral bending modes, where the largest was 10.83% and lowest being 0.06% (see Table 21). The physical model is theoretically built to be statically determined but factoring in friction and the limitations of the mount's design it will act stiffer in practise, hence pinned-pinned was the most comparable.

The analytical modal analysis of the adjusted finite element method model gave similar results to the experimental modal analyses' (CMA and OMA) lateral modes (see Table 12 and Figure 45 under chapter 7.3). However, the AMA gave no clear vertical or torsional modes; thus, the experimental modal analyses were only compared to the AMA using the lateral modes.

8.2 Discrepancies in the experimental modal analyses

The results from the classical modal analysis (CMA) (see Table 5) were treated as a control because of the sensors used and the lack of post-processing opportunities. The sensors used were shock sensors normally used for projects measuring high impact forces like in car crashes etc. This means the sensitivity of the sensors are very low, because of this the impact force of the vibration stimulation needs to be significant to be able to get a good reading. This caused significant noise in the measurements due to ripples in the bridge model.

The sensors used for the operational modal analysis (OMA) are high sensitivity sensors used to measure concrete floors. These sensors are significantly heavier than the sensors used in the CMA (7.5 grams vs 157 grams). This noticeably impacts the frequencies as the CMA results are on average 2.44% higher than the OMA in the first 6 lateral bending modes (see Table 12).

The postprocessing of the accelerometer data was done in two different methods. The CMA accelerometer data was processed using a FFT through MATLAB. The data from the OMA was processed using a FDD through the software from the sensor manufacturer, Pulse OMA. To ensure there were no major differences between the two post processing methods, a FFT was performed of the OMA results as well. The two methods gave less than one percent difference and thus deemed negligible (see Table 6, Table 7, Table 8, Table 9, Table 10 and Table 11). Therefore, the FDD results from the PULSE OMA software was used as it allows for easier identification of closely spaced modes.

8.3 Mode shapes

By using the PULSE OMA software when post processing the vibration data from the OMA, we were able to extract the mode shapes from the measurements. By comparing these to the mode shapes from the FEM AMA in ANSYS we were able to identify the bending and torsional modes. We looked at lateral movement (y-direction) and vertical movement (z-direction) separately because of the uniaxial accelerometers.

Figure 9 on page 9 in the theory chapter (3.4.1) shows an illustration that describes how the first and second bending mode of a clamped-clamped beam theoretically should move. In both the OMA result from the physical model and the AMA result from the numerical model we can see the same movements appear. This tells us the bridge moves as expected and validates our analyses.

The first 6 modal frequencies found in both the OMA and the AMA were lateral bending modes. This is due to the low bending stiffness of the design in the y-direction. These modes were found in the 0-110 Hz range. A comparison of the OMA and AMA mode shapes for the 1st, 2nd and 6th bending mode are shown in Figure 46, Figure 48 and Figure 49 under chapter 7.4. The mode shapes from the physical testing show clear comparable movements to the analytical counterpart.

The bridge design is substantially stiffer in the vertical plane, which means the vertical modes should appear in the higher frequency ranges. The first vertical bending- and torsional mode shapes were found in OMA in the higher frequency scale 110-210 Hz. This tells us that the result we got, was as we expected. Since the vertical mode shapes from the AMA were difficult to identify, due to little movement in the Z direction, we focused on lateral bending modes in the comparison between the two modal analyses.

Some complex mode shapes containing multiple peaks and arches were difficult to identify from the OMA. This is due to the OMA post processing software only showing movements in the bridge's nodes as this is where the measurements were made. Because of this, modes with the peaks in between nodes sometimes appeared cluttered as the full movement was not shown.

Some of the mode shapes from the OMA often contained noise and unsymmetric movements compared to the theoretically ideal mode shapes from the AMA. This is likely caused by inaccuracies and slight dissymmetry in the design of the physical truss bridge. This is more apparent in modes with higher frequencies and more complex mode shapes, thus making it more difficult to identify these modes.

From PULSE OMA we had both the Modal complexity factor (MCF) and the Modal assurance criterion (MAC) to help with the identification of the mode shapes. Most of the mode shapes found from the undamaged case had low MCF, around 0-1 %. This tells us that the movements of the mode shape were mostly in phase or 180 degrees apart in phase (opposite movements). High MCF values indicates that the mode shapes contain a lot of noise and unsynchronised movements. This might be a sign of inconsistencies in the bridge model or in the vibration recordings as a result of poor stimulation.

The first vertical bending mode containing a single arch were found at both 121.2 Hz and 158.2 Hz, with only some differences (see Figure 52 on page 54). The first one has most of the movement in the top half of the bridge, while the other one in the bottom half. The two mode shapes had a MAC value of 0.7401 out of 1, where 1 is identical movements (see Table 13 on page 54). Both the visual movement in the mode shape and the MAC tells us that the two modes are similar.

8.4 Damage cases

The damage cases focused on in this study aimed for simulating realistic damage scenarios. Damage case 1 served as a control to analyse the effect of applying a relatively significant change in the geometry by removing a diagonal truss element. By analysing the results from this case, the group could decide how significant the damage of the main case would need to be to achieve sufficient change in frequency. This damage case could also easily be replicated in the FEM AMA to give a theoretical comparison. The diagonal truss element is a key element for the vertical stiffness of the bridge as it transfers the vertical and lateral forces of the connecting nodes. The element contributes little to lateral stiffness. This was reflected in the results from the OMA. The average change in frequency from the undamaged case for the lateral modes was -0.87% and -6.49% for the vertical modes. The FEM AMA with the same damage case gave an average reduction of -9.74% in the lateral modes.

On basis of the results from the first damage case the second damage case was chosen. The first damage case gave adequate change in stiffness, any lower could be hard to identify so a similar case was used. The truss element previously removed was kept but loosened instead. By doing this the truss element will not absorb any forces but the weight is still present. This is comparable to realistic damage scenarios with considerable mechanical damage from corrosion, cracking etc.

As a result of the added weight in damage case 2, we saw a further decrease of frequencies. The lateral and vertical modes for damage case 2 were reduced by -1.79% and -8.37% compared to -0.87% and -6.49% for damage case 1.

Other damage cases were considered. Simulating other mechanical damage cases by i.e., bending a key element to reduce the axial stiffness of that element by creating an eccentric load case. This significantly reduces the critical buckling load and increased the displacement to load ratio (see 7.7.6). To see how this affects the modal frequencies a FEM modal analysis of an eccentric cross-sections case was done (see 7.7.5). This analysis showed a relatively low impact on the frequencies; thus, it was deemed too small of an impact and was scrapped.

When examining the lateral modal shapes of the damage cases from the OMA recordings we saw little visual discrepancies beyond expected noise or inaccuracies in the recordings. The differences were more apparent in the vertical modes as the damage cases more significantly impacts the vertical stiffness. The vertical bending modes are dependent on each vertical plane to move in phase at the same frequency. Because the damage is only applied to one side of the bridge it creates unsymmetric properties. The resulting dissymmetry in stiffness causes uneven natural frequencies on each side. This causes the vertical bending modes in the damage cases to either disappear or lag out of phase. Hence some of the vertical modes from the OMA were not observed.

Both damage cases produced measurable change in frequencies due to the damage applied to the model. This shows that modal analysis based structural health monitoring is a viable method for uncovering damage in bridges. In the cases presented the damage mainly affected the vertical stiffness which was reflected in the results.

8.5 Limitations and challenges

There are several challenges with this study, some of the most important once will be listed in an overview below:

- The group had limited access to the Pulse OMA software, since we only had the simplest version. Which mean we lacked some functions that could have helped us locating the different mode shapes.

- The physical bridge model had increased stiffness due to the mounting brackets, which had an impact on the results.

- Identification of the modes and mode shapes in the z-direction was challenging. This was especially true in the damage cases as some of the mode shapes were cluttered. This made comparing the mode shapes a challenge.

- The sensors used in the OMA were significantly heavier than the ones used in the CMA. This impacted the frequencies noticeably. In addition, it may have some impact on the mode shapes.

9 Conclusion

How to monitor the structural health condition of a steel bridge based on vibration measurements?

Structural health monitoring based on vibration measurements can be achieved by instrumenting the bridge with accelerometers in key locations. By doing this we are able to measure the free vibrations of the bridge's superstructure. The raw vibration data from the measurements can then be decomposed to identify the bridge's modal frequencies. The eigenfrequencies are dependent on the bridge's structural stiffness and weight. Knowing this, any change in the eigenfrequencies can be treated as a change in stiffness of the superstructure. This may be caused by structural damage and should be investigated.

- Instrumenting the truss bridge with sensors to obtain the dynamic properties of the structure can be done by mounting sensors in the bridge's nodes. This will effectively pick up the global modes of the bridge. For simple recordings, instrumenting key nodes is adequate. For studies requiring advanced post-processing, all nodes must be measured. If there are more nodes on the bridge than sensors available, a stationary reference sensor can be used to combine multiple recordings in post-processing.
- Applying damage to the truss bridge altered the dynamic properties due to reduced stiffness in the superstructure. Both the damage case with an element removed (a), and the damage case with an element loosened (b) produced significant reduction of the bridge's modal frequencies. The damage was applied to a key element contributing to vertical stiffness, this was reflected in the results as the vertical modes were affected more. The vertical modes were reduced by -6.49% (a) and -8.37% (b) and the lateral modes by 0.87% (a) and -1.79% (b) on average. Some modes were not observed in the damage cases due to unsymmetric stiffness caused by the damage. Other modes experienced decreased clarity in the corresponding mode shapes.
- Damage can be detected by analysing the sensor data. By monitoring a bridge using accelerometers, the modal frequencies can be identified. If the modal frequencies change, an alteration in the bridge's stiffness has likely occurred. This may be a result of structural damage. These changes can be detected by either taking periodical measurements or by constantly monitoring the bridge.
- There are some discrepancies between the results from the modal analyses. On average, the analytical modal analysis gave 1.31% higher modal frequencies compared to the operational modal analysis in the undamaged case. In the damage case (a), the analytical modal analysis gave a significantly larger decrease in frequencies (-9.83% on average) compared to the operational modal analysis (-0.87%). The operational modal analysis had consistently lower frequencies than the classic modal analysis due to the heavier sensors used (-2.44% on average).

10 Suggestions for Further Work

This study examines the change in the truss bridge's dynamic response when altering the physical properties. Although the study gave good results, the numerical model had some limitations, like being simplified version of the physical bridge model. Which is why building on this thesis, the group suggest further work will be to:

- Make a 1:1 digital model (digital twin) for the analytical modal analysis.
- Take the bridge with the sensors attached and monitor outside, to get random excitation of the bridge vibration by rain or wind loads.
- Making a true digital twin that gets the accelerometers data from the sensors in real time.
- Implement damage localization methods.
- After this, further work would be to implement this to a real steel truss bridge.
- Perform a life cycle assessment (LCA) to really see if doing structural health monitoring would have an economical and resource usage benefit over traditional maintenance of a bridge.
- Making an artificial neural network and training it to detect damage, which by having a digital twin with real time data would give a continuous monitoring of the bridge.

11 Bibliography

[1] F. Magalhães, A. Cunha og E. Caetano, «Vibration based structural health monitoring of an arch bridge,» 7 June 2011. [Internett]. Available: https://www.sciencedirect.com/science/article/abs/pii/S0888327011002330. [Funnet 19 May 2022].

[2] Y. Ni, «Structural health monitoring of cable-supported bridges based on vibration measurments,» 30 June 2014. [Internett]. Available: https://web.fe.up.pt/~eurodyn2014/CD/papers/009_SKN_ABS_2019.pdf. [Funnet 19 May 2022].

[3] B. Peeters, G. Couvreur, O. Razinkov, C. Kündig, H. Van der Auweraer og G. De Roeck, «CONTINUOUS MONITORING OF THE ØRESUND BRIDGE,» 2003. [Internett]. Available: https://www.researchgate.net/publication/228675249_Continuous_monitoring_of_the_Oresund_Bridge_System_and_data_analysis. [Funnet 19 May 2022].

[4] B. Siem, «Nrk.no,» 12 April 2022. [Internett]. Available: https://www.nrk.no/vestland/5600-bruer-har-skader-som-reduserer-trafikktryggleiken-1.15921518. [Funnet 19 May 2022].

[5] B. Siem, «Nrk.no,» 04 April 2022. [Internett]. Available: https://www.nrk.no/vestland/1000-norske-bruer-har-skader-som-trugar-bereevna-1.15819652. [Funnet 19 May 2022].

[6] NRK, «Nrk.no,» 3 mars 2019. [Internett]. Available: https://www.nrk.no/norge/271-bruer-har-skader-som-ma-folges-opp-1.14455277. [Funnet 5 mars 2022].

[7] G. T. Frøseth, «ntnuopen.ntnu.no,» 24 februar 2019. [Internett]. Available: https://ntnuopen.ntnu.no/ntnu-xmlui/bitstream/handle/11250/2604884/Gunnstein%20Froseth_PhD.pdf?sequence=1&isAllowed=y. [Funnet 3 mars 2022].

[8] S. Hakdaoui, A. Emran og F. Oumghar, «Mobile Mapping, Machine Learning and Digital Twin for Road Infrastructure Monitoring and Maintenance: Case Study of Mohammed VI Bridge in Marocco,» 2020. [Internett]. Available: https://ieeexplore.ieee.org/stamp/stamp.jsp?tp=&arnumber=9121882&tag=1. [Funnet 19 May 2022].

[9] FN-sambandet, «fn.no,» 23 ferbruar 2022. [Internett]. Available: https://www.fn.no/om-fn/fns-baerekraftsmaal/industri-innovasjon-og-infrastruktur. [Funnet 29 april 2022].

[10] J. Fuchs, «The Strength and Mystery of Triangles,» 22 October 2012. [Internett]. Available: https://techblog.ctgclean.com/2012/10/the-strength-and-mystery-of-triangles/. [Funnet 10 February 2022].

[11] T. Megson, «Chapter 4 - Analysis of Pin-Jointed Trusses,» i *Structural and Stress Analysis*, Butterworth-Heinemann, 2019.

[12] S. W. W. H. Albert Fink, «Britannica,» 16 September 2019. [Internett]. Available: https://www.britannica.com/technology/truss-bridge. [Funnet 27 January 2022].

[13] HILTI, Corrosin Handbook, Hilti Corporation, 2015.

[14] National Transport Safety Board, «Collapse of the Interstate 5 Skagit River Bridge,» 23 May 2013. [Internett]. Available: https://www.ntsb.gov/investigations/AccidentReports/Reports/HAR1401.pdf. [Funnet 8 February 2022].

[15] B. Monk, «Puget Sound Business Journal,» *What caused the Skagit River bridge to collapse?,* 25 May 2013.

[16] W.-L. J. Yong Bai, «Science Direct, Buckling/Collapse of Columns and Beam-Columns,» 2016. [Internett]. Available: https://doi.org/10.1016/B978-0-08-099997-5.00015-0. [Funnet 8 February 2022].

[17] B. J. G. James M. Gere, Mechanics of materials, 2011.

[18] Unknown, «Buckling of Eccentrically Loaded Columns,» [Internett]. Available: https://www.continuummechanics.org/eccentriccolumnbuckling.html. [Funnet 5 March 2022].

[19] K. Worden, C. R. Farrar, G. Manson og G. Park, «The royal society publishing,» 3 April 2007. [Internett]. Available: https://royalsocietypublishing.org/doi/full/10.1098/rspa.2007.1834. [Funnet 8 Mars 2022].

[20] M. Williams, Structural Dynamics, Boca Raton: CRC Press, 2016.

[21] H. Benaroya, M. Nagurka og s. Han, Mechanical Vibration: Analysis, Uncertainties, and Control, Fourth Edition, Boca Raton: CRC Press, 2017.

[22] B. a. Kjær, «Webinar Operational Modal Analysis,» [Internett]. Available: https://hbm.wistia.com/medias/u454cf9cwf.

[23] J. He og Z.-F. Fu, Modal Analysis, Oxford: Butterworth Heinemann, 2001.

[24] P. S. Rao og C. Rtnam, «Engineeringresearch.org,» 2012. [Internett]. Available: https://engineeringresearch.org/index.php/GJRE/article/view/298. [Funnet 14 May 2022].

[25] W.-X. Ren, T. Zhao, I. E. Harik og M.ASCE, «researchgate.net,» July 2004. [Internett]. Available: https://www.researchgate.net/publication/228695134_Experimental_and_Analytical_Modal_Analysis_of_Steel_Arch_Bridge. [Funnet 14 May 2022].

[26] D. J. Inman, Engineering Vibrations fourth edition, Michigan: Pearson, 2013.

[27] M. Pastor, M. Binda og T. Harþarik, «Sciencedirect,» Elsevier, 2012. [Internett]. Available: https://www.sciencedirect.com/science/article/pii/S1877705812046140. [Funnet 18 April 2022].

[28] B. &. Kjær, «Brüel & Kjær.com OMA,» Brüel & Kjær, [Internett]. Available: https://www.bksv.com/en/analysis-software/structural-dynamics-software/modal-analysis-software/operational-modal-analysis. [Funnet 04 April 2022].

[29] M. Imregun og D. J. Ewins, «COMPLEX MODES - ORIGINS AND LIMITS,» 1995. [Internett]. Available: https://www.scribd.com/document/407974516/sem-org-IMAC-XIII-13th-13-13-3-Complex-Modes-Origins-Limits-pdf. [Funnet 19 May 2022].

[30] P. B. Andersen, «snl.no,» 23 januar 2018. [Internett]. Available: https://snl.no/FFT. [Funnet 15 mars 2022].

[31] R. Brincker, L. Zhang og P. Andersen, «vbn.aau.dk,» June 2000. [Internett]. Available: https://vbn.aau.dk/ws/files/203990023/Modal_Identification_of_Output_Only_Systems_using_Frequency_Domain_Decomposition.pdf. [Funnet 18 April 2022].

[32] S. Amador, M. Ø. Ø. Juul, T. Friis og R. Brincker, «Researchgate.net,» Juni 2019. [Internett]. Available: https://www.researchgate.net/publication/323254720_Application_of_Frequency_Domain_Decomposition_Identification_Technique_to_Half_Spectral_Densities. [Funnet 04 Mai 2022].

[33] M. K. Thompson og J. M. Thompson, ANSYS Mechanical APDL for Finite Element Analysis, Oxford: Butterworth-Heinemann, 2017.

[34] K. Vertes, «Canvas.no BYG506 FEMpresentation4 2020,» 26 Janaur 2021. [Internett]. Available: https://uia.instructure.com/courses/8386/pages/26-dot-01-dot-2021?module_item_id=254957. [Funnet 13 May 2022].

[35] G. Liu og S. Quek, «elsevier.com,» Elsevier, 7 August 2013. [Internett]. Available: https://www.elsevier.com/books/the-finite-element-method/liu/978-0-08-098356-1. [Funnet 14 Februar 2022].

[36] K. Vertes, «BYG 506 Lecture note 1 FEM.pdf,» 19 January 2021. [Internett]. Available: https://uia.instructure.com/courses/8386/pages/19-dot-01-dot-2021?module_item_id=252225. [Funnet 26 May 2022].

[37] K. Vertes, *BYG506 Elementmetoden i Konstruskjoner,* Grimstad : UIA, 2021.

[38] J. Gardiner, «Xceed Engineering & Consulting P.C.,» 27 March 2017. [Internett]. Available: https://www.xceed-eng.com/finite-element-analysis-convergence-and-mesh-independence/. [Funnet 14 May 2022].

[39] OMEGA, 28 August 2018. [Internett]. Available: https://www.omega.com/en-us/resources/accelerometers.

[40] Nortek Group, «Nortek,» [Internett]. Available: https://www.nortekgroup.com/knowledge-center/wiki/new-to-subsea-navigation. [Funnet 22 February 2022].

[41] P. L. Walter, «qringtech.com,» 2006. [Internett]. Available: https://qringtech.com/TryMe/wp-content/uploads/2014/01/HistoryOfTheAccelerometer.pdf. [Funnet 29 april 2022].

[42] Grampian Fasteners, [Internett]. Available: https://www.grampianfasteners.com/files/95b2c19b-1d29-4624-abdf-0813df2db3ac/Torque_Settings.pdf.

[43] ENDEVCO, « Data sheet for ENDEVCO 713-2k-240,» [Internett]. Available: https://buy.endevco.com/ContentStore/MktgContent/Endevco/Datasheet/713-713F_DS_083019.pdf.

[44] P. Dolec, Interviewee, *Training on structural vibration measurements w/ Bruel & Kjær via Scanditest AS.* [Intervju]. 11 Mars 2022.

[45] DEWESoft, «DEWSoft products,» DEWESoft, 2022. [Internett]. Available: https://dewesoft.com/products/daq-systems/sirius. [Funnet 21 February 2022].

[46] Ansys, «Ansys.com,» Ansys, 27 01 2022. [Internett]. Available: https://www.ansys.com/company-information. [Funnet 27 01 2022].

[47] B. &. Kjær, «Brüel & Kjær.com,» Brüel & Kjær, [Internett]. Available: https://bkconnect.bksv.com/. [Funnet 04 April 2022].

[48] Cambridge, «Cambridge Dictionary,» [Internett]. Available: https://dictionary.cambridge.org/dictionary/english/superstructure. [Funnet 27 January 2022].

[49] CME Engineering, «UConn Today,» 11 August 2016. [Internett]. Available: https://today.uconn.edu/2016/08/keeping-connecticuts-bridges-strong/bridge_9_16_02-020/. [Funnet 31 Januar 2022].

[50] ASM Handbooks, « Failure Analysis and Prevention,» i *Metal Handbook*, 1975.

[51] M. Yashinsky, «Bridge of the week,» 1 April 2018. [Internett]. Available: http://www.bridgeofweek.com/2018/04/humboldt-county-bridges-highway-101.html. [Funnet 31 January 2022].

[52] G. M. Smith, «DEWESoft,» 29 January 2020. [Internett]. Available: https://dewesoft.com/daq/measure-strain-and-pressure. [Funnet 18 Febuary 2022].

[53] ALTHEN, «ALTHEN,» [Internett]. Available: https://www.althensensors.com/sensors/strain-sensors-strain-gauges/special-application-straingauges/4476/dsf-series-for-high-endurance-strain-gauges/.

[54] National Instruments, «National Instruments,» 15 July 2020. [Internett]. Available: https://www.ni.com/en-no/innovations/white-papers/07/measuring-strain-with-strain-gages.html. [Funnet 18 febuary 2022].

[55] Micro Measurements, «Vishay PG,» 30 May 2018. [Internett]. Available: http://www.vishaypg.com/docs/11055/tn505.pdf.

[56] T. G. Beckwith, Mechanical measurements, Addison-Wesley Pub. Co., 1982.

[57] Baumer, «Baumer,» 2022. [Internett]. Available: https://www.baumer.com/nl/en/service-support/function-principle/functionality-and-technology-of-optical-distance-sensors/a/Know-how_Function_optical-distance-sensors.

[58] J.-S. Kang, K. Chung og E. J. Hong, «www.Link.springer.com,» 17 February 2021. [Internett]. Available: https://link.springer.com/article/10.1007/s11042-021-10649-x#citeas. [Funnet 08 Mars 2022].

[59] Siemens, «Siemens.Mindsphere.com,» Siemens , [Internett]. Available: https://siemens.mindsphere.io/en. [Funnet 08 Mars 2022].

[60] E. P. Carden og P. Fanning, «CiteSeerx,» 2004. [Internett]. Available: https://citeseerx.ist.psu.edu/viewdoc/summary?doi=10.1.1.118.3093. [Funnet 8 Mars 2022].

[61] H. Holden, «snl.no,» 28 november 2019. [Internett]. Available: https://snl.no/fouriertransformen. [Funnet 15 mars 2022].

[62] MathWorks, «MathWorks.com,» MathWorks, [Internett]. Available: https://se.mathworks.com/products/matlab.html?s_tid=hp_ff_p_matlab. [Funnet 25 03 2022].

[63] E. Chatzi og D. Straub, «TUM Institute for Advanced study,» Technische Universität München, 20 May 2021. [Internett]. Available: https://www.ias.tum.de/ias/event-pages/didis-workshop/home/. [Funnet 13 May 2022].

12 Appendices

- Appendix A, collection of the scripts made throughout the thesis
- Appendix B, collection of all the meeting rapports
- A3-poster